THERAPEUTIC DEVELOPMENT FOR FACIOSCAPULOHUMERAL MUSCULAR DYSTROPHY UTILIZING A NOVEL HUMAN SKELETAL MUSCLE XENOGRAFT MODEL

by
Yuanfan Zhang

A dissertation submitted to the Johns Hopkins University in conformity with the requirements of the degree of Doctor of Philosophy.

Baltimore, Maryland
March 2016

© 2016 Yuanfan Zhang
All Rights Reserved

Abstract

Genetic muscle disorders such as facioscapulohumeral muscular dystrophy (FSHD) deprive patients of their physical strength and quality of life. Animal models have been indispensable in the research investigation and therapeutic development for genetic muscle disorders. But the successful leap from bench to bedside rarely happens because the animal model is not human and cannot predict human response to therapy precisely. Herein, we try to create a 'living and breathing' human muscle inside a mouse host and demonstrate the feasibility and validity of human to mouse xenografts as a preclinical model of myopathy. Human skeletal muscle biopsies as well as autopsies transplanted into the anterior tibial compartment of the hindlimbs of NOD-Rag1null IL2rγnull (NRG) immunodeficient host mice regenerate new vascularized and innervated myofibers from human myogenic precursor cells. The grafts exhibit contractile and calcium release behavior, characteristic of functional muscle tissue.

The validity of the human graft as a model of FSHD is demonstrated in disease biomarker studies, showing that gene expression profiles of xenografts mirror those of the donor muscles. These findings illustrate the value of a new experimental model of muscle disease as a feasible and valid preclinical tool to better investigate the pathogenesis of human genetic myopathies and to more accurately predict their response to novel therapeutics.

We also report a proof-of-concept study using antisense phosphorodiamidate morpholino oligonucleotides (PMOs) to suppress DUX4 expression, which is believed to be the causative genetic defect of FSHD currently, in FSHD myotubes and xenografts derived from patients. The most effective PMO FM10 had no significant cell toxicity.

RNA-seq analyses of FSHD and control myotubes revealed that FM10 down-regulated many transcriptional targets of DUX4, without overt off-target effects. Treatment with FM10 in FSHD patient muscle xenografts also down-regulated *DUX4* and DUX4 targets. These findings demonstrate the potential of antisense PMOs as an FSHD therapeutic option.

Advisor:

Dr. Kathryn R. Wagner

Thesis Committee:

Dr. Robert A. Casero, Jr. (Chair)

Dr. Peter A. Campochiaro (Reader)

Dr. Terence A. Partridge

Acknowledgements

This thesis work would not have been possible without the help, support and inspiration from the bright minds and kind souls I have worked with. I would like to extend my sincere gratitude to them.

I would like to first thank my advisor and mentor Dr. Kathryn Wagner, for her endless guidance and support through this PhD journey. She introduced me to the beauty of muscle and taught me so much about the exciting yet challenging translational research. Her undivided passion and dedication for clinic and research will always inspire me. She and Dr. Terry Partridge were the ones who started this human muscle in mouse project triggered by scientific curiosity. I truly appreciate my thesis committee members Drs. Bob Casero, Peter Campochiaro, and Terry Partridge for their critical input and support through the years.

Thanks to Kathryn, I was part of the amazing team of Senator Paul D. Wellstone Muscular Dystrophy Cooperative Research Center for FSHD. As a predoctoral trainee, I had the opportunity to go to research meetings and discuss science with the brightest scientists. I would like to thank our collaborators Drs. Charlie Emerson, Oliver King, Takako Jones, Jennifer Chen and Miguel Esteves at University of Massachusetts Medical School, Drs Louis Kunkel and Fedik Rahimov at Harvard, and Nicholas Clayton and Dr. Bruce Wentworth at Genzyme. The whole Wellstone team and scientific advisory board has provided thoughtful insights for my research. I thank Drs. Gabsang Lee, Warren Grayson, and Thomas Lloyd at Hopkins to include me in their research teams.

My research project wouldn't be possible without the devoted patient community of FSHD. I sincerely thank all the patient families in this study. Special thanks to Daniel

Perez and the FSH Society, Inc. for assistance with patient recruitment and biopsy procurement.

I would also like to thank the great team at the Center for Genetic Muscle Disorders. They have been helpful not only in experiments but as friends in my daily life: Naili Liu, Adam Moyer, Jessica Miciak, Kenneth Estrellas, Tatiana Cohen and Melanie Branagan in the lab; and Drs. Genila Bibat, Doris Leung, Elba Gerena Maldonado, and Carla Grosmann in clinic. Thank you to Karen Smith-Connor and Larry Frelin for making the 4th floor of KKI a happy place to work. A special thanks to the members of the MRB animal facility for their vigilance regarding the wellbeing of my mice.

Dr. Jennifer Elisseeff, advisor of my Master's thesis in Biomedical Engineering, opened my eyes to regenerative medicine and led me to the CMM program. Working in her lab intrigued me to stay at Hopkins and pursue my PhD. I am so fortunate to be in the CMM graduate program with the strongest support team of Colleen Graham, Leslie Lichter and Dr. Rajini Rao. They have guided me through life as a graduate student.

Thanks to my friends, I have not felt lonely or helpless as an international student at Baltimore. To my family, your love and support are the source of my strength and happiness. Special thanks to my husband Zhaoying Hu, for his extraordinary friendship, encouragement and support while we were working on our PhDs 360 miles apart.

Table of Contents

List of Figures and Tables

Chapter 1. Introduction

Chapter 2. Human skeletal muscle xenograft as a new preclinical model for muscle disorders

Chapter 3. Morpholino-Mediated Knockdown of DUX4 Towards

Facioscapulohumeral Muscular Dystrophy Therapeutics

Chapter 1. Introduction

Overview

In **Chapter 1**, I will provide an introduction to the disease facioscapulohumeral muscular dystrophy (FSHD), the challenges faced in creating animal models for FSHD, and the use of xenograft models in therapeutic development. In **Chapter 2**, I will present the establishment of the human skeletal muscle xenograft model, specifically for FSHD. In **Chapter 3**, I will present a proof-of-concept study of using antisense phosphorodiamidate morpholino oligonucleotides (PMOs) as a potential FSHD therapeutic. In **Chapter 4**, I will discuss the future directions.

Introduction

Skeletal muscle tissues, composing a third of the body mass in a healthy individual (1), are essential for support, protection and movement of the body. There are many disorders of skeletal muscle, and most individuals will suffer from a skeletal muscle disorder at some point in their lives. These include genetic disorders of muscle, acquired primary myopathies (including toxic, metabolic, and inflammatory myopathies), acquired myopathy secondary to a chronic illness (including infections, cancer, and congestive heart failure), or sarcopenia, the age related loss of muscle. Our lab is devoted to developing novel therapies for muscle disorders in order to improve function and quality of life.

Animal models are essential in the investigation of disease pathogenesis and therapeutic development. The significance of the project detailed here is that a human muscle xenograft model independent of specific molecular hypothesis may translate well to human clinical trials and could be made rapidly available for diseases which do not currently have an accepted animal model. Such an *in vivo* model would facilitate entry of novel therapeutics to clinical trials in underserved disease population, and in the present study this is demonstrated specifically with facioscapulohumeral dystrophy (FSHD).

Facioscapulohumeral dystrophy

Facioscapulohumeral dystrophy (FSHD) was first described in 1885 by the French neurologists Landouzy and Dejerine (2) It is characterized by asymmetric muscle weakness and wasting (atrophy) of specific muscle groups indicated by the name: those of the face (facio-), around the shoulder blades (scapulo-), and in the upper arms

(humeral) (Figure 1.1). FSHD is one of the most prevalent neuromuscular disorders, affecting 1-9 : 100,000 individuals worldwide (3).

FSHD is classically considered an autosomal dominant muscle disorder; however, up to 30% of cases are sporadic, caused by *de novo* mutations (4). Traditionally, physicians believe the progression of disease starts with asymmetric weakness of muscles in the face and shoulder-girdle, later involving pelvic and proximal lower limb muscles. Recent whole body MRI studies have revealed that while FSHD can go on to affect most any skeletal muscle, the most frequently and severely involved muscle overall is the semimembranosus. Paraspinal muscles and muscles of the abdominal wall are also among the most frequently involved(5). In rare cases, there are extramuscular manifestations including a retinal exudative retinopathy (Coats disease) and hearing loss (6). Disease onset appears from infancy to late life but typically in the second decade for men and by the third decade of life for women. The clinical spectrum is widely variable, ranging from asymptomatic gene carriers to wheelchair bound patients, which matches the great variety in severity of muscle pathology (Figure 1.2). Interestingly, FSHD affects males more severely and more frequently than females, although the cause is not yet clear (7). FSHD has no particular racial, geographic or ethnic distribution, and studies worldwide show similar prevalence across races (8-10). Currently genetic testing is the only way to confirm a FSHD diagnosis, while no biochemical, histological, or instrumental markers are available for diagnosis.

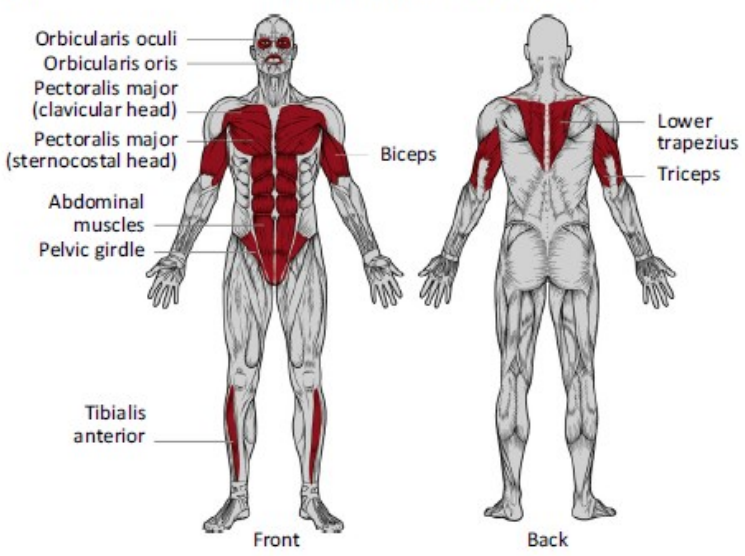

Figure 1.1 Clinical features of FSHD (11).

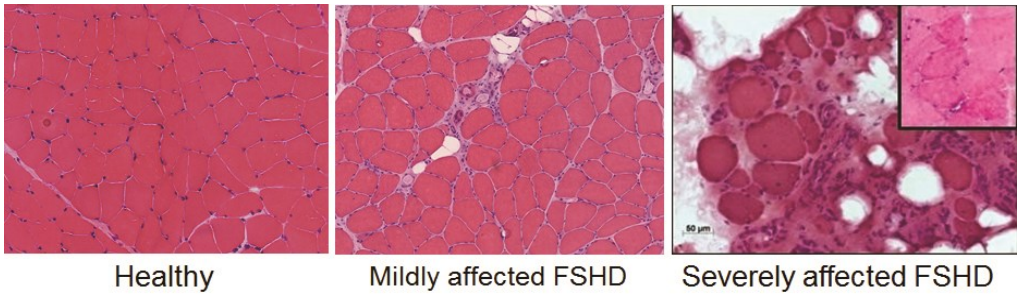

Figure 1.2 Example images of H&E stained muscle sections from healthy, mildly affected, and severely affected FSHD donors.

FSHD pathogenesis has been one of the most puzzling enigmas in human genetics for the past two decades. There was always a consensus that the disease was caused by a gain-of-function mutation that activate the transcription of a region that is normally repressed post development. There are two subtypes of FSHD based on the genetics and epigenetics as shown in Figure 1.3 summarized by Himeda et al.: FSHD1, the classical form accounting for 95% of FSHD cases, is associated with pathogenic contraction of D4Z4 macrosatellite repeats on a 4qA subtype of chromosome 4; and FSHD2 is

contraction-independent but associated with mutations in the chromatin regulator gene *SMCHD1* (structural maintenance of chromosomes hinge-domain protein 1). In healthy individuals, the D4Z4 macrosatellite repeat array in the subtelomere of chromosome 4 at 4q35 varies between 11 and 100 repeat units and is marked by hypermethylation and compact chromatin structure, indicating the state of transcriptional repression. In FSHD1, the repeat units are contracted to 1-10 units and are associated with local hypomethylation and chromatin relaxation on chromosome 4. With the disease-permissive 4qA allele, the toxic DUX4-fl (double homeobox protein 4-full length) expression is no longer silenced in skeletal muscle. Recent studies have shown an imperfect correlation between the size of the repeat units and disease severity, as FSHD1 patients with 1-3 repeat units tend to be more clinically severe with younger onset ages while patients with 8-10 repeat units usually present milder symptoms or may be asymptomatic even in late adulthood. In FSHD2, mutations in *SMCHD1* cause hypomethylation of chromosomes 4 and 10, allowing chromosome 4 to express the toxic *DUX4* transcript in the case of the permissive 4qA allele. It is recently suggested that *SMCHD1* may act as a genetic modifier of FSHD1 because *SMCHD1* gene mutations are identified in individuals with more severe phenotype and *SMCHD1* protein directly binds to D4Z4 and suppresses somatic expression of D4Z4 (12, 13). The high variability of disease severity between FSHD individuals, even within the same family with the same contracted D4Z4 allele and permissive haplotype, suggests that there are likely other genetic modulators of the clinical manifestations.

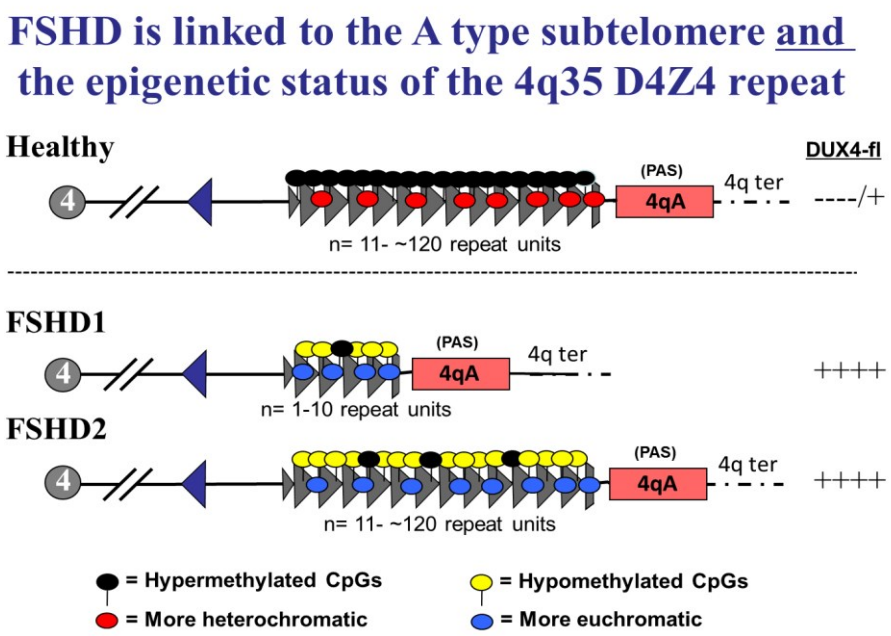

Figure 1.3 FSHD is a genetic and epigenetic disorder (14)

While there is consensus on the genetic cause of the disease, the pathogenesis of FSHD is still under investigation. Several candidate genes located within or close to the D4Z4 locus, including *FRG1* (FSHD region gene 1) (15, 16), *FRG2* (FSHD region gene 2) (17), *ANT1* (adenine nucleotide translocase 1) (18), *FAT1* (FAT Atypical Cadherin 1) (19), and *DUX4c* (20), have been proposed as FSHD pathogenesis mediators based on differential expression between FSHD and healthy myoblasts, but little consensus is reached in subsequent validation using large cohort studies. However one gene that has been consistently shown to be misexpressed in FSHD myoblasts and patient biopsies is *DUX4*, a retrogene exclusive to Old World Primates. Although located within each D4Z4 repeat unit, DUX4 is only transcribed from the last D4Z4 unit and its mRNA needs to be stabilized by splicing to a polyadenylation signal present only in a 4qA disease-permissive allele. *DUX4* encodes two different protein isoforms generated through

alternative mRNA splicing: a non-pathogenic short form, DUX4-s, that is often expressed in healthy somatic cells and a toxic full-length form DUX4-fl, which is expressed in muscle and other tissues during development and post development in testis, but silenced in healthy somatic cells (Figure 1.4). However even in FSHD myoblasts *in vitro* DUX4-fl is expressed at very low levels, around 1:1000 nuclei. DUX4-fl expression is shown to be cytotoxic in myoblasts and disrupts myotube formation *in vitro*. The current hypothesis is that DUX4-fl expression activates a network of DUX4 targets, including germline genes and immune modulators, and eventually causes muscle pathology. Nevertheless, recent large family cohort studies where many asymptomatic patients with detectable DUX4 expression were identified indicate other disease modulators may be important in FSHD manifestation.

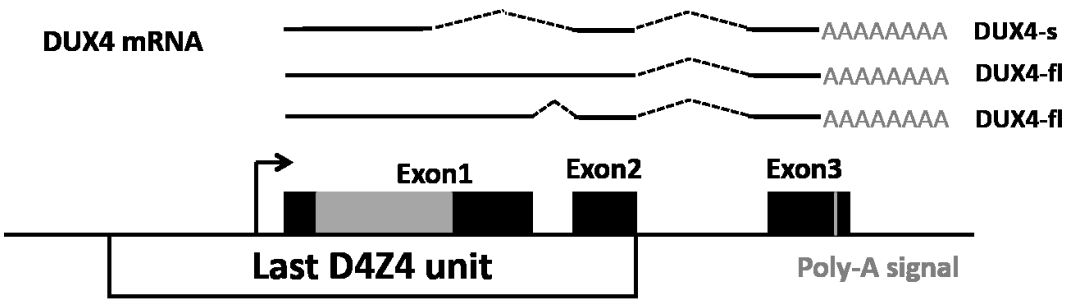

Figure 1.4. Alternate *DUX4* transcript splicing creates multiple isoforms.

Models for FSHD

Researchers have built various cell models to advance understanding of this complex disease. Experiments over-expressing DUX4-fl in various cell types with plasmid or viral constructs showed DUX4 is a transcription factor that can turn on a panel of downstream targets. Transfection studies expressing DUX4 in cell lines showed

that DUX4 transcripts and protein localize to the nucleus and are directly toxic to cells leading to apoptosis. DUX4 expression can also inhibit myogenesis (21-24).

In primary myoblasts derived from FSHD patient muscle, it is found that DUX4 was expressed at low levels, being found in approximately 1 out of every 1,000 nuclei, and has a curious pattern of being expressed in a gradient in aligned nuclei as shown in Figure 1.5 (25). In addition, the nuclei that showed abundant expression of DUX4 also showed changes consistent with DUX4-mediated toxicity, including nuclear aggregation of DUX4 protein and apoptosis (26). Transcriptomic analyses in human and mouse cells in response to ectopic DUX4 expression demonstrated that DUX4 regulates human and mouse transcriptomes differentially; specifically inflammation, BMP signaling and NRF-2 mediated oxidative stress are the top three affected pathways in human muscle cells while p53 signaling, cell cycle regulation and cellular energy metabolism are the top hits in mouse C2C12 cells (27).

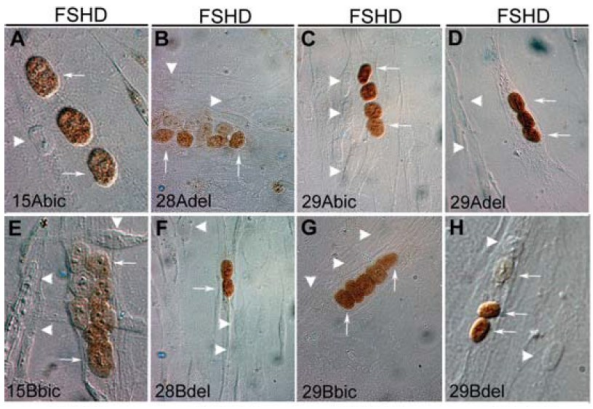

Figure 1.5 DUX4 immunostaining in primary myotube culture derived from FSHD patient biopsy (25).

Animal models are essential to study potential disease mechanisms, to identify therapeutic targets, and eventually to test potential therapeutic strategies. However, the complexity of the disorder and the underlying uncertainty about the pathogenesis make FSHD a challenging disorder for the creation of animal models. Even the near-consensus causal gene *DUX4* is only found in Old World primates and not in any common laboratory animal species (28), which eliminates the possibility of having a 'natural' model of disease like the mdx mouse and GRMD dog models for DMD (Duchenne muscular dystrophy) (29). Additionally, the extremely low level of DUX4 expression in FSHD patient cells and biopsies highlights yet another challenge to create a model where DUX4 expression is near the physiological level found in patients. Furthermore, emerging evidence indicates other modifier genes may be essential for disease manifestation as studies identify DUX4 expression in non-manifesting patients.

Zebrafish are considered an ideal model organism to study the vertebrate muscle development because of the ease of visualization of muscle abnormalities (30). Mitsuhashi *et al*. created a DUX4 zebrafish model by directly injecting *DUX4-fl* mRNA at the one-cell stage of embryogenesis, which resulted in embryonic lethality at high dosage. Nevertheless, at low levels *DUX4* mRNA induced disorganization of muscle structure, asymmetric abnormality of the eyes and fins, and disrupted swimming patterns, indicating the zebrafish model may be helpful in high-throughput screening of potential therapeutics in current medical chemistry libraries by assaying birefringence and swim pattern (31).

Researchers have been working on creating a mouse model for FSHD, but the fact that DUX4 and a number of DUX4-fl gene targets are primate specific presents a big

challenge. The first mouse model was created by Wallace *et al*. by intra-muscular injection of DUX4-overexpressing adeno-associated virus type 6 (AAV6). As DUX4 expression is detected one week post-injection, significant muscle damage was presented by degenerating myofibers and infiltrating mononuclear cells and positive staining of apoptosis markers, indicating DUX4 toxicity *in vivo.* They also demonstrated this myopathic effect is p53 dependent (32). Recently, researchers attempted to insert the *DUX4*-containing human D4Z4 locus to the mouse genome to create a transgenic mouse model. Krom *et al*. integrated an FSHD contraction including 2.5 D4Z4 repeats on a permissive haplotype background (termed D4Z4-2.5 mouse), while also generating a control mouse with 12.5 D4Z4 repeats representing the normal size in healthy humans (33). Even though DUX4 transcript expression is detected in multiple muscle groups in the D4Z4-2.5 mice, no muscle weakness or wasting was observed, nor were abnormalities in morphology or histology. The only phenotype is keratitis detected at 8-12 weeks. Despite the recapitulation of the FSHD hypomethylation epigenetics and sporadic DUX4 expressing genetics, the lack of relevant pathology indicates other players in FSHD pathogenesis.

Overall there is not an accepted animal model of FSHD, which has had a direct negative impact on therapeutic development for FSHD: there have been very few clinical trials. For other neuromuscular diseases, such as Amyotrophic Lateral Sclerosis (ALS) and DMD which have mouse models (SOD1G93A and mdx) there are dozens of ongoing trials. Because of this, my work has aimed to create a novel animal model using affected human muscle.

Xenograft model

Primary xenograft models have become widespread in the study of various cancers and development of novel chemotherapeutics (34-36). In these models, patient tumor cells are typically dissociated and injected into the subcutaneous space or the flank of mice to determine if the human tumor will respond to a specific therapeutic regime. Such human tumor xenografts have led to the successful development of effective treatments for common cancers including multiple myeloma, as well as personalized therapeutic approaches for individual patients. For example, the efficacy of Velcade and Melphalan was first demonstrated in xenografts and are now used as standard of care in multiple myeloma (37, 38).

Human muscle xenografts have previously been attempted only from dissociated cells. Several laboratories have injured and/or irradiated the legs of mice and injected human muscle progenitor cells. The engraftment of human muscle cells in these studies is not high, and tends to be largely perifascicular (39, 40). In addition, this technique also leads to a high rate of human-mouse hybrid myofibers because it is highly difficult to eliminate all mouse myoblasts from the graft area.

The abundance of stem cells in skeletal muscle makes a tissue based xenograft possible. Satellite cells, which account for ~2–6% of the nuclei in adult skeletal muscle, are the main source of stem cells for repair of postnatal skeletal muscle through regenerative myogenesis, induced by muscle wear-and-tear, injury, or disease-related atrophy (41). During regeneration, satellite cells are induced to proliferate and form myoblasts while also maintaining a pool of quiescent stem cells. The activated myoblasts

then differentiate and fuse with the damaged myofiber or with other myoblasts to form multinucleated myotubes, regenerating functional muscle.

Researchers have experimented with free muscle grafts in multiple animal models in the past, where a piece of muscle is excised from its original site by both tendons and transplanted into another site within the same animal. Collins et al. isolated single myofibers with their associated satellite cells and transplanted into the muscles of radiation-ablated muscles of an mdx host (42). They showed the great myogenic potential of satellite cells in a single fiber in that one myofiber can produce sufficient differentiation-competent progeny to generate thousands of myonuclei (Figure 1.6).

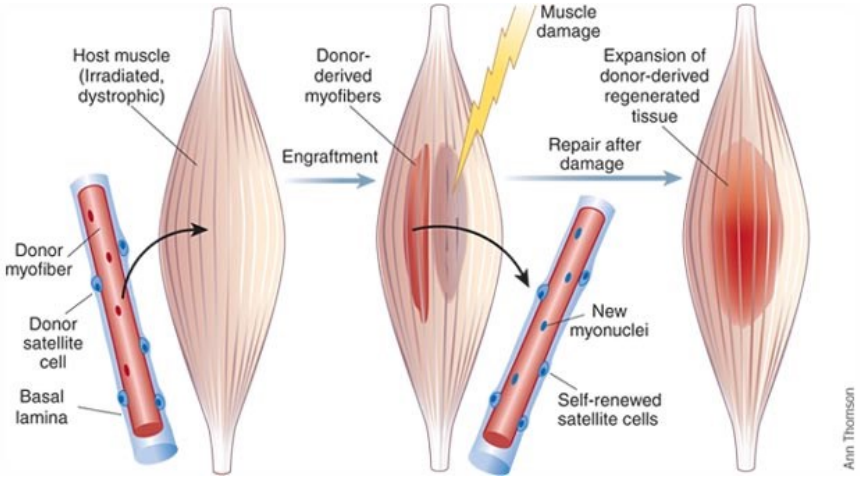

Figure 1.6 Myogenic Potential of Satellite Cells in Single Myofiber Grafts. (41)

Summary

A tissue-based xenograft model for human muscle disorders, depicted in Figure 1.7, has many advantages. Specifically for FSHD, these include that the graft features the

complex genetic and epigenetic abnormality that exists in the human disease which may never be reproducible in a genetically engineered mouse model. Additionally, the actual human tissue response to drugs that can be studied in these mice will more likely translate to patients. There are also disadvantages, including labor intensive nature of creating individual mice, limitations from the availability of FSHD muscle and the inability to study whole animal function. In the next two chapters, I will demonstrate the both feasibility and functionality of such a model.

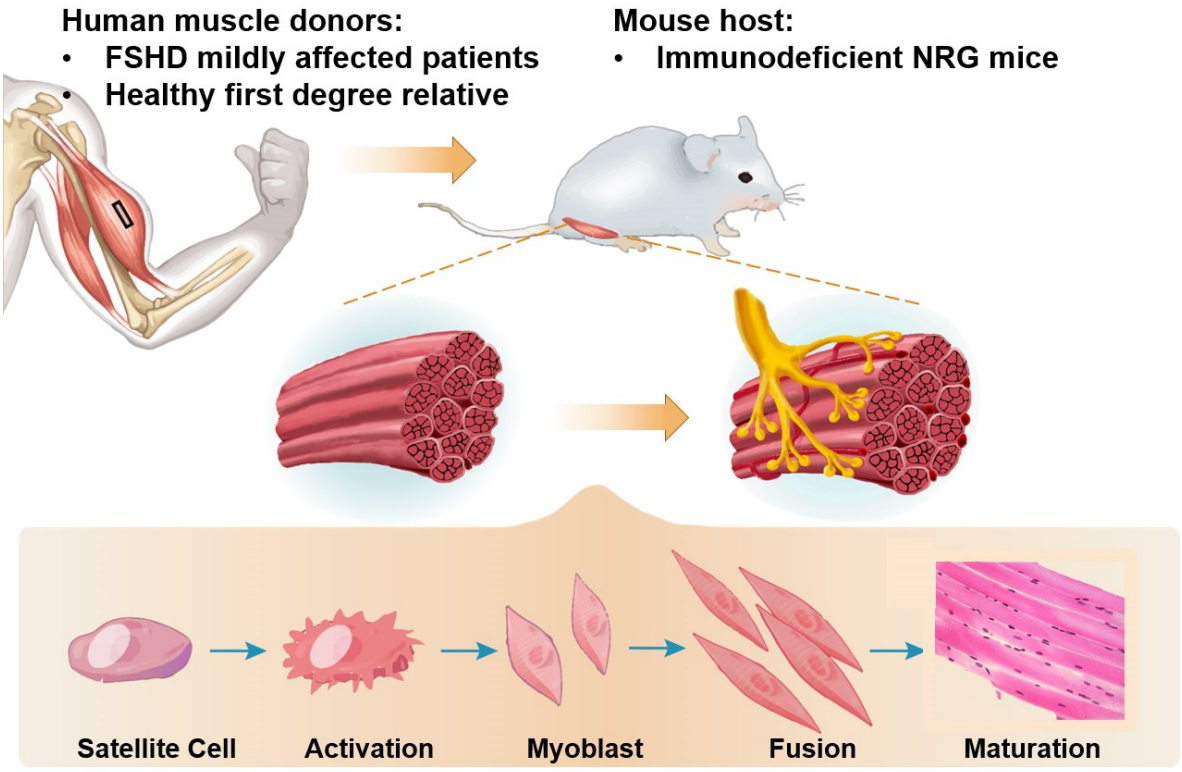

Figure 1.7. Summary of the xenograft concept for modeling human skeletal muscle disease in mouse.

Chapter 2. Human skeletal muscle xenograft as a new preclinical model for muscle disorders

Yuanfan Zhang, Oliver D. King, Fedik Rahimov, Takako I. Jones, Christopher W. Ward, Jaclyn P. Kerr, Naili Liu, Charles P. Emerson, Jr, Louis M. Kunkel, Terence A. Partridge, and Kathryn R. Wagner. Human skeletal muscle xenograft as a new preclinical model for muscle disorders. Hum. Mol. Genet. (2014) 23 (12): 3180-3188.

Abstract

Development of novel therapeutics requires good animal models of disease. Disorders for which good animal models do not exist have very few drugs in development or clinical trial. Even where there are accepted, albeit imperfect models, the leap from promising preclinical drug results to positive clinical trials commonly fails, including in disorders of skeletal muscle. The main alternative model for early drug development, tissue culture, lacks both the architecture and, usually, the metabolic fidelity of the normal tissue in vivo. Herein, we demonstrate the feasibility and validity of human to mouse xenografts as a preclinical model of myopathy. Human skeletal muscle biopsies transplanted into the anterior tibial compartment of the hindlimbs of NOD-Rag1null IL2rγnull immunodeficient host mice regenerate new vascularized and innervated myofibers from human myogenic precursor cells. The grafts exhibit contractile and calcium release behavior, characteristic of functional muscle tissue. The validity of the human graft as a model of facioscapulohumeral muscular dystrophy is demonstrated in disease biomarker studies, showing that gene expression profiles of xenografts mirror those of the fresh donor biopsies. These findings illustrate the value of a new experimental model of muscle disease, the human muscle xenograft in mice, as a feasible and valid preclinical tool to better investigate the pathogenesis of human genetic myopathies and to more accurately predict their response to novel therapeutics.

Introduction

Animal models of myopathy are an important feature of the development of novel therapies for humans. Of these, the mouse is certainly the most convenient and popular mammalian model. However, mouse models for many human diseases such as Duchenne muscular dystrophy (DMD) are frequently criticized for their limitations, especially the lack of translation from positive preclinical studies to positive clinical trial (43, 44). As a notable example, the only drugs proven in randomized, placebo-controlled, clinical trials to benefit boys with DMD are glucocorticosteroids, which do not improve the condition of the murine mdx model in long term studies (45-47). Despite this, preclinical efficacy testing in animal models remains a near obligatory requirement in industry and academia for neuromuscular diseases prior to clinical trials. For several complex and rare neuromuscular disorders, there is no accepted animal model, a lack that has stymied therapeutic development.

Facioscapulohumeral muscular dystrophy (FSHD) is one such complex neuromuscular disorder affecting approximately 4-7 per 100,000 individuals (48). Weakness in the muscles of the face, scapular region, and arms typically begins in late adolescence and early adulthood; however, there is a range of severity from infant to late adult onset, loosely correlating to genotype. The disorder is relentlessly progressive, eventually affecting most skeletal muscles and resulting in the lack of ability to smile, to raise arms overhead, and to lift. Approximately one third of patients with FSHD lose the ability to ambulate.

The pathogenesis of FSHD has remained elusive. The disease is due to a loss of macrosatellite repeats on chromosome 4q (49, 50). Within this region, there are 3.3 kb

hypermethylated repetitive DNA segments termed D4Z4 repeats. Unaffected people have >100 copies of D4Z4 units, while those with FSHD have 1-10 units (51). Although the genetics and pathophysiology are yet to be fully elucidated, the chromosome 4q deletion, when it occurs in the appropriate context, appears to lead to the misexpression of a transcription factor DUX4-fl, which in turn activates a number of other genes (23, 52, 53). Due to the complexity of this epigenetic disorder, there is no accepted animal model of FSHD that recapitulates the disease, and there are no current ongoing clinical trials in the disorder.

In cancer research, xenografts of human tumors in immunocompromised mice have been used successfully to predict their clinical response to therapeutic drugs (54, 55). Previous attempts to use xenografts to model muscle disease by injecting dissociated human myoblasts into injured mouse muscle have produced low engraftment of human cells, mainly in a perifascicular position (39, 56-58). However, grafts of whole muscle from the mdx mouse placed into normal mice retained the dystrophic phenotype of the donor mouse (59). This finding encouraged us to investigate whether human muscle could be similarly grafted into immunodeficient mice and recapitulate key features of normal and diseased human muscle for preclinical therapeutic studies.

Results

Regeneration of human skeletal muscle in immunodeficient mice

Human volunteers donated biceps muscle specimens through a protocol approved by the Johns Hopkins Medicine Institutional Review Board. The donor muscle was trimmed and transplanted into the anterior compartment of the hindlimbs of immunodeficient NOD-*Rag1*^{null}*IL2r*γ^{null} mice in place of the host tibialis anterior and extensor digitorum longus muscles and sutured to the proximal and distal tendons of the peroneus longus as

described in Methods (see Supplementary Fig. 1). Such grafts were spontaneously vascularized and survived through 36 weeks post-transplantation (Fig. 2.1A). Myofibers of donor muscle degenerated and nascent fibers regenerated within the existing basal lamina of the donor specimen (Fig. 2.1B-E). Regenerated fibers showed the predominant peripheral relocation of nuclei characteristic of human but not murine muscle regeneration(60) (55 $\pm$ 3% central nucleated fibers at day 14 versus 21 $\pm$ 3% central nucleated fibers at day 140, mean $\pm$ sd, n = 3 for each, $p<0.001$ by two-tailed t-test). Beyond 90 days post transplantation, grafts were fully regenerated with predominantly peripheral nuclei and stable average cross sectional areas (CSA) approximately one half that of myofibers in the donor biopsy from which they originated (1348 $\pm$ 966 μm2 versus 3382 $\pm$ 945 μm2, mean $\pm$ sd) (Fig. 2.1F).

Xenografts were composed entirely of myofibers uniformly expressing human membrane proteins such as spectrin (Fig. 2.2A). Multi-labeling immunohistochemistry (see Methods and Supplementary Fig. 2.2) was used to identify total human nuclei, human myonuclei and human myogenic precursor cells, satellite cells. Within the xenograft area as defined by positive anti-human spectrin reactivity, 91.4 ± 3.4% of all nuclei, 95.2 ± 3.2% of all myonuclei and 90.2 ± 4.0% of all satellite cells were human (mean $\pm$ sd),(Fig. 2.2B). Capillaries within the xenograft were both human and mouse in origin with some appearing to be anastomoses of human and mouse capillaries (Fig. 2.2C). Mouse erythrocytes within capillaries indicate patency of the human vasculature within the xenograft (Fig 2.2D).

Functional competency of skeletal muscle xenografts

Having established the xenograft as a feasible model of human muscle, containing predominantly human myofibers and nuclei, we sought evidence of functional competence. As described in Methods, the graft of human biopsy sample was sutured to the peroneus longus muscle overlying a branch of the peroneal nerve (freed after tibialis resection). Figures 2.3A and 2.3B reveal neuromuscular junctions (NMJs) in cryosections of xenografts indicating innervation of the xenograft. Furthermore, the presence of both type 1 and type 2 fibers (Fig. 2.3C) indicate re-innervation by more than one motor neuron.

While the graft is innervated, *in situ* or *in vivo* assessment of xenograft function could not be technically differentiated from function of the host peroneus longus to which it was sutured. Graft specific contractility was assessed in explanted xenografts *in vitro* with trains of action potentials (APs) delivered with increasing frequency (i.e. force frequency response) (61-63). The xenograft exhibited a steep force frequency response indicative of functionally competent muscle (Fig. 2.4A and 2.4B). Functional assessments were also made on intact, single myofibers enzymatically isolated from xenografts and verified as human in origin (Fig. 2.4C) (62, 64). Myofibers were loaded with the Ca^{2+} indicator dye Indo-1-PE and stimulated to contract with electrical field pulses. The presence of robust responses to brief single pulses or tetanic trains of pulses (Fig. 2.4D and 2.4E) indicate a fully competent excitation-contraction (EC) coupling system in these fibers.

A xenograft model of Facioscapulohumeral muscular dystrophy

To test the suitability of the xenograft as a model for muscle disease, we grafted mildly weak muscle from subjects with FSHD into the anterior compartment of NOD-

Rag1^{null}*IL2rγ*^{null} host mice**.** Biceps muscle was donated from families (cohort numbers 29, 30, 33 and 37) with affected (indicated by letters, "A", "B" or "C") and unaffected (indicated by letter "U") members to serve as close genetic controls(65). Muscle from FSHD individuals, as well as unaffected family members, regenerated in immunodeficient mice (Fig. 2.5A). DUX4-fl expression, assayed by nested RT-PCR, was detected in xenografts which originated from FSHD affected muscle donors but not in xenografts which originated from control unaffected donors (Fig. 2.5B).

We next assessed whether the gene expression differences between FSHD and control biopsies were also present in FSHD versus control xenografts. Probably because they have passed through a round of degeneration and regeneration, grafted muscles showed not-unexpectedly different baseline gene expression levels from human biopsies. However, the ordinal levels of expression of FSHD and control biopsies are concordant with those observed between FSHD and control xenografts derived from these biopsies. These comparisons were made between xenografts derived from 5 individuals from 2 families (see Methods). We measured expression levels for a panel of 25 genes in 22 xenograft samples, and the 5 human biopsies of origin with real-time quantitative PCR (qPCR). This panel consisted of: 15 genes identified as differentially expressed in a microarray study of FSHD versus control biopsies(66), 8 genes (*MBD3L5*, *PRAMEF1*, *PRAMEF6*, *SLC34A2*, *SPRYD5, TRIM43*, *TRIM49*, *ZSCAN4*) that are dramatically upregulated by ectopic overexpression of DUX4-fl in cell-cultures(67), and *PPIA* and *GUSB*, which were used for normalization.

Expression differences in FSHD versus control xenografts were compared with the differences between the FSHD and control biopsies from which they had been

derived; this was performed separately for three pairs of affected and unaffected individuals within a family (Supplementary Fig. 2.3). In each case, the $\log_2$(fold-changes) for FSHD vs. control of the xenografts was strongly concordant with those of their biopsies of origin (Pearson correlation 0.63, 0.89, 0.66 respectively; $p < 0.001$ for each). For two of the three comparisons, there was a significant agreement in the direction of the changes (i.e., the sign of the $\log_2$(fold-changes); $p = 0.07$, $p = 0.002$, $p = 0.0004$ respectively by Fisher's exact test). Most of the genes with discordant direction of change had $\log_2$(fold-changes) close to zero. The consistency of the relationship between biopsy and xenograft is epitomized by the finding that the strong upregulation of *MYH8* reported in a larger FSHD collection(66) was not seen in either the biopsy, or the corresponding xenografts of FSHD individuals 33A and37B, but was seen for both the biopsy and xenografts of 33C (Fig. 2.5D and Supplementary Fig. 2.3).

Although the xenografts in the gene expression analysis were derived from a small population of biopsies (3 FSHD and 2 control), it is encouraging that the differences in FSHD versus control samples from the pooled xenografts not only have good agreement with the differences between the pooled biopsies from which they were derived (Fig. 2.5C; Pearson correlation 0.87; p =2e-08 for correlation test; p = 0.003 for agreement in direction of changes by Fisher's exact test), but also reflect the FSHD-related differences reported in larger populations of unrelated samples: upregulation of *MYH8* (albeit mild, for the reasons discussed above) and downregulation of *EXTL1*, *G0S2*, *GLT25D2*, *IDI2*, and *TECRL* (66), and upregulation of the DUX4-induced genes *MBD3L5*, *PRAMEF1*, *PRAMEF6*, *SLC34A2*, *SPRYD5, TRIM43*, *TRIM49*, and *ZSCAN4(67)*. Figure 2.5D highlights the genes with the strongest down-regulation and

up-regulation in the pooled FSHD versus control biopsies (*EXTL1* and *TRIM49*) and xenografts (*IDI2* and *ZSCAN4*), excluding those genes that were not detected in all samples.

Autopsy skeletal muscle specimens as donors for xenografting

Recognizing that many laboratories will not have easy access to fresh muscle biopsy tissues, we evaluated whether autopsy material could be similarly used as donor muscle. Autopsy material from the biceps of an octogenarian with FSHD was transplanted into immunodeficient mice approximately 48 hours after death of the donor. This autopsy specimen, which was neither ideal in age of donor nor time from death to transplantation, regenerated well in the NOD-*Rag1*^{null} *IL2rγ*^{null} host. Since satellite cells have been shown to survive for many days in postmortem muscle (68) this new model might be easily generated by other laboratories (Supplementary Fig. 2.4).

Discussion

Our results establish the feasibility of grafting human muscle into immunocompromised mice, where it regenerates, becomes innervated, and displays functional contractility. The grafted muscle retains human characteristics including the peripheral migration of centralized nuclei during regeneration. The xenograft may, therefore, provide a unique opportunity to study human muscle regeneration over time with a degree of access and invasive experimental scrutiny that is not available in human subjects. A limitation of the model in this regard is the requisite immunodeficiency of

the host mice, in our study NOD-*Rag1*^{null} *IL2rγ*^{null} , which lack functional T cells, B cells, and Natural Killer cells (69). More directly important to muscle regeneration than lymphocytes, however, are macrophages that in NOD-*Rag1*^{null} *IL2rγ*^{null} appear to be present, although reduced in number (69).

For muscular dystrophies without animal models, or with suboptimal animal models –which is true to some extent with all of them – the human muscle xenograft will be a useful new preclinical tool. FSHD is a complex genetic disorder for which the relative lack of clinical trials is attributable in part to the absence of an accepted mouse model for preclinical testing. Each of the proposed animal models of FSHD has its own distinct strengths and weakness. One early mouse model transgenically overexpressed FRG1, which previous studies had shown was increased in expression in FSHD patient derived muscle biopsies (15). Although the model exhibits skeletal muscle pathology, the failure of subsequent studies of muscle biopsies from FSHD individuals to replicate the misexpression of FRG1 (66, 70) raises questions about the validity of this mouse. Conditional expression of DUX4 in zebrafish produces an intriguing constellation of eye, ear, and muscle abnormalities reminiscent of FSHD (71), however a conditional model of DUX4 expression in mice is not yet available in that constitutive expression of DUX4 is toxic to cells (72, 73). More recently, a mouse model has been developed carrying the FSHD permissive subtelomeric region and demonstrating DUX4 transcripts in multiple tissues including skeletal muscle (33). This will be a useful model to study de-repression of DUX4, but as the lack of muscle pathology in this model suggests, it may not be as helpful in studying pathogenesis downstream from DUX4, which necessarily depends on mouse genes. The xenograft model described in this paper also has limitations; namely,

an inability to assess whole animal function such as grip strength or treadmill endurance. Since the xenograft expresses genes mirroring the human muscle from which it originated, we anticipate that it will be especially useful for studies with molecular outcomes (such as gene replacement or silencing studies).

In general, for detailed cell and molecular biology investigation of human muscle, investigators have resorted heavily to tissue culture for short-term ex-vivo maintenance of human muscle. However, even superficial assessment tells us that this is remote in many ways from functional muscle in vivo. At the molecular level, too, tissue culture can be deceptive. For example exon skipping studies in the dystrophic GRMD dog and the mdx mouse reveal that data from tissue cultures do not provide a reliable guide to in vivo behavior (74, 75). The graft procedure we have described here should not only be applicable to genetic diseases of muscle for which we lack suitable animal models but should also hold promise for gaining a more detailed understanding of a number of acquired muscle conditions. The vigor of regeneration of our autopsy graft from an octogenarian donor opens new avenues into the study of the effects of age and disease on the innate regenerative and growth capacity of human skeletal muscle.

Materials and Methods

Human muscle acquisition

This study was approved by The Johns Hopkins School of Medicine Institutional Review Board. Subjects with FSHD and their first degree unaffected relatives, were recruited and screened for biomaterial contributions. Subjects had their FSHD genetic status confirmed by the University of Iowa Diagnostic Laboratories by pulse-field gel electrophoresis (PFGE) and Southern blotting as previously described (65). Subjects were categorized as "affected" (and labeled "A", "B" or "C") if they had contraction of the D4Z4 array (fewer than 11 repetitive units) associated with the 4qA allele and "unaffected" (and labeled "U") if they had no contraction. Open muscle biopsy was performed on biceps muscles having strength greater than 4- out of 5 (MRC scale). A portion of the harvested tissue was dissected into several small strips of longitudinal fibers approximately 1 cm long and taken immediately to the animal suite for xenografting.

Surgical procedure

The Institutional Animal Care and Use Committee at the Johns Hopkins University School of Medicine approved the animal and surgical procedures performed in this study. Female NOD.Cg-*Rag1*^{tm1Mom} *Il2rg*^{tm1Wjl}/SzJ immunodeficient mice (The Jackson Laboratory) were used for this study. Donor human muscle was trimmed to 8 mm x 3 mm x 1 mm strips. Host mice were anaesthetized with isofluorane. The tibialis anterior and extensor digitorum longus were removed from the anterior tibial compartment. The neurovascular bundle was severed leaving maximal length. A strip of human muscle was placed in the empty anterior compartment and ligated with nonabsorbable suture (6/0

POLYPRO, CP medical) to the tendons of the peroneus longus. Skin was closed with surgical glue (Histoacryl, B. Braun) and stainless steel wound clips (Reflex Wound Clips, CellPoint Scientific). Rimadyl 5mg/kg was given subcutaneously after the surgery for pain control.

Immunohistochemistry and morphometric analysis

Mice were sacrificed at a variety of time points up to 36 weeks post transplantation. The graft was harvested with the entire mouse lower limb, frozen, and serially sectioned as previously described (76). Ten micron cryosections were stained with H&E or processed for immunohistochemistry. Ice-cold methanol fixed sections were blocked with anti-mouse IgG (MKB-2213, Vector Laboratories). The primary antibodies used were anti-human spectrin (NCL-SPEC1, Leica, 1:50), anti-human collagen IV (M3F7, DSHB, 1:50), anti-human lamin A/C (Ab40567, AbCam, 1:200), anti-synaptic vesicle 2 (SV2, DSHB, 1:50), anti- type I myosin heavy chain (A4.840, DSHB, 1:50), anti-type II myosin heavy chain (A4.74, DSHB, 1:50), anti-human CD31 (M0823, DAKO, 1:20), anti-mouse CD31 (550274, BD, 1:50), anti-mouse TER-119 (550565, BD, 1:50), anti-human laminin (2E8, DSHB, 1:100), anti-Pax7 (PAX7, DSHB, 1:10). The secondary antibodies used were AlexaFluor 488 goat anti-mouse IgG1, AlexaFluor 594 goat anti-mouse IgG2b, AlexaFluor 647 goat anti-mouse IgM and AlexaFluor 594 goat anti-rat IgG (all Invitrogen, 1:500). Tetramethylrhodamine α-Bungarotoxin (T-1175, Invitrogen, 1:50) was used for detecting postsynaptic membranes. All nuclei were labeled with DAPI in mounting medium (P36930, Invitrogen). Image capture was performed using an upright microscope for brightfield, DIC, and epifluorescence with apotome structured illumination digital imaging system (Zeiss). The image stacks consisted of 6 optical

sections with 1.4-μm Z-steps. Nuclei staining positive for DAPI but outside anti-human laminin were considered interstitial cells while those inside laminin were considered myonuclei. Satellite cells were identified by Pax7+ staining within anti-human laminin staining. Muscle fiber cross-sectional areas were determined by using Scio Image Software (NIH) on anti-human spectrin stained sections as previously described(77). Central nucleated fibers were counted in anti-human spectrin and lamin A/C positive regions as previously described(78).

In vitro functional assessment

Grafts were carefully dissected away from the mouse peroneus longus muscle belly and affixed at the suture sites. Following equilibration, the force vs. frequency relationship was evaluated as previously described (61). Peak isometric tension was normalized to the calculated cross-sectional-area using the length (mm) and mass (mg) of the muscle between the sutures.

Single intact myofibers were enzymatically isolated from the xenograft using Collagenase A (Roche) in DMEM and adhered to glass-bottom imaging dishes as described previously (61, 64, 79). Myofibers were loaded with the dual emission, ratiometric, fluorescent Ca^{2+} indicator, Indo-1 PE AM (5 μM in 20% pluronic/DMSO), for 45 min in a normal rodent Ringer (in mM: 140 NaCl, 4 KCl, 1.8 CaCl, 1 $MgSO_4$, 5 NaHCO3, 10 HEPES, 5 glucose, pH 7.4). Dishes were washed and incubated for 30 min in Ringer to allow Indo-1 deesterification. Myofibers were imaged on an IonOptix dual PMT imaging platform mounted to an IX-70 inverted fluorescence microscope (40x

water UV objective) equipped with a Sutter DG-4 excitation source (excitation: 340+/- 10 nm). The Indo-1 PE emission ratio (emission: 405/485 nm, sampled at 1KHz) was taken as the estimate of myoplasmic Ca^{2+} concentration ($[Ca^{2+}]$). The Indo1 ratio was assessed in quiescent myofibers to determine the resting myoplasmic $[Ca^{2+}]$. Action potential induced fluorescent transients were elicited with brief (200μsec, square pulse) trains of pulses delivered at 10 or 100 Hz.

FSHD xenograft *DUX4*-fl expression

Total RNA was isolated from frozen muscle biopsy samples and xenografts using Trizol (Invitrogen) and RNeasy mini kit (Qiagen). DUX4-fl expression was determined using 100 ng of poly(A)+ cDNA by a nested reverse transcription polymerase chain reaction (RT-PCR) as described previously (25). PCR products were sequenced and specificity of reaction products was confirmed.

Gene expression analysis

High-throughput real-time qPCR was performed on the BioMark 96.96 Dynamic Array (Fluidigm) with TaqMan Gene Expression Assays (Applied Biosystems), as previously described (66). Gene expression analyses were done on xenografts derived from 5 individuals from 2 families: FSHD subjects 33A, 33C and control subject 33U from family 33 (previously reported (66)), and FSHD subject 37B and control subject 37U from family 37. There were six xenograft samples derived from the biceps of 33C, and four xenograft samples derived from the biceps of each of the other four individuals.

We tested whether the TaqMan primers for the 25 assayed human genes (assay IDs listed in Supplementary Table 1) were specific to human as opposed to mouse

mRNA by including two samples of tibialis anterior muscle from non-xenograft mice (TA1 and TA2). *CAB39L* and *OXCT1* were detected in these samples, with raw Cts (threshold cycles) 18 and 32 respectively, but the other 23 genes were not. The raw Cts for the xenograft mice averaged 15 for *CAB39L* and 17 for *OXCT1*. As the value for *OXCT1* in xenografts is 15 Ct lower (suggesting $2^{15} \approx 30{,}000$ times greater signal) than in the non-xenograft mice, the signal for it in xenografts should be largely from human mRNA. For *CAB39L,* the difference is ~3 Ct, so mouse mRNA levels may potentially partially mask differences in human mRNA levels in the xenografts.

Statistical Analysis

The raw Ct value for each gene for each sample was computed as the median value of the Cts from three technical qPCR replicates. These values are given in Supplementary Table 2. Sample names are in the top row: names with prefix "biop" are biopsies (biceps) from the indicated subject, those with prefix "xg" are xenografts derived from the indicated subject (with mouse index number and L/R leg as a suffix), and TA1 and TA2 are the non-xenograft mouse controls. ND indicates that the gene was not detected in the sample.

To account for differences in quantities of input RNA for each sample, and in the case of xenografts for differences in relative abundances of human vs. mouse RNA, raw Cts were normalized to ΔCt values by subtracting the mean Ct of *PPIA* and *GUSB,* which were previously identified as stable internal controls genes(66).

Estimates of $\log_2$(fold-changes) for FSHD/control comparisons would typically be computed as the mean ΔCt for control samples minus the mean ΔCt for FSHD samples, but because many of the DUX4-induced genes are near the qPCR detection threshold

(where the variance increases sharply and genes may not be detected in some samples) we first performed a variance-stabilizing transformation (vst) on the ΔCt values. Modeling the standard deviation as independent of the mean for ΔCt < 5 (corresponding roughly to raw Ct < 20) then increasing linearly by 25% of the baseline standard deviation per additional Ct, by the delta method the asymptotic variance-stabilizing transformation is given by $\text{vst}(x) = \int_{t=0}^{x} (1 + 0.25 \cdot \max\{t - 5, 0\})^{-1} dt$, so $\text{vst}(x) = x$ for $x \leq 5$ and $\text{vst}(x) = 5 + 4(\ln(x - 1) - \ln(4))$ for $x > 5$. To avoid infinite fold-changes, non-detected genes were assigned the value ΔCt = 25 (approx. 1 Ct higher than the highest value for any detected gene in any sample) prior to applying the vst; these genes are indicated by special symbols in Figure 5 and Supplementary Figure 3. The tests for significant differences between FSHD and control xenografts for individual genes used non-parametric Wilcoxon rank-sum tests, so were not affected by the monotonic vst or by the precise choice of value assigned to the non-detected genes, which are regarded as tied for having the highest Ct value. These tests used the function wilcox.exact in the R package exactRankTests, which allows for tied observations.

For the simple pairwise comparisons (33A vs. 33U, 33C vs. 33U, 37B vs. 37U), $\log_2$(fold-changes) were computed from mean values of variance-stabilized ΔCt values. For the pooled comparisons of all FSHD vs. all control, as there were differences in the number of individuals per family (three from family 33 and two from family 37) and the number of xenograft mice per individual (six for 33C; four for the others), we used mixed-effect models to compute the $\log_2$(fold-changes) from the variance-stabilized ΔCt values. For humans this model had a fixed effect for Class (FSHD vs. control) and a random effect for Family (model specification vst.values ~ Class + (1 | Family) in R

package lme4). For xenografts, the model also included blocking factors for replicate mice derived from the same individual (model specification vst.values ~ Class + (1 | Family) + (1+ Class | Individual)). Tests for agreement in direction of expression changes used Fisher's exact test (fisher.test in R, one tailed) on the 2×2 contingency tables of gene counts, with the sign of the $\log_2$(fold-change) in xenografts in one margin and the sign of the $\log_2$(fold-changes) in biopsies in the other margin. Genes were excluded if their $\log_2$(fold-change) was exactly zero in either margin, which happened only for genes that were detected in neither the FSHD nor the control samples.

Figures

Figure 2.1. Human muscle regenerates in immunodeficient NOD-Rag1null IL2rγnull mice. (A) Human muscle graft at 130 days post-transplantation into mouse hindlimb. Black sutures indicate ends of graft. (B) Hematoxylin and eosin (H&E) stained cross-section of original donor biceps biopsy. (C) H&E stained cross-section of human graft at 14 days post-transplant. Large myofibers continue to degenerate (arrow) and clusters of small myofibers regenerate (arrowhead and box) within original myofiber basal lamina (insert, anti-human spectrin in red, anti-human collagen IV in green). (D) H&E stained cross-section of human graft at 60 days demonstrating increasing size of grouped myofibers. Asterisk indicates neighboring host mouse muscle. (E) H&E stained cross-section of host hindlimb with fully regenerated human graft at 130 days. Graft within dotted lines. Asterisk indicates mouse muscle. Scale bars, 200 μm. (F) Histograms of cross sectional area (CSA) of myofibers from xenograft at 130 days (left) and donor muscle (right), n = 1300-1400 fibers each.

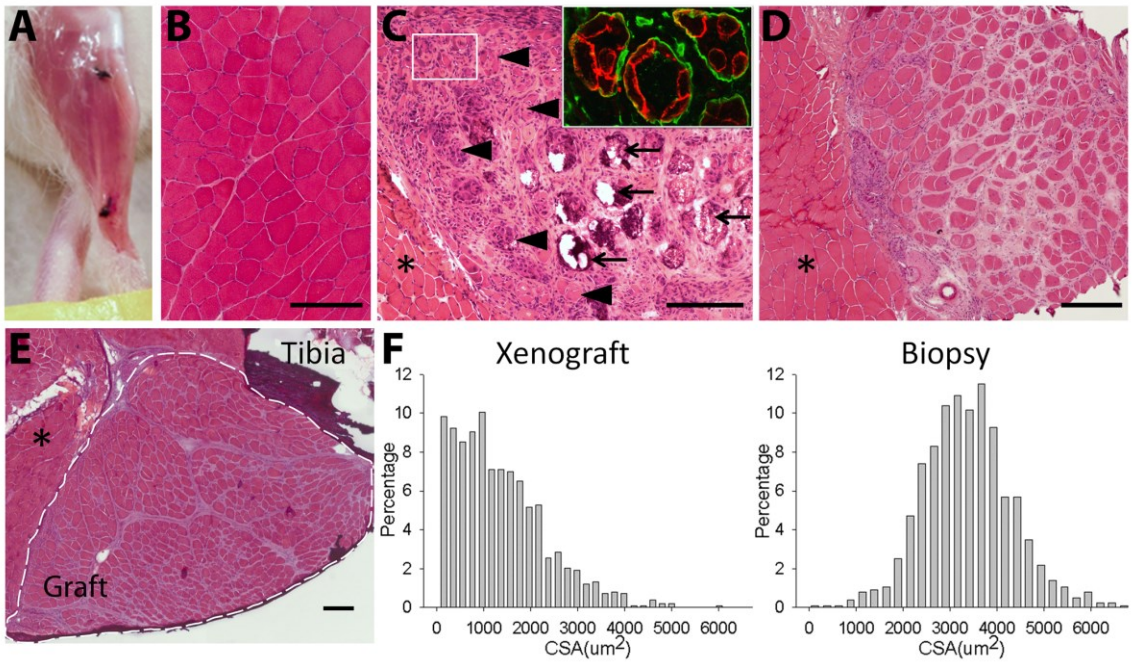

Figure 2.2. Skeletal muscle xenografts have human myofibers, nuclei and capillary immunoreactivity. (A) Anti-human spectrin antibodies (red) define discrete boundaries (insert) of xenograft (serial section of 1E) from neighboring mouse muscle (asterisk) and uniformly recognize myofiber membrane. Scale bar, 200 μm. (B) Within anti-human spectrin defined xenograft, 91.6 ± 5.3% of all nuclei (DAPI+), 92.4 ± 3.8% of myonuclei, and 90.1 ± 3.8% of Pax7+ satellite cells are human as recognized by anti-human lamin A/C. (n = 6). Data are shown as the mean ± sd. (C) Both human (green) and mouse (red) vascular networks were identified with species-specific CD31 antibodies, which appear to anastomose (insert). Scale bar, 200 μm. (D) Human capillaries (green) within the xenograft contain mouse erythroid cells identified with species-specific antibodies (red). Xenografts in these images are all 130 days post transplantation. Scale bar, 50 μm.

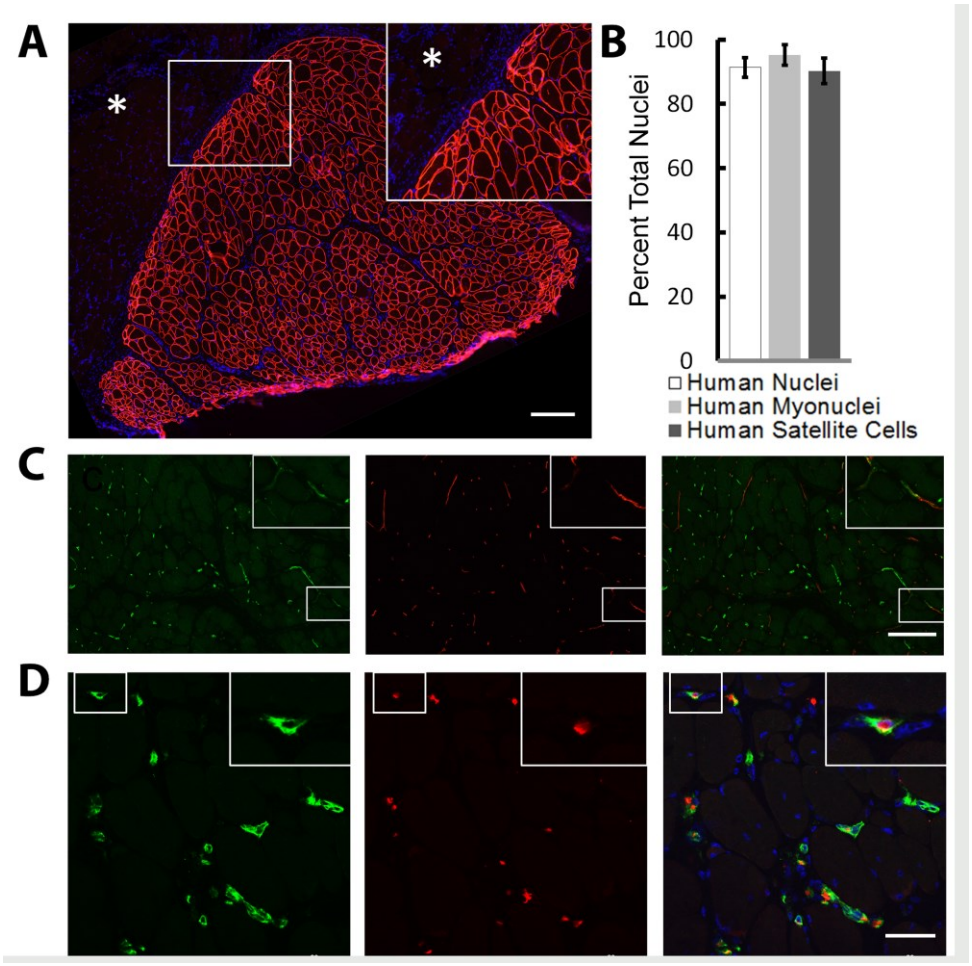

Figure 2.3. Xenografts are innervated. (A) Cross-section and (B) longitudinal section of 130-day xenografts demonstrate co-localization of presynaptic anti-SV2 reactivity (green) and postsynaptic α-bungarotoxin reactivity (red). Scale bars, 20 μm. (C) Immunohistochemistry demonstrates both type I (purple) and type II (green) myofibers in mature xenograft with a predominance of type I fibers. Asterisk indicates mouse muscle.

Scale bar, 200 µm.

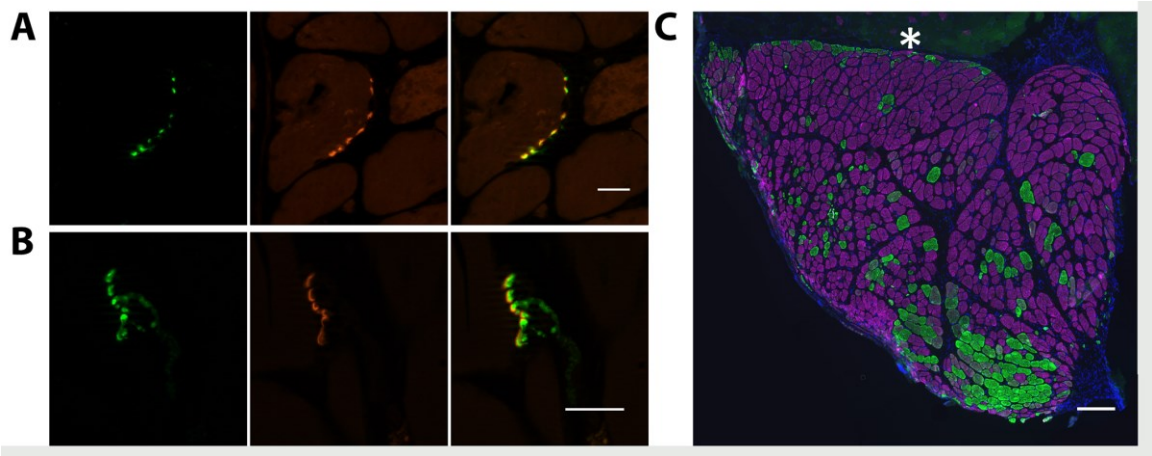

Figure 2.4. Xenografts are functionally competent. (A) Xenograft explants were suspended in a temperature-controlled, physiological saline contained bath and electrically-evoked force measurements were recorded with 250msec trains of pulses delivered between 1-300Hz. Representative isometric force traces are shown normalized to the calculated cross-sectional area of the xenograft. (B) Force-frequency relationship of aggregate data from 3 xenografts derived from 3 healthy donors. (C) Single enzymatically isolated myofiber from xenograft identified post-physiology as human with immunohistochemistry using anti-human spectrin (red), anti-human lamin A/C (green) antibodies and DAPI (blue). (D) Single myofibers were loaded with the ratiometric calcium (Ca^{2+}) dye Indo-1PE and electrically stimulated to elicit calcium transients. Representative twitch (single square 0.2usec square field pulses, black trace) or tetanic trains (100Hz, blue trace) are shown from fibers isolated from xenograft explants (n=3) of healthy donors. (E) Aggregate Ca^{2+} transient data (Box whisker plot; box = 5-95%; line = population median; whiskers = min/max).

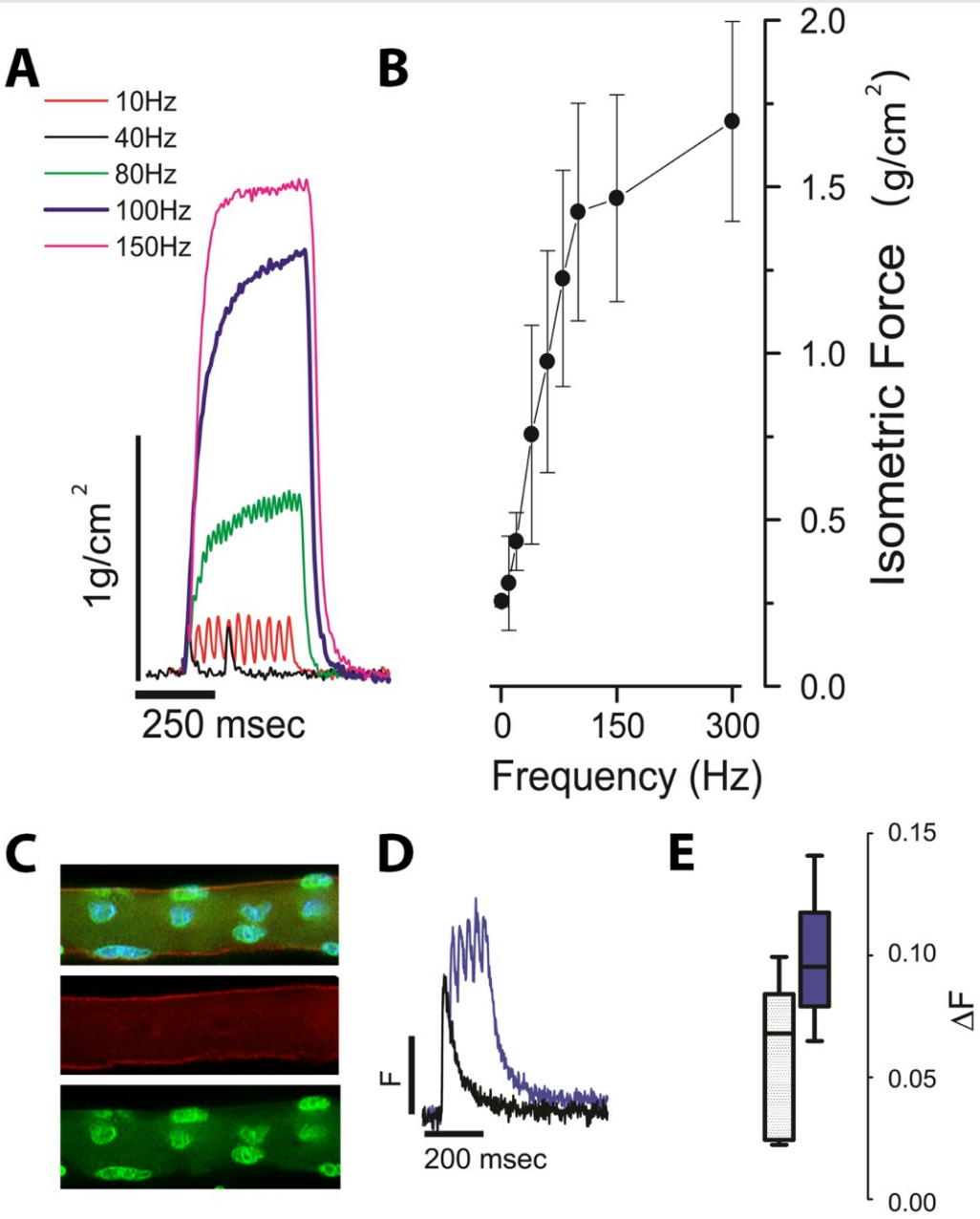

Figure 2.5. Validation of the model for FSHD. (A) H&E stained section (left) of FSHD xenograft next to host mouse peroneus (asterisk) at 140 days, human muscle fibers identified by anti-human spectrin (right, red). (B) DUX4-fl mRNA is specifically expressed in xenografts from FSHD muscle biopsies. Polyadenylated DUX4-fl mRNA expression was analyzed by RT-PCR in xenograft muscle originating from FSHD and

control biopsy. Expression of DUX4-fl mRNA in the original muscle biopsy specimen was similarly assayed by RT-PCR, and DUX4-fl mRNA expression in the 29A muscle biopsy was confirmed previously (25). All RT-PCRs were repeated at least three times. All products were sequenced to confirm the presence of spliced DUX4-fl mRNA (arrow) in samples from FSHD1 xenografts (29A, 30B, 37A and 37B) and FSHD1 biopsy (30B, 37A and 37B). RT–PCR for GAPDH mRNA expression controlled for integrity of the mRNA and first strand cDNA synthesis. (C and D) Expression differences between FSHD and control biopsies are correlated with expression differences in the xenografts derived from these biopsies. In (C), log2(fold-changes) for FSHD vs. control biopsies (horizontal axis) are plotted against the corresponding log2(fold-changes) for FSHD vs. control xenografts (vertical axis) for the 25 genes assayed by qPCR. For both axes positive values represent higher expression in FSHD samples than control samples. The log2(fold-changes) were fit using mixed-effect models on variance-stabilized normalized Ct values for 5 individuals (3 FHSD, 2 control) from 2 families, and 22 xenografts derived from these individuals (see Methods). The log2(fold-changes) for lowly expressed genes may be compressed due to the variance stabilization, and log2(fold-changes) should be regarded with particular caution for genes represented by triangles (not detected in at least one xenograft) and squares (not detected in at least one xenograft and at least one biopsy. Dashed black line: perfect agreement; dashed red line: best fit using orthogonal regression. In (D), ΔCt values are shown for five genes: TRIM49, ZSCAN4, EXTL1, IDI2, and MYH8. Each column represents a biopsy subject, with 33U repeated to clarify its relation to both 33A and 33C. Meanings of colors and symbols are defined in figure. Upward sloping lines indicate higher expression (lower ΔCt) in the

FSHD sample than the control. Solid and dashed lines between two subjects slope in the same direction when xenografts display the same direction of difference as the biopsies from which they were derived.

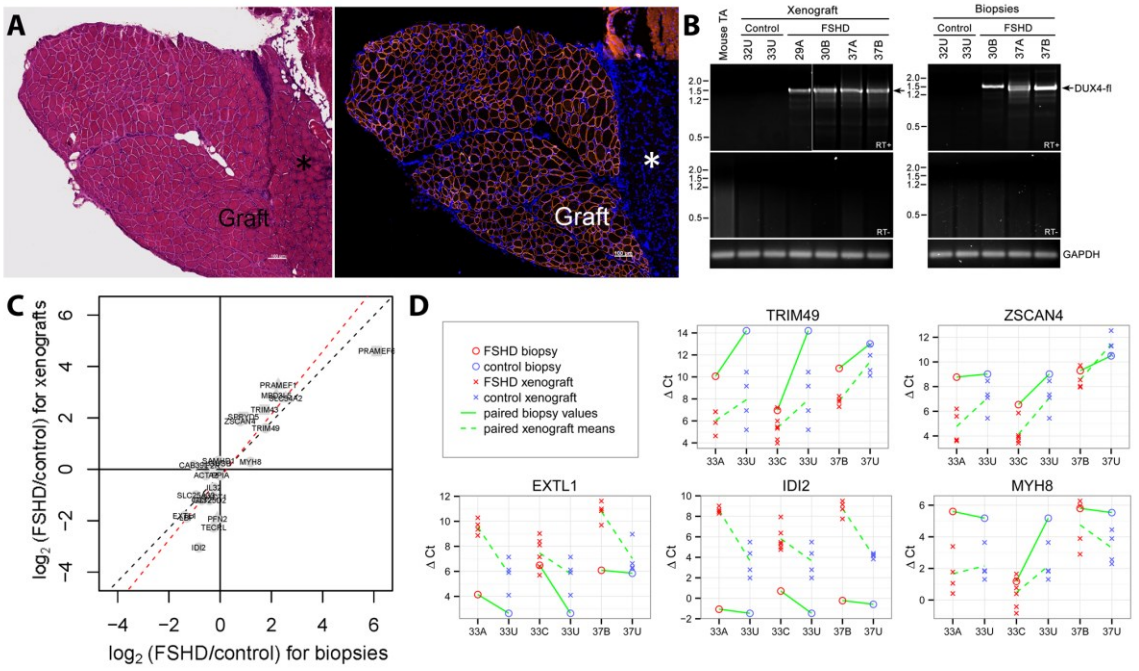

Supplementary Data

Figure S2.1. Human muscle transplanted to mouse limb: surgical procedure. (**A**) With the mouse hair removed on the lower hindlimb, and skin cleansed, an incision is made overlying the tibialis. (**B**) Graft site is created by complete excision of the host tibialis anterior and extensor digitorum longus. Sutures (shown proximally with black thread) are looped around the peroneus longus tendons. (**C**) Donor graft is implanted into the site and tied to the proximal and distal tendons of peroneus longus muscle. (**D**) The skin over the graft site is closed with surgical glue and later stapled.

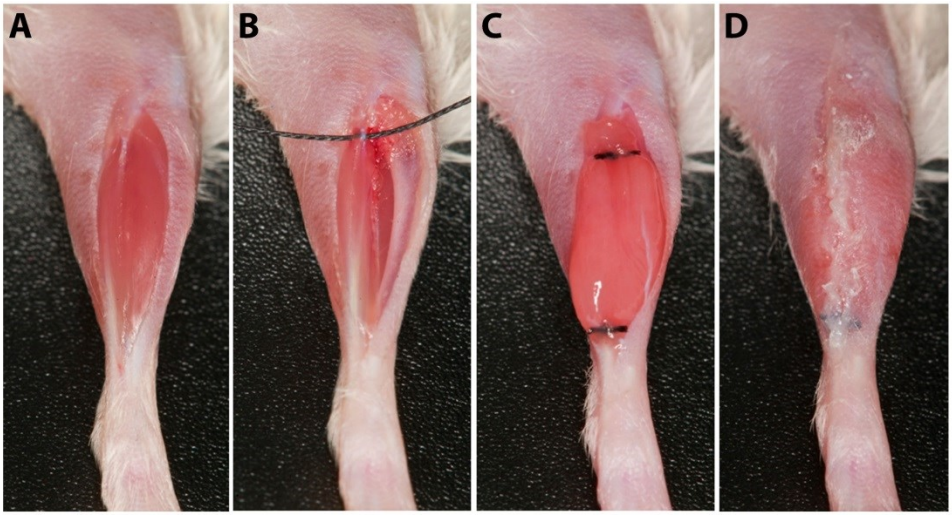

Figure S 2.2. Human muscle regenerates and survives through 41 weeks post-transplantation. (A) H&E staining of the xenograft harvested 41 weeks after transplantation. (B) Immunohistochemistry of a serial section with anti-human spectrin (red), anti-human lamin A/C (green) and DAPI (blue). Asterisk indicates host mouse muscle. Scale bar, 200 μm.

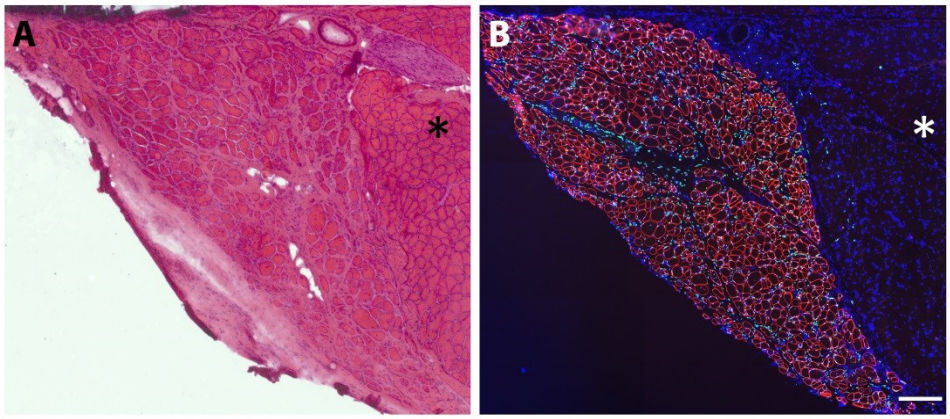

Figure S 2.3. Identification of various types of human nuclei in the xenograft by immunofluorescence. Immunohistochemistry of cross-section of xenograft 120 days post-

transplantation. (**A**) Anti-human lamin A/C identifies all human nuclei (red). (**B**) Anti-pax7 (green) identifies satellite cells. (**C**) Anti-human laminin identifies basal lamina (purple). (**D**) Merge image with DAPI (blue). Three types of human nuclei can be identified: myonuclei (★), satellite cells (⬅) and interstitial cells (◄). Scale bar, 10 μm.

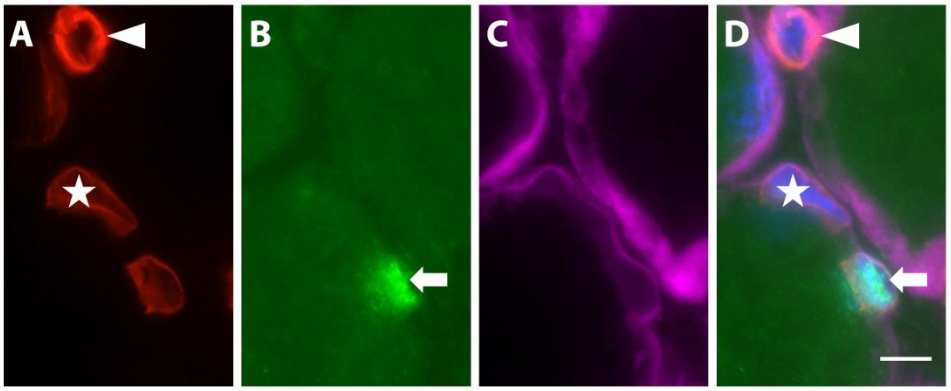

Figure S2.4. Pairwise expression differences between FSHD and control biopsies are correlated with expression differences in the xenografts derived from these biopsies. Nomenclature: 33A, 33C and 33U are individuals from the same family where 33A and 33C are FSHD affected, and 33U is unaffected, confirmed by 4qA allele genotyping. Similarly, 37B and 37U are individuals from a different family where 37B is affected and 37U is unaffected. Each subplot shows log2(fold-changes) for a pairwise FSHD vs. control biopsy (horizontal axis) plotted against the corresponding log2(fold-changes) for FSHD vs. control xenografts derived from these biopsies (vertical axis) for the 25 genes assayed by qPCR: at top is 33A vs. 33U, in the middle 33C vs. 33U, and at bottom 37B vs. 37U. For both axes, positive values represent higher expression in FSHD samples than control samples. Genes in the upper-right and lower-left quadrants show consistent direction of change for biopsies and xenografts. The log2(fold-changes) for xenografts are differences in means of variance stabilized normalized Ct values for multiple FSHD and control xenografts ($n = 6$ for 33C, $n = 4$ for others). Genes are colored green if the FSHD and control xenografts differ at $p < 0.05$ by the Wilcoxon rank-sum test. (Statistical tests are not done for the biopsies as there is just one FSHD and one control sample in each comparison.) The log2(fold-changes) for lowly expressed genes may be compressed due to the variance stabilization, and log2(fold-changes) should be regarded with particular caution for genes represented by triangles (not detected in at least one xenograft) and squares (not detected in at least one xenograft and at least one biopsy), for which non-detected transcripts were assigned Cts near the detection limit (see Methods). The dashed diagonal black line indicates perfect agreement and the dashed red line is the line of best fit by orthogonal regression.

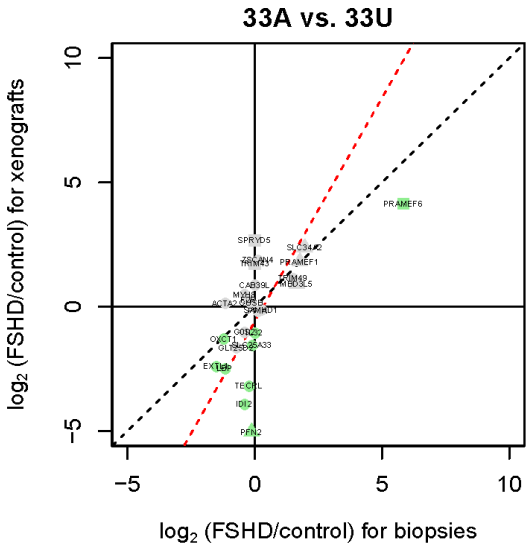
33A vs. 33U
log2 (FSHD/control) for xenografts
log2 (FSHD/control) for biopsies
10
5
0
−5
−5
0
5
10
PRAMEF6
SPRYD5
SLC34A2
ZSCAN4
PRAMEF1
TRIM43
CABS1
MBD3L5
MYH8
ACTA2
OXCT1
GLT25D2
EXTL1
TECTL
IDI2
PFN2

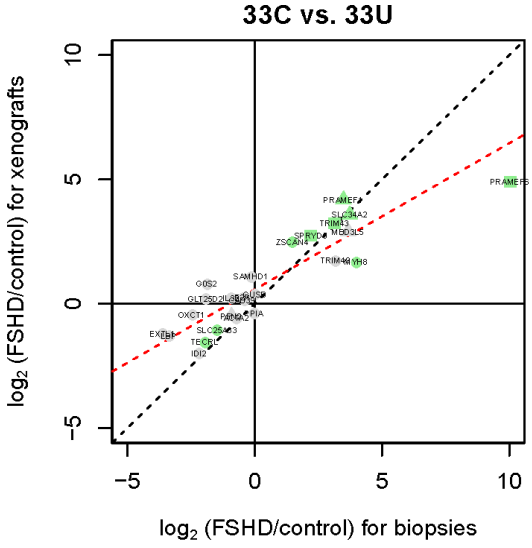
33C vs. 33U
log2 (FSHD/control) for xenografts
log2 (FSHD/control) for biopsies
10
5
0
−5
−5
0
5
10
PRAMEF6
PRAMEF1
SLC34A2
TRIM43
SPRYD5
MBD3L5
ZSCAN4
TRIM49
SAMHD1
GOS2
GLT25D2
OXCT1
EXTL1
TECTL
IDI2

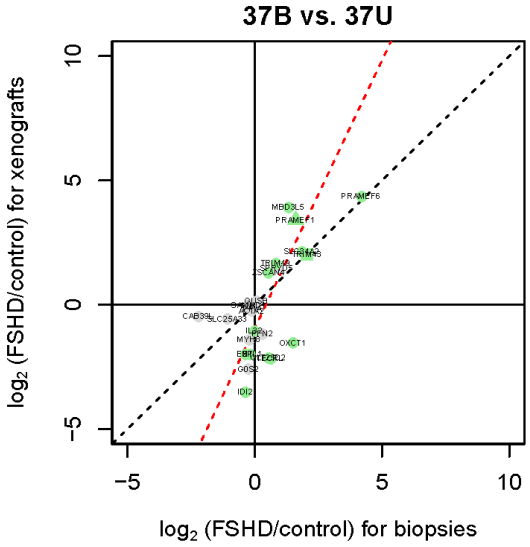
37B vs. 37U
log2 (FSHD/control) for xenografts
log2 (FSHD/control) for biopsies
10
5
0
−5
−5
0
5
10
PRAMEF6
MBD3L5
PRAMEF1
TRIM43
ZSCAN4
CABS1
OXCT1
GOS2
IDI2

Figure S2.5. Human muscle xenograft generated from muscle sample harvested 48 hours postmortem. (A) H&E staining of the autopsy generated xenograft 110 days after transplantation. (B) Immunohistochemistry of a serial section with anti-human spectrin (red), anti-human lamin A/C (green) and DAPI (blue). Asterisk indicates host mouse muscle. Scale bar, 200 μm.

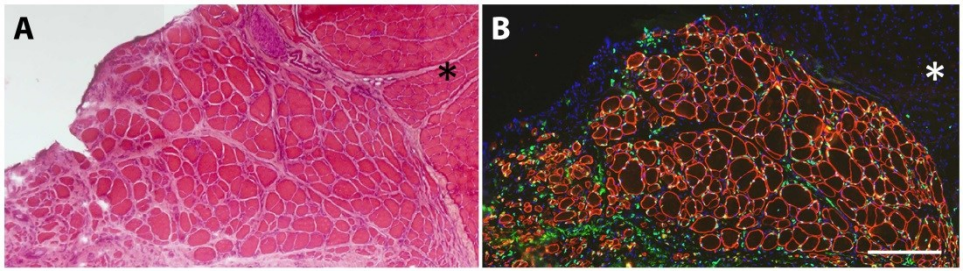

Table S 2.1. TaqMan Gene Expression assays from Life Technologies (www.lifetechnologies.com). PPIA and GUSB were used as normalization genes.

TaqMan Assay ID	Gene
Hs00426835_g1	ACTA2
Hs00229488_m1	CAB39L
Hs00184929_m1	EXTL1
Hs00169258_m1	F2R
Hs00274783_s1	G0S2
Hs00362851_m1	GLT25D2
Hs99999908_m1	GUSB
Hs00264442_m1	IDI2
Hs00170403_m1	IL32
Hs01084621_m1	LBP
Hs04190573_mH	MBD3L5
Hs00267293_m1	MYH8
Hs00166467_m1	OXCT1
Hs00160050_m1	PFN2
Hs99999904_m1	PPIA
Hs00363780_m1	PRAMEF1
Hs04192778_mH	PRAMEF6
Hs00210019_m1	SAMHD1
Hs00757629_s1	SLC25A33
Hs00197519_m1	SLC34A2
Hs00827634_m1	TRIM51 (SPRYD5)
Hs01399058_m1	TECRL
Hs00299174_m1	TRIM43
Hs00220514_m1	TRIM49
Hs00537549_m1	ZSCAN4

Chapter 3. Morpholino-Mediated Knockdown of DUX4 Towards Facioscapulohumeral Muscular Dystrophy Therapeutics

Jennifer C. J. Chen*, Oliver D. King*, **Yuanfan Zhang***, Nicholas P. Clayton, Carrie Spencer, Bruce M. Wentworth, Charles P. Emerson Jr, Kathryn R. Wagner. Morpholino-Mediated Knockdown of DUX4 Towards Facioscapulohumeral Muscular Dystrophy Therapeutics. *Submitted*.

Morpholino-Mediated Knockdown of DUX4 Towards Facioscapulohumeral Muscular Dystrophy Therapeutics

Jennifer C. J. Chen[1]*, Oliver D. King[1]*, Yuanfan Zhang[2,3]*, Nicholas P. Clayton[4], Carrie Spencer[1], Bruce M. Wentworth[4†], Charles P. Emerson Jr[1]§, Kathryn R. Wagner [2,3,5]§

[1] Departments of Cell and Developmental Biology and Neurology, University of Massachusetts Medical School, Worcester, MA 01655, USA
[2] The Hugo W. Moser Research Institute, Kennedy Krieger, Baltimore, MD 21205, USA
[3]Graduate Program in Cellular and Molecular Medicine, The Johns Hopkins School of Medicine, Baltimore, MD 21205 USA
[4]Sanofi Genzyme, Cambridge, MA 02152 USA
[5]Departments of Neurology and Neuroscience, The Johns Hopkins School of Medicine, Baltimore, MD 21287, USA

*These three first authors contributed equally
§These two senior authors contributed equally

†Current address:
Bruce M. Wentworth, PhD
Vice President, Biology
Sarepta Therapeutics
215 First St.
Cambridge MA 02142

Corresponding Author:
Kathryn R. Wagner, MD, PhD
Center for Genetic Muscle Disorders
Kennedy Krieger Institute
707 North Broadway
Baltimore, MD 21205
443-923-9525
wagnerk@kennedykrieger.org

Abstract

Derepression of DUX4 in skeletal muscle has emerged as a likely cause of pathology in facioscapulohumeral muscular dystrophy (FSHD). Here we report on the use of antisense phosphorodiamidate morpholino oligonucleotides (PMOs) to suppress DUX4 expression and function in FSHD myotubes and xenografts. The most effective was PMO FM10, which targets the polyadenylation signal of *DUX4*. FM10 had no significant cell toxicity, and RNA-seq analyses of FSHD and control myotubes revealed that FM10 down-regulated many transcriptional targets of DUX4, without overt off-target effects. Electroporation of FM10 into FSHD patient muscle xenografts in mice also down-regulated *DUX4* and DUX4 targets. These findings demonstrate the potential of antisense PMOs as an FSHD therapeutic option.

Introduction

FSHD1 and 2 are genetic diseases whose primary manifestations are weakness and wasting of muscles of the face, shoulder girdle and upper arms. FSHD1, representing ~95% of cases, is associated with deletions of macrosatellite D4Z4 repeats in the subtelomeric region of chromosome 4q35, leaving 1-10 D4Z4 repeats (80). FSHD2 is in most cases associated with mutations in SMCHD1 on chromosome 18 (81). Both of these mutations lead to relaxation of chromatin at the 4q35 D4Z4 repeat array, allowing aberrant transcription in muscle of a full-length form of *DUX4* mRNA (*DUX4-fl*), which encodes a double homeobox transcription factor (23, 81-84). Development of laboratory animal models of FSHD have been challenging, due in part to the unknown pathophysiologic mechanism of DUX4 action and the restricted emergence of the D4Z4-DUX4 chromosomal architecture in primates and Afrotheria (6, 85). Nevertheless, the evidence that *DUX4* is an FSHD disease gene is compelling, including the findings that: (1) both FSHD1 and 2 are associated with particular "permissive" 4q35A haplotypes that include a polyadenylation signal required for production of stable *DUX4-fl* mRNA from the telomeric D4Z4 repeat; (2) overexpression of *DUX4-fl* induces a large cohort of germline genes that are also up-regulated in FSHD muscle (67, 83, 86); and 3) overexpression of full-length DUX4 protein is toxic in muscle, both *in vitro* and *in vivo* (24, 87).

These findings identify DUX4 as a promising therapeutic target for antisense therapy. Antisense oligonucleotides (AONs) are being developed as therapeutics for other neuromuscular diseases including Duchenne muscular dystrophy (DMD), spinal muscular atrophy (SMA) and myotonic dystrophy (88-91). Here we report a proof-of-

concept study of the therapeutic potential of antisense phosphorodiamidate morpholino oligonucleotides (PMOs) for the treatment of FSHD, by targeting *DUX4* and demonstrating efficacy in both FSHD myogenic cells and human muscle xenografts.

Results and Discussion

Transcriptome sequencing (RNA-seq) was performed on cultured myotubes derived from the biceps of 6 FSHD subjects and their unaffected first-degree relatives to establish a reference transcriptional signature (Fig. 3.2A, Table S 3.1). Consistent with previous studies (86), FSHD myotubes expressed elevated levels of direct and indirect transcriptional targets of DUX4 (67). The mRNA levels of DUX4 targets serve as biomarkers of DUX4 activity, and can be more readily quantified than levels of *DUX4* mRNA or DUX4 protein, which are often quite low (67).

PMOs that target the *DUX4-fl* transcript (Fig. 3.1A; Table S 3.2) were tested for their ability to suppress the expression of DUX4 protein and selected DUX4 target genes (92-94). Differentiating myotube cultures derived from FSHD subjects were treated for four days with control or *DUX4* PMOs, and then analyzed for biomarker expression to assay knockdown efficiency. FM10 and, to a lesser extent, FM9 had the greatest effects, consistently decreasing levels of DUX4 target genes *ZSCAN4*, *MBD3L2*, and *TRIM43* (Fig. 3.1B; Fig. S 3.1), establishing that these compounds block DUX4 function. Both FM10 and FM9 target the polyadenylation signal region of the *DUX4* transcript. In contrast, other PMOs tested in this series did not decrease biomarker expression. Notably, PMOs did not disrupt expression of myosin heavy chain, a marker of myogenic cell differentiation. FM10 down-regulation of DUX4 target genes in FSHD cells was dose-dependent, with ED50 in the range from 1-3 uM, and maximal response between 10 and 20 uM, without evidence of cell toxicity (Figs. S 3.2, S 3.3).

PMO effects on protein levels of DUX4 were evaluated in control and *DUX4* PMO-treated FSHD myotube cultures by immunostaining with an antibody targeting a C-

terminal region in the full-length DUX4 protein that is absent from the alternatively spliced "short" DUX4, which is not thought to be a toxic protein (83). DUX4-positive nuclei were reduced in FM9-treated myotubes and almost undetectable in FM10-treated myotubes (Fig. 3.1C), establishing their inhibition of DUX4 protein expression.

Transcriptomes of FSHD and control myotube cultures treated with FM10 or standard control PMO were determined by RNA-seq, using $p < 10^{-4}$ as the cutoff for significance to control for the number of false positives. In myotube cultures from two FSHD subjects, 47 genes differed significantly between FM10 versus control PMO treatment, with an associated false discovery rate (FDR) of 0.066 (Fig 2B, Table S3). Of these 47 transcripts, 46 had lower expression with FM10 treatment than with control PMO.

To assess whether these changes reflected a suppression of FSHD-associated transcription, we compared PMO transcriptome results to the RNA-seq data from myotubes of six FSHD subjects versus their unaffected relatives, in which 121 genes were significantly upregulated in FSHD and 5 were significantly downregulated (FDR = 0.021; Table S 3.1), and to the 213 DUX4 targets from Table S1, Yao et al (86), which includes 94 of the 121 genes significantly upregulated in FSHD versus unaffected myotubes. Both false positives and false negatives have a stochastic component (including sampling error), which limits how well sets of significantly altered genes from different studies will agree, even for identically designed and equally powered studies (which these are not). As a more relaxed measure of agreement, though still subject to sampling error, we checked whether the significantly altered genes in one study were changed in a consistent direction in the other study, regardless of significance. Of the 46

genes that were significantly decreased by FM10, 41 showed elevated expression in FSHD versus control myotubes, significantly for 32, and 30 were among the DUX4 targets from Table S3.1 of Yao et al. (86). Thus most of the genes significantly decreased by FM10 are elevated in FSHD. Conversely, 116 of the 121 genes that were significantly elevated in FSHD versus unaffected myotubes, and 162 of the 185 detected DUX4 target genes from Yao et al. (86) showed at least some reduction by FM10. The reduction was not typically to the level of DUX4 targets observed in control cells: many DUX4 targets were elevated more than 16-fold in FSHD versus unaffected myotubes ($\log_2$ fold-change > 4 in Fig. 3.2A), whereas few showed more than 4-fold decrease by FM10 versus control PMO ($\log_2$ fold-change < -2 in Fig. 3.2B), and this is not because the two FM10-treated FSHD samples had particularly low levels of the DUX4 targets pre-treatment (Fig. S3.3).

RNA-seq analysis of FM10 myotube cultures from the two unaffected first-degree relatives provides another view of off-target effects, unclouded by DUX4 target genes, as unaffected cells express little if any DUX4-fl. For these cells, only 3 genes differed significantly between GZ10 and the control PMO (p-value < 10^{-4}), and this is roughly what one expects by chance when testing ~37,000 genes for differential expression, even if the null hypotheses of equal expression are all true (Fig 2C). No genes had p-value < 10^{-5} or FDR < 0.72. Thus we observed no clear off-target effects of FM10 based on these samples.

We evaluated FM10 PMO knockdown of *DUX4-fl* in human muscle *in vivo* using an FSHD xenograft model created by transplanting FSHD affected donor muscle into the hindlimbs of *NOD-Rag1*^{null}*IL2r*□^{null} immunodeficient mice (95). Engrafted muscle from

FSHD biopsy donors and FSHD autopsy donors regenerated and was re-vascularized and re-innervated by four months post-transplant. Importantly, *DUX4-fl* as well as DUX4 target gene expression in these xenografts have been shown to mirror those of the donor muscle tissue (95). FM10 or standard control PMO was electroporated into FSHD xenografts, and mice were analyzed after two weeks (Fig. 3.3A) (95). Human xenografts were confirmed by immunohistochemistry using anti-human spectrin and anti-human lamin a/c antibodies to stain specifically for human muscle fiber membranes and human nuclei, respectively (Fig. 3.3B). In FSHD xenografts, FM10 reduced *DUX4-fl* expression to nearly undetectable levels compared to control PMO (Fig. 3.3C). FM10 treatment also reduced the expression of DUX4 target genes *MBD3L5* and *ZSCAN4* in xenografts compared to control PMO (Fig. 3.3D).

Our study provides proof-of-concept that antisense PMO targeted specifically to the essential *DUX4* polyadenylation signal can significantly diminish the expression of *DUX4-fl* and DUX4 target genes that serve as biomarkers of DUX4 activity (83, 96, 97), both *in vitro* and in human xenografted muscle *in vivo*. Previously, PMOs and other AONs targeting 3' elements of DUX4-fl, including splice acceptor sites 2 and 3 and the polyadenylation signal, have been shown to reduce expression of DUX4 and select DUX4 targets *in vitro* (98, 99). Our *in vitro* studies provide a global view of transcriptional changes associated with DUX4 knockdown, and provide experimental data on off-target effects that complement *in silico* predictions. In particular, the 25 nucleotide sequence targeted by FM10 is the same as that targeted by PMO-PAS in Marsollier et al., which did not have strong off-target candidates based on BLAST search and predictions of binding energies (23). Our studies of FM10 PMO also evaluate its cell

toxicity and *in vivo* effect on DUX4, which are essential in pursuing therapeutic development. Future studies will be needed to evaluate the efficacy of repeated and systemic administration of PMOs in knocking down DUX4 target gene expression, and although the pathophysiology of FSHD remains incompletely understood, we anticipate that one or more of these DUX4 target genes is responsible for FSHD muscle weakness and could serve as a direct therapeutic target. Our findings, therefore, provide comprehensive evidence that antisense PMO technology is a potential therapeutic option for FSHD.

Materials and Methods

Statistics. Statistical methods for each experiment are described in the main text and Supplementary Methods. P-values ≤ 0.05 were considered significant, except for the RNA-seq analyses in which p-value $< 10^{-4}$ was considered significant.

Study approvals. This study was approved by The Johns Hopkins School of Medicine Institutional Review Board. Written informed consent was received from participants prior to inclusion in the study. All animal procedures were carried out in accordance with an approved IACUC protocol from Johns Hopkins University School of Medicine.

Human subjects, genotyping, and biopsy. This study was approved by the Johns Hopkins School of Medicine Institutional Review Board. Subjects with FSHD and their first degree unaffected relatives were recruited and screened for biomaterial contributions. FSHD status was determined by pulsed field electrophoresis and southern blotting of leukocyte DNA by Dr. Steven A. Moore and the University of Iowa Diagnostic Laboratories, and included identification of the EcoRI/BlnI 4q35 D4Z4 repeat length with a p13E11 probe, and 4qA/4qB allele typing of HindIII fragments (100-103). Subjects with a positive FSHD diagnosis were categorized with an A, B or C designation, and unaffected control subjects with a confirmed negative genotype were categorized with a U, V, or W designation. Open muscle biopsy was performed on biceps from living donors and deltoid muscle was harvested from autopsy (66). Clinical data for subjects 33A, 33U, 41A, 58A, 61A and 61B are presented in Supplemental Table S5; data for remaining subjects were published previously (25).

Morpholinos. Phosphorodiamidate morpholino oligonucleotides (PMOs) were synthesized by Gene Tools, LLC with a 5' primary amine modification to facilitate conjugation with a cell penetrating peptide (CPP). Sequences of PMOs are shown in Supplemental Table S2.

Cell Culture & *in vitro* morpholino treatment. Primary muscle cells from FSHD subjects 03A, 13B, 14A, 15A, 15B, 16A, 17A, 18A, 21A, 33A, 41A and first-degree, unaffected relatives 03U, 13U, 14W, 16U, 21U, 33U were cultured as previously described (104). To assess PMO activity, cells were cultured until >95% confluent, rinsed briefly with PBS (Cellgro), and then differentiated in Opti-MEM (Invitrogen) supplemented with 10 uM *DUX4*-targeting PMO or standard control PMO (Gene Tools, LLC). The standard control PMO designed by Gene Tools, LLC targets a human beta-globin intron mutation that causes beta-thalassemia, and this target is restricted to beta-thalessemic hematopoietic cells (www.gene-tools.com). Cells were treated with PMOs for four days without a medium change, and then harvested for RT-qPCR analysis or immunocytochemistry. To identify ED50 of FM10, cells were cultured as above and treated with 0-15 uM standard control or FM10 PMO for four days and assayed for RT-qPCR analysis. Toxicity was assessed with 17A primary muscle cells treated with 0-500 uM standard control or FM10 morpholinos conjugated to CPP Peptide B (105) in triplicate, using the Celltiter-Glo® Luminescent Viability Assay (Promega) according to manufacturer's instructions. Fluorescence was measured using a Tecan Safire II plate reader operated by Xfluor4 software.

Antibodies and immunostaining. Myotube cultures treated with DUX4-targeting PMOs or standard control PMOs were fixed with 4% formaldehyde, pH 7.4 and immunostained with C-terminal specific mouse-anti-DUX4 clone P4H2 (kindly provided by Drs. Stephen Tapscott and Linda Geng) as previously described (25). Secondary detection was performed using the ABC Elite kit (Vector Labs) and DAB staining. DUX4-positive nuclei were counted using DIC microscopy, and total number of nuclei was estimated by counting 10 random fields and multiplying by a factor accounting for area screened. Muscle cryosections (10 μm) were fixed in ice-cold methanol, blocked with anti-mouse IgG (MKB-2213, Vector Laboratories) for 2 hours, incubated in the primary antibodies for 1 hour [anti-human spectrin (NCL-SPEC1, Leica, 1:50) and anti-human lamin A/C (Ab40567, AbCam, 1:200)], followed by 45 minute incubation with secondary antibodies [AlexaFluor 488 goat anti-mouse IgG1, AlexaFluor 594 goat anti-mouse IgG2b (Invitrogen, 1:500)] at room temperature. All nuclei were labeled with DAPI in mounting medium (P36930, Invitrogen).

RNA isolation, cDNA synthesis and RT-qPCR analyses. RNA was isolated from cells or xenografts as previously described (4, 5). cDNA was synthesized using Oligo $(dT)_{16}$ and Superscript III reverse transcriptase (Invitrogen). Primers were synthesized by Integrated DNA Technologies. Primer sequences are listed in Supplemental Table S4. Cell RT-qPCR reactions were set up in triplicate using iQ SYBR Green Supermix (Bio-Rad) and amplified on a CFX96 Touch Real-time PCR Detection System (Bio-Rad). Results were analyzed using CFX Manager Software, and visualized graphically using Microsoft Excel and Graphpad Prism 6. Expression was normalized to RPL13A. From

the xenografts, DUX4-fl expression was determined using 100 ng of poly(A)+ cDNA by a qRT–PCR as described previously (106). qPCR reactions were performed using Taqman Master Mix (BioRad) with specific Taqman assays for *ZSCAN4* (Hs00537549_m1, Life Tech), *MBD3L5* (Hs04190573_mH, Life Tech), *GUSB* (Hs99999908_m1, Life Tech) and *PPIA* (Hs99999904_m1, Life Tech) and run on a CFX PCR machine (BioRad). Reactions were set up in duplicate. Statistical tests were performed on Cts, normalized to the mean Ct of *PPIA* and *GUSB*. The samples where *DUX4* was not detected were given a Ct of 45 (total cycle number). The control PMO-treated biopsy group included two 58A, one 61A and one 61B xenograft, and the FM10-PMO biopsy group included three 58A, one 61A and two 61B xenografts. To address between-donor rather than within-donor variance in response to FM10, multiple xenografts from the same donor in each treatment were averaged at the ΔCt level, then these average levels were used in the paired t-tests of control PMO vs. FM10. Autopsy xenografts (n=10 Ctrl and n=6 FM10) were from a single donor, and were analyzed with a two tailed t-test, assuming unequal variance.

RNA sequencing and analysis. High throughput TruSeq stranded mRNA sequencing (RNA-seq, 50- or 51-bp paired end) was performed by Expression Analysis. To identify differences between FSHD and unaffected muscle cells, sequencing was performed on 4-day differentiated myotube cells from FSHD subjects 03A, 13B, 14A, 16A, 21A, 33A and their first-degree, unaffected relatives 03U, 13U, 14W, 16U, 21U, and 33U (respectively). To identify effects of FM10 PMO treatment (both DUX4-dependent and off-target effects), 4-day myotubes from FSHD subjects 15A and 17A, and first degree,

unaffected relatives, 15V and 17U (respectively), treated with FM10, standard-control morpholino, or Opti-MEM medium alone were sequenced. Samples from 17A and 17U were treated and sequenced in duplicate, which allows estimation of within-subject variance in response to treatment, but the statistical tests reported here depend on between-subject variance in response to treatments, and use just the first replicate so that all subjects are treated uniformly. (Data from both replicates is shown in Supplemental Fig. S3.4). FASTQ files of raw RNA-seq reads were mapped to Ensembl human GRCh37 reference genome and transcript annotations (version 75) from Illumina iGenomes using Tophat2 (2.1.0) (107) and Bowtie2 (2.2.6) (108) with options -r 70 --mate-std-dev 40 for the FSHD vs. unaffected data and -r 60 --mate-std-dev 40 for the PMO data (which was done later and had a bit shorter average insert length). Counts of reads mapping unambiguously to ~63,000 annotated genes were computed using htseq-count (HTSeq-0.6.1p1, strand-specific mode) (109), and imported into R for tests of differential expression using the package edgeR (3.12) (110). Total per-sample counts of these reads ranged from 74 - 113 million for the FSHD vs. unaffected data, and from 63 - 72 million for the PMO data. Normalization factors for each sample were computed in edgeR with the TMM method, and used as offsets when modeling the data with negative binomial distributions with the function glmFit. The dispersion parameters were computed with the estimateGLMTagwiseDisp function, shrinking the per-gene estimates toward trended dispersion estimates, with prior degrees of freedom set to 5. Likelihood-ratio tests for differential expression were performed with the function glmLRT. The model formula for the FSHD vs. unaffected comparison was ~ 0 + diseaseGroup + family, and the model formula for the PMO comparisons was ~ 0 + diseaseGroup:treatment + subject. Here the

diseaseGroup factor has levels FSHD and unaffected, the treatment factor has levels FM10, control, and Opti-MEM, and the family factor and subject factor account for the pairings between first-degree relatives and between multiple treatments of subjects, respectively. To make the coefficients identifiable, the sum of the coefficients for family was constrained to be zero in the first model, as were the sums of the coefficients for FSHD and unaffected subjects in the second model. The three treatments were modeled jointly to allow for shared estimates of dispersion parameters. Results for Opti-MEM were generally similar to the standard control PMO (e.g. Supplemental Fig. S3.4). All subjects in the FSHD vs. unaffected study were female except for 14A and 14W, which were male; thus an additive effect for sex can be absorbed into the family factor, so is not used. All subjects in the PMO study were male, except from 15V; as there is just one female sample we did not attempt to adjust for sex, but do note that the gene with the most significant change for FM10 in unaffected samples was XIST, which is expressed from inactivated X-chromosomes; this may be due to the negative-binomial model being a particularly poor fit for this gene, whose read count was >10,000-fold higher for the female unaffected subject than for the male unaffected subject, as the direction of change with FM10 was not consistent in the two subjects. In Fig. 3.2, Supplemental Table S3.1 and Supplemental Fig. S3.4, a prior count of 1 was used in computing the $\log_2$(counts per million) and $\log_2$(fold-changes), to avoid infinite values; this does not affect the p-values. The ~25,000 genes with zero counts in all samples (separately for the FSHD vs. unaffected data and PMO data) were excluded when computing false-discovery rates.

Xenograft procedure and local delivery of PMO-ASO. The Institutional Animal Care and Use Committee at the Johns Hopkins University School of Medicine approved all procedures performed in this study. NOD-Rag1^{null}IL2r□^{null} immunodeficient mice (NRG) (Stock 007799, The Jackson Laboratory) were used. The xenografting procedure was performed with biceps muscle biopsies from FSHD subjects 58A, 61A, and 61B, as previously described (95). Human skeletal muscle xenografts which had fully regenerated in host NRG mice for 4~6 months were used in this study. For delivery of PMO-ASO, xenografts were first injected with 12 µl of 0.4U/µl bovine hyaluronidase (Sigma Aldrich). Two hours later, xenografts were injected with 20 µg (1 µg /µl) of PMO-Standard ASO or PMO-FM10 ASO. Immediately following injection, the ASO was electroporated using the parameters of 50 V/cm, 10 pulses at 1 Hz, and 20 ms duration per pulse. Mice were euthanized 2 weeks after electroporation and human xenograft muscles were collected and snap frozen until analysis.

Figures

Figure 3.1. DUX4 and DUX4 target gene knockdown in FSHD myotubes *in vitro*. (A) Schematic demonstrating *DUX4-fl* transcript and relative targets of PMOs; PAS, polyadenylation signal. (B) FSHD biomarker expression analysis of 4-day FSHD myotube cultures treated with standard control or DUX4-targeting morpholinos. Significant decreases in *CCNA1*, *MBD3L2*, *TRIM43*, and *ZSCAN4* biomarker expression were observed in myotube cultures treated with 10 uM FM10 (*p-value<0.05, Student's t-test performed on DCts normalized to RPL13A); an intermediate effect was observed in FM9-treated cultures. Data are presented as the mean fold change ± SEM relative to standard control morpholino. (C) DUX4 protein expression analysis of 4-day FSHD myotube cultures treated with standard control or DUX4-targeting morpholinos. DUX4 protein was detected by immunostaining with C-terminal DUX4-specific P4H2 antibody. The greatest decrease in DUX4-positive nuclei was observed in myotube cultures treated with 10 uM FM10; an intermediate effect was observed in FM9-treated cultures.

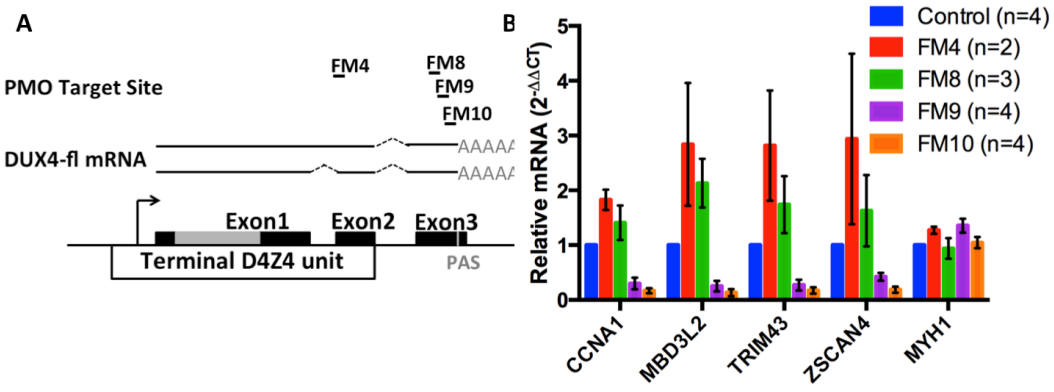

C

Morpholino Treatment (10 uM)	Total # DUX4+ Cells	Total # DUX4+ Nuclei	Est. total # of nuclei screened	Rate of DUX4+ nuclei per 10000
-	25	135	34287	39.37
FM4	36	153	39099	39.13
FM8	28	153	35859	42.67
FM9	12	69	50778	13.59
FM10	1	1	44733	0.22

Figure 3.2. RNA-seq analysis of FSHD vs. unaffected myotube cultures and FM10 vs. control PMO-treated myotube cultures. These volcano plots show $\log_2$(fold-change) versus $-\log_{10}$(p-value) for tests of differential expression of approx. 37,000 genes detected by RNA-seq, for three comparisons: (A) myotube cultures from FSHD subjects vs. unaffected first-degree relatives (n=6 pairs); (B) FM10 vs. control (CTRL) PMO-treated myotube cultures from FSHD subjects (n=2); and (C) FM10 vs. control (CTRL) PMO-treated myotube cultures from unaffected subjects (n=2). The two subjects in (B) are first-degree relatives of the two subjects in (C), and are unrelated to the 12 subjects in (A). To aid in comparisons between plots, the color-coding of points in all plots is determined by direction and significance of changes in (A): genes whose expression is higher in FSHD than control myotubes are colored red if p-value $< 10^{-4}$ and pink otherwise; genes whose expression is lower in FSHD than control myotubes are colored blue if p-value $< 10^{-4}$ and light blue otherwise. In all plots, black squares are overlaid on the DUX4 targets from Table S1 of Yao et al. (10). P-values are from likelihood-ratio tests for negative binomial regression (R package edgeR), and prior counts of 1 were used to avoid infinite log fold-changes; see Supplemental Methods for details.

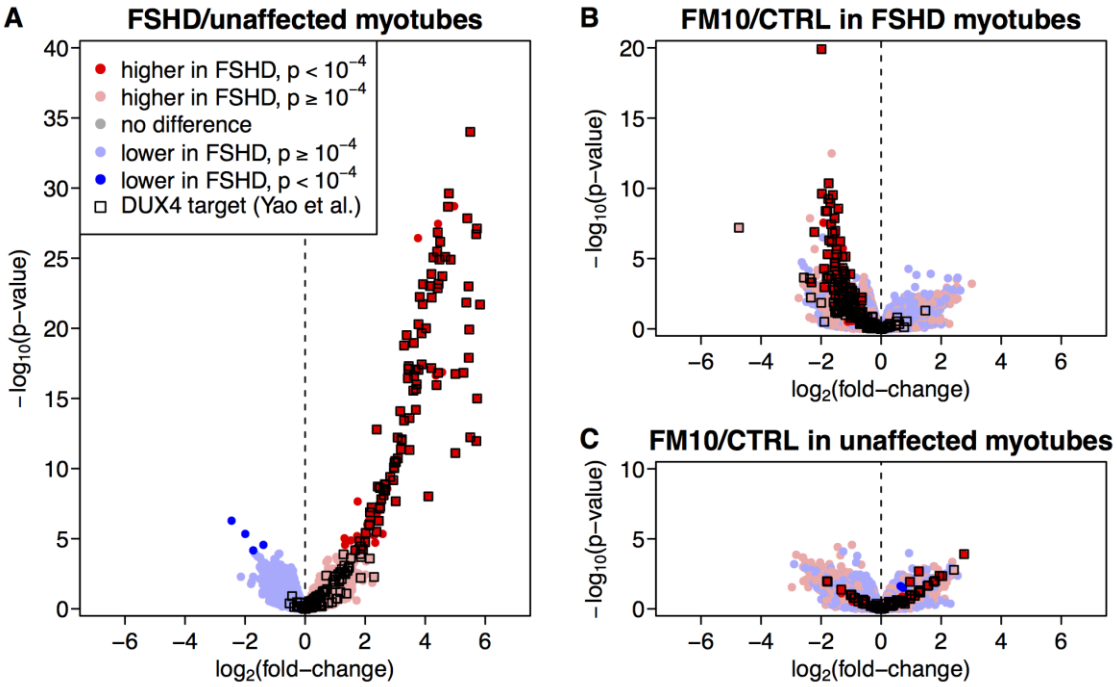
A
FSHD/unaffected myotubes
higher in FSHD, p < 10^−4
higher in FSHD, p ≥ 10^−4
no difference
lower in FSHD, p ≥ 10^−4
lower in FSHD, p < 10^−4
DUX4 target (Yao et al.)
−log10(p−value)
log2(fold−change)
B
FM10/CTRL in FSHD myotubes
−log10(p−value)
log2(fold−change)
C
FM10/CTRL in unaffected myotubes
−log10(p−value)
log2(fold−change)

Figure 3.3. *In vivo* validation of FM10 knockdown of *DUX4-fl* and DUX4 target genes in a human FSHD xenograft model. (**A**) Schematic of the *in vivo* study design. FSHD patient muscle was transplanted into the *tibialis anterior* space of NRG mice. Xenografts fully regenerated in the mouse leg for more than four months, were treated with Control- or FM10- PMO via electroporation, and harvested after two weeks. (**B**) Histology of a four-month FSHD xenograft. Immunohistochemistry of the human-specific muscle membrane protein spectrin and nuclear envelope protein lamin A/C confirmed that the xenograft was well regenerated. Human spectrin (red), human lamin A/C (green), DAPI (blue). Scale bar: 200 μm. **(C)** Expression analysis of *DUX4-fl* and **(D)** of DUX4 target genes *MBD3L5* and *ZSCAN4* in xenografts from biopsy and autopsy donor groups treated with Control- and FM10-PMOs. Significant decreases were observed for all three genes with FM10 treatment (**P < 0.01; *P < 0.05, all tests two-tailed). Statistical tests were performed on DCts, normalized to *PPIA* and *GUSB*. The biopsy group consisted of xenografts from three donors (n=4 Ctrl; n=6 FM10); to address between-donor rather than within-donor variance in response to FM10, DCts for xenografts from each donor were averaged, and a paired t-test performed on the per-donor averages. All xenografts in the autopsy group were from a single donor (n=10 Ctrl; n=6 FM10), and an unequal variance t-test was used for this data. Expression levels for each xenograft are shown as fold-changes relative to the per-donor mean DCt for the Ctrl PMO ($2^{-\Delta\Delta Ct}$), with mean of the per-donor averages (biopsy) or mean ± SEM (autopsy) also indicated.

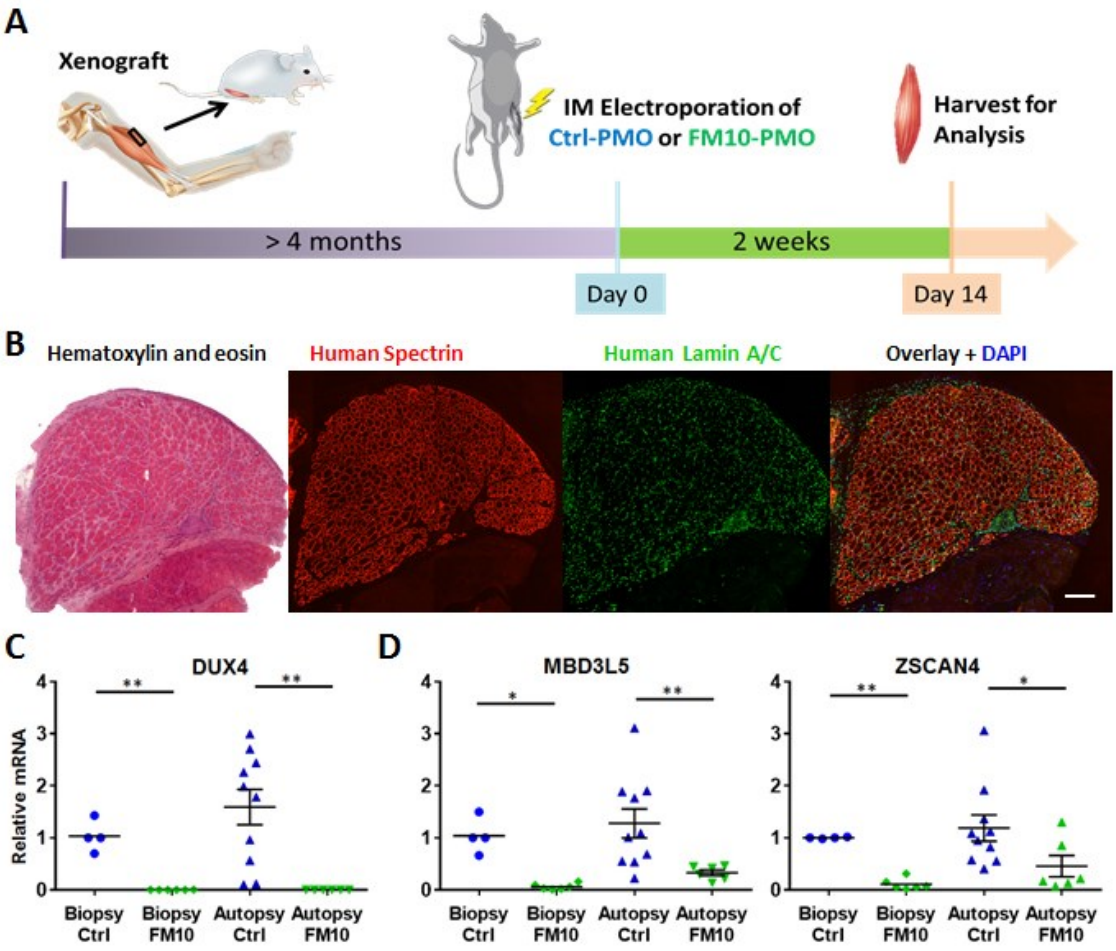

Supplemental Data

Supplemental Table S 3.1. 125 genes differentially expressed (with p-value < 10^{-4}) in myotubes of FSHD patients versus unaffected first degree relatives, sorted by p-value. Column names beginning LCPM, LFC, P and FDR indicate $\log_2$(counts per million), $\log_2$(fold-change), p-value, and false-discovery rate, respectively, and the suffix of the column name indicates the comparison: FvsU for FSHD vs. control myotubes; FM10.F for FM10 vs. control PMO in FSHD myotubes;

and FM10.U for FM10 vs. control PMO is unaffected myotubes. The column Yao.S1 is Y if the gene appears in Supplemental Table S1, “Robust DUX4 regulated genes in human myoblasts transduced with human DUX4”, of Yao et al (86), N otherwise.

gene_id	gene_name	LCPM.FvsU	LFC.FvsU	P.FvsU	FDR.FvsU	LFC.FM10.F	P.FM10.F	FDR.FM10.F	LFC.FM10.U	P.FM10.U	FDR.FM10.U	Yao.S1
ENSG00000229571	PRAMEF26	-1.16	5.5	9.80E-35	3.90E-30	-1.67	3.60E-08	8.90E-05	0	1.00E+00	1	Y
ENSG00000180532	ZSCAN4	1.94	4.79	2.40E-30	4.80E-26	-1.65	6.70E-07	1.00E-03	0.43	4.10E-01	1	Y
ENSG00000268799	RP11-321E2.13	-1.43	4.97	1.90E-29	2.10E-25	-1.47	1.70E-04	1.10E-01	0.57	2.50E-01	1	N
ENSG00000204455	TRIM51BP	-2.07	4.76	2.10E-29	2.10E-25	-1.55	3.60E-05	3.40E-02	-0.01	9.80E-01	1	Y
ENSG00000128253	RFPL2	-0.41	5.4	1.40E-28	1.10E-24	-1.43	8.40E-04	3.30E-01	0.74	3.20E-01	1	Y
ENSG00000176979	TRIM60	-2.28	4.43	3.50E-28	2.30E-24	-1.92	2.80E-08	7.90E-05	0	1.00E+00	1	N
ENSG00000251258	RFPL4B	0.83	5.72	7.70E-28	4.40E-24	-1.55	1.40E-08	4.20E-05	0.08	8.90E-01	1	Y
ENSG00000128250	RFPL1	-2.25	4.42	1.50E-27	7.30E-24	-1.65	2.70E-04	1.50E-01	-0.59	2.40E-01	1	Y
ENSG00000116721	PRAMEF1	0.75	5.7	2.00E-27	8.60E-24	-1.97	2.40E-10	2.20E-06	-0.05	9.40E-01	1	Y
ENSG00000267908	ZSCAN5D	-0.96	3.76	3.80E-27	1.50E-23	-1.51	1.90E-07	3.60E-04	1.01	1.00E-01	1	N
ENSG00000232423	PRAMEF6	-2.21	4.5	6.80E-27	2.40E-23	-1.15	2.10E-03	5.50E-01	0	1.00E+00	1	Y
ENSG00000204449	TRIM49C	-2.57	4.4	3.40E-26	1.10E-22	-1.02	1.30E-03	4.10E-01	-0.6	2.30E-01	1	Y
ENSG00000249620	RP11-321E2.10	-1.1	4.67	8.10E-26	2.50E-22	-1.28	4.70E-05	4.30E-02	-0.01	1.00E+00	1	Y
ENSG00000225581	TRIM53AP	-1.75	4.27	8.80E-26	2.50E-22	-1.52	4.40E-03	7.90E-01	0	1.00E+00	1	Y
ENSG00000168930	TRIM49	-1.56	4.48	1.20E-25	3.10E-22	-0.7	3.60E-02	1.00E+00	0.58	2.40E-01	1	Y
ENSG00000179412	HNRNPCP5	-0.89	4.85	1.30E-25	3.10E-22	-1.36	5.90E-07	9.20E-04	1	9.80E-02	1	Y
ENSG00000204495	PRAMEF13	-2.41	4.21	1.30E-24	3.10E-21	-1.49	2.10E-06	2.80E-03	0.97	1.10E-01	1	Y
ENSG00000182315	MBD3L3	-1.81	4.57	1.90E-24	4.30E-21	-1.24	1.20E-04	9.20E-02	0.57	2.50E-01	1	Y
ENSG00000223638	RFPL4A	-1.41	4.45	6.70E-24	1.40E-20	-1.01	5.70E-03	8.60E-01	-0.76	3.00E-01	1	Y
ENSG00000243073	PRAMEF4	-2.12	3.93	7.10E-24	1.40E-20	-1.48	4.80E-06	6.00E-03	0	1.00E+00	1	Y
ENSG00000239810	WI2-3308P17.2	-1.97	4.16	9.70E-24	1.80E-20	-1.45	1.40E-04	9.90E-02	0	1.00E+00	1	Y
ENSG00000179172	HNRNPCL1	-0.25	5.44	1.00E-23	1.90E-20	-1.76	5.70E-10	3.50E-06	1.54	2.30E-02	1	Y
ENSG00000124900	TRIM51	-1.73	4.42	1.40E-23	2.40E-20	-1.27	7.90E-04	3.30E-01	0	1.00E+00	1	Y
ENSG00000254104	RP11-63E5.1	-1.71	3.82	5.80E-23	9.60E-20	-1.06	1.20E-03	3.90E-01	0.01	1.00E+00	1	Y
ENSG00000150244	TRIM48	-2.96	4.22	6.40E-23	1.00E-19	-0.58	2.20E-01	1.00E+00	-1.78	1.20E-02	1	Y
ENSG00000120952	PRAMEF2	0.67	5.37	1.50E-22	2.20E-19	-1.75	4.40E-11	5.40E-07	1.57	2.10E-02	1	Y
ENSG00000214325	AC025287.1	-2.35	3.92	1.90E-22	2.80E-19	-0.95	1.70E-02	1.00E+00	-0.02	9.70E-01	1	Y
ENSG00000213921	LEUTX	1.41	5.83	2.00E-22	2.90E-19	-1.62	1.50E-07	3.00E-04	2.04	4.60E-03	1	Y
ENSG00000249910	TRIM51CP	-2.52	3.78	5.10E-21	7.00E-18	-1.14	4.10E-02	1.00E+00	1.25	5.90E-02	1	Y
ENSG00000144188	TRIM43CP	-2.92	4.03	9.90E-21	1.30E-17	-0.99	2.40E-03	5.90E-01	-0.02	9.70E-01	1	Y
ENSG00000144015	TRIM43	0.31	5.47	1.20E-20	1.60E-17	-1.85	4.10E-09	1.60E-05	2.76	1.20E-04	0.78	Y
ENSG00000254764	TRIM53CP	-1.95	3.88	2.30E-20	2.80E-17	-1.38	2.80E-04	1.50E-01	0	1.00E+00	1	Y
ENSG00000204480	PRAMEF19	-3.59	3.38	3.10E-20	3.70E-17	-0.64	5.90E-03	8.70E-01	0	1.00E+00	1	Y
ENSG00000233834	AC005083.1	-2.59	3.62	1.10E-19	1.30E-16	-1.89	1.10E-03	3.70E-01	0.56	2.60E-01	1	Y
ENSG00000256980	KHDC1L	-2.29	3.3	1.70E-19	1.90E-16	-1.19	6.40E-04	3.00E-01	-0.01	9.80E-01	1	Y
ENSG00000235268	KDM4E	0	5.45	1.30E-18	1.40E-15	-1.52	2.20E-05	2.30E-02	-0.01	9.90E-01	1	Y
ENSG00000251163	CTD-2325A15.2	-2.91	3.88	3.80E-18	4.00E-15	-1.44	4.70E-04	2.50E-01	-0.57	2.40E-01	1	Y
ENSG00000219061	TRIM51FP	-2.67	3.45	5.00E-18	5.20E-15	-0.86	5.70E-02	1.00E+00	0.97	1.10E-01	1	Y
ENSG00000133101	CCNA1	3.94	4.2	6.90E-18	7.00E-15	-1.73	5.00E-07	8.20E-04	0.96	1.20E-02	1	Y
ENSG00000166013	TRIM53BP	-2.74	3.44	7.60E-18	7.50E-15	-0.95	1.40E-02	1.00E+00	-0.59	2.40E-01	1	Y
ENSG00000250782	RP11-432M8.13	-2.68	3.68	8.50E-18	8.30E-15	-0.96	9.80E-03	9.50E-01	-0.6	2.30E-01	1	Y
ENSG00000187545	PRAMEF10	-3.12	3.78	9.20E-18	8.60E-15	-1.32	7.60E-04	3.20E-01	0	1.00E+00	1	Y
ENSG00000269466	RP11-432M8.17	-0.47	4.57	1.30E-17	1.20E-14	-1.67	5.00E-05	4.50E-02	1.27	5.30E-02	1	N
ENSG00000144010	TRIM43B	0.22	5.27	1.50E-17	1.30E-14	-1.61	3.00E-10	2.20E-06	0.3	6.30E-01	1	Y
ENSG00000251360	KHDC1P1	-1.03	4.43	1.50E-17	1.30E-14	-1.42	1.30E-03	4.10E-01	-0.01	1.00E+00	1	Y
ENSG00000204513	PRAMEF11	-1.08	5.01	1.80E-17	1.50E-14	-1.53	1.10E-07	2.30E-04	0.97	1.90E-01	1	Y
ENSG00000258873	DUXA	-0.68	4.35	2.20E-17	1.90E-14	-1.07	7.10E-03	9.20E-01	0.56	2.50E-01	1	N
ENSG00000237194	SNAI1P1	-2.61	3.63	2.50E-17	2.10E-14	-0.7	6.10E-02	1.00E+00	-1.01	9.40E-02	1	Y
ENSG00000249357	RP11-432M8.8	-2.07	3.42	3.70E-17	3.00E-14	-0.72	6.70E-02	1.00E+00	0.97	1.90E-01	1	Y
ENSG00000204481	PRAMEF14	-3.31	3.72	9.90E-17	7.90E-14	-1.43	2.80E-09	1.30E-05	0	1.00E+00	1	Y
ENSG00000182053	TRIM49B	-1.48	4.38	1.10E-16	8.80E-14	-1.19	1.30E-04	9.20E-02	-0.03	9.70E-01	1	Y
ENSG00000250386	RP11-432M8.11	-1.25	3.7	2.10E-16	1.60E-13	-1.25	7.70E-05	6.20E-02	1.75	1.20E-02	1	Y
ENSG00000230268	SSU72P8	-3.3	3.61	2.80E-16	2.10E-13	-0.36	4.80E-01	1.00E+00	0	1.00E+00	1	Y
ENSG00000257951	RP11-554D14.4	2.13	5.73	1.00E-15	7.40E-13	-1.25	3.20E-03	6.90E-01	1.95	4.40E-03	1	Y
ENSG00000229292	RFPL4AL1	-2.4	3.69	6.40E-15	4.60E-12	-0.71	6.30E-02	1.00E+00	-1.33	4.20E-02	1	Y
ENSG00000249156	RP11-432M8.9	-1.85	3.17	8.00E-15	5.70E-12	-0.75	8.70E-02	1.00E+00	0.34	6.30E-01	1	Y
ENSG00000255855	RP11-735A19.2	-2.94	3.48	2.50E-14	1.70E-11	-1.28	9.70E-04	3.60E-01	-0.01	9.80E-01	1	Y
ENSG00000220948	TRIM51GP	-3.21	3.3	3.80E-14	2.60E-11	-1.81	2.50E-04	1.40E-01	0	1.00E+00	1	Y
ENSG00000178928	TPRX1	-1.44	2.38	1.60E-13	1.10E-10	-0.62	6.10E-02	1.00E+00	-0.88	1.70E-01	1	Y
ENSG00000116726	PRAMEF12	1.21	5.5	5.90E-13	3.90E-10	-1.69	1.10E-09	5.90E-06	-0.54	4.50E-01	1	Y
ENSG00000218725	RP11-174C7.2	-3.25	3.08	6.20E-13	4.00E-10	-0.65	6.00E-03	8.70E-01	0	1.00E+00	1	Y
ENSG00000239275	RP4-675G8.2	-3.72	3.22	8.20E-13	5.30E-10	-1.29	7.50E-06	8.50E-03	0	1.00E+00	1	Y
ENSG00000186232	SSU72P3	-3.77	3.21	1.00E-12	6.50E-10	0.16	7.50E-01	1.00E+00	0	1.00E+00	1	Y
ENSG00000157765	SLC34A2	3.38	5.7	1.10E-12	6.70E-10	-1.99	1.20E-20	4.60E-16	1.25	2.10E-03	1	Y
ENSG00000236217	C1DP2	-2.74	3.19	4.20E-12	2.60E-09	-1.78	5.00E-06	6.00E-03	0	1.00E+00	1	Y
ENSG00000165929	TC2N	-1.41	3.48	4.70E-12	2.80E-09	-1.06	1.80E-03	5.00E-01	-0.61	4.00E-01	1	Y
ENSG00000230522	MBD3L2	0	5	7.80E-12	4.60E-09	-0.96	1.90E-03	5.00E-01	1.29	4.80E-02	1	Y
ENSG00000189253	TRIM64B	-3.64	3.09	1.90E-11	1.10E-08	-1.08	8.20E-03	9.30E-01	0	1.00E+00	1	Y
ENSG00000224199	WI2-2994D6.1	-3.6	3	2.90E-11	1.70E-08	-1.37	1.70E-02	1.00E+00	0	1.00E+00	1	Y
ENSG00000237247	MBD3L5	-3.8	3.02	3.50E-11	2.00E-08	-0.61	2.80E-01	1.00E+00	0	1.00E+00	1	Y

ENSG00000229542	SSU72P7	-3.77	2.98	3.80E-11	2.10E-08	-0.7	2.50E-01	1.00E+00	0.57	2.60E-01	1	Y
ENSG00000223417	TRIM49D1	-3.74	2.96	8.20E-11	4.50E-08	-0.87	2.90E-03	6.50E-01	-0.6	2.30E-01	1	Y
ENSG00000237706	TRIM51EP	-3.55	2.97	9.40E-11	5.10E-08	-1.79	4.30E-09	1.60E-05	0	1.00E+00	1	Y
ENSG00000255194	SSU72P2	-3.76	2.83	4.00E-10	2.10E-07	-0.55	2.50E-01	1.00E+00	0	1.00E+00	1	Y
ENSG00000249666	RP11-432M8.12	-3.35	2.94	6.70E-10	3.60E-07	-0.72	2.00E-01	1.00E+00	0	1.00E+00	1	Y
ENSG00000188460	ACTBP11	-3.57	2.65	1.30E-09	6.70E-07	-1.02	6.10E-02	1.00E+00	0	1.00E+00	1	Y
ENSG00000214534	ZNF705E	-1.32	2.68	1.40E-09	7.10E-07	-1.19	7.30E-06	8.50E-03	0.28	5.50E-01	1	Y
ENSG00000188536	HBA2	-4.3	2.42	1.90E-09	9.70E-07	-1.9	5.30E-05	4.60E-02	0.57	2.50E-01	1	Y
ENSG00000197123	ZNF679	-4.04	2.49	2.40E-09	1.20E-06	-0.08	8.80E-01	1.00E+00	0	1.00E+00	1	Y
ENSG00000214295	FOXO1B	-3.38	2.74	2.60E-09	1.30E-06	-0.51	4.30E-01	1.00E+00	0	1.00E+00	1	N
ENSG00000251076	RP11-526F3.1	-3.59	2.63	2.90E-09	1.40E-06	-0.92	2.80E-02	1.00E+00	1.29	4.90E-02	1	Y
ENSG00000204479	PRAMEF17	-4.06	2.67	3.70E-09	1.80E-06	-0.9	6.90E-02	1.00E+00	0	1.00E+00	1	Y
ENSG00000229978	RP13-221M14.3	-4.08	2.61	7.90E-09	3.80E-06	-1.03	1.20E-04	9.20E-02	0	1.00E+00	1	Y
ENSG00000196946	ZNF705A	-1.12	4.1	9.70E-09	4.60E-06	-1.55	1.80E-05	2.00E-02	1.12	1.20E-01	1	Y
ENSG00000166007	TRIM51HP	-4.25	2.53	1.60E-08	7.30E-06	-1.55	2.50E-02	1.00E+00	0	1.00E+00	1	Y
ENSG00000205622	AF064858.6	-2.58	3.02	2.20E-08	9.90E-06	-1.11	1.40E-02	1.00E+00	-1.8	1.10E-02	1	Y
ENSG00000251393	RP1-240K6.3	-2.71	1.75	2.30E-08	1.00E-05	-0.02	9.50E-01	1.00E+00	-0.95	2.90E-01	1	N
ENSG00000204532	ZSCAN5C	-3.99	2.5	5.30E-08	2.40E-05	-2.22	1.30E-07	2.70E-04	0	1.00E+00	1	Y
ENSG00000128276	RFPL3	-4.25	2.21	5.90E-08	2.60E-05	0	1.00E+00	1.00E+00	0	1.00E+00	1	Y
ENSG00000187569	DPPA3	-3.21	2.48	7.10E-08	3.10E-05	-0.17	6.50E-01	1.00E+00	0	1.00E+00	1	Y
ENSG00000236941	RP11-366M4.8	-0.98	2.25	9.10E-08	4.00E-05	-1.27	1.90E-06	2.70E-03	-0.54	3.10E-01	1	N
ENSG00000269118	FAM90A28P	-3.67	2.42	9.60E-08	4.20E-05	-0.79	1.60E-01	1.00E+00	0	1.00E+00	1	N
ENSG00000206172	HBA1	-4.46	2.16	1.30E-07	5.60E-05	-0.68	1.90E-01	1.00E+00	1.8	1.00E-02	1	Y
ENSG00000188782	CATSPER4	-3.84	2.4	1.40E-07	6.10E-05	0	1.00E+00	1.00E+00	0	1.00E+00	1	N
ENSG00000204711	C9orf135	-4.18	2.21	4.60E-07	1.90E-04	-0.97	1.60E-01	1.00E+00	-0.59	2.40E-01	1	N
ENSG00000269067	ZNF728	-3.76	2.14	4.70E-07	1.90E-04	-0.95	1.30E-01	1.00E+00	-0.56	2.50E-01	1	N
ENSG00000147256	ARHGAP36	-1.88	-2.44	5.10E-07	2.10E-04	-0.18	6.70E-01	1.00E+00	0.14	7.00E-01	1	N
ENSG00000229361	UBTFL7	-3.71	2.45	5.30E-07	2.20E-04	-0.65	9.80E-03	9.50E-01	0	1.00E+00	1	Y
ENSG00000227160	RP1-65P5.1	-4.25	2.23	5.60E-07	2.30E-04	-1.07	5.20E-02	1.00E+00	-0.43	5.60E-01	1	N
ENSG00000087510	TFAP2C	-3.19	2.07	9.40E-07	3.70E-04	-0.69	2.40E-01	1.00E+00	1.17	1.30E-01	1	N
ENSG00000189348	FAM90A27P	-4.17	2.14	9.70E-07	3.80E-04	-1	5.20E-03	8.40E-01	0	1.00E+00	1	Y
ENSG00000204503	PRAMEF3	-4.49	2.15	1.10E-06	4.40E-04	-0.2	4.40E-01	1.00E+00	0.01	1.00E+00	1	Y
ENSG00000171872	KLF17	-0.74	2.37	3.10E-06	1.20E-03	-0.45	1.90E-01	1.00E+00	-0.27	6.10E-01	1	Y
ENSG00000214003	ATP5F1P3	-4.62	2.01	3.20E-06	1.20E-03	-0.28	5.40E-01	1.00E+00	0	1.00E+00	1	N
ENSG00000196589	CTB-25J19.1	-4.59	2.02	3.80E-06	1.40E-03	0.08	8.90E-01	1.00E+00	0	1.00E+00	1	Y
ENSG00000261723	CTD-2196E14.3	-3.15	2.58	4.30E-06	1.60E-03	-1.05	1.60E-02	1.00E+00	-1.3	4.60E-02	1	N
ENSG00000197584	KCNMB2	-1.91	-1.99	4.60E-06	1.70E-03	-0.14	7.30E-01	1.00E+00	0.73	3.10E-02	1	N
ENSG00000272382	CTD-2035E11.4	-1.42	2.3	5.70E-06	2.10E-03	-1.12	4.00E-03	7.60E-01	0.5	4.50E-01	1	N
ENSG00000228709	AP001065.15	-2.2	1.74	6.40E-06	2.30E-03	-1.02	1.00E-02	9.60E-01	0.52	4.90E-01	1	N
ENSG00000206077	ZDHHC11B	-3.93	1.92	8.30E-06	3.00E-03	-1.11	3.10E-01	1.00E+00	-1.32	7.60E-02	1	N
ENSG00000156453	PCDH1	1.46	1.32	9.50E-06	3.40E-03	0.05	8.60E-01	1.00E+00	0.21	3.80E-01	1	N
ENSG00000235890	TSPEAR-AS1	-3.41	1.52	1.30E-05	4.80E-03	-0.97	2.90E-01	1.00E+00	-0.77	3.40E-01	1	N
ENSG00000223912	EEF1A1P36	-4.79	1.82	1.50E-05	5.40E-03	-2.32	5.00E-04	2.60E-01	0	1.00E+00	1	Y
ENSG00000204478	PRAMEF20	-4.3	2	1.80E-05	6.20E-03	-0.81	1.30E-01	1.00E+00	0	1.00E+00	1	Y
ENSG00000257842	NOVA1-AS1	-3.87	2.34	1.90E-05	6.70E-03	-1.16	1.60E-02	1.00E+00	-0.58	2.40E-01	1	N
ENSG00000108602	ALDH3A1	-0.11	-1.39	2.60E-05	8.90E-03	-0.29	3.30E-01	1.00E+00	0.65	2.40E-02	1	N
ENSG00000130303	BST2	-1.23	1.33	2.70E-05	9.20E-03	-0.96	2.10E-02	1.00E+00	0.7	1.30E-01	1	N
ENSG00000255065	RP11-680E19.2	-4.17	1.86	3.60E-05	1.20E-02	-1.57	1.70E-03	4.80E-01	-0.01	9.80E-01	1	Y
ENSG00000255268	RP11-707M1.9	-4.72	1.71	4.90E-05	1.60E-02	-0.79	3.10E-01	1.00E+00	0	1.00E+00	1	N
ENSG00000154639	CXADR	-1.45	1.71	4.90E-05	1.60E-02	-1.09	1.30E-04	9.20E-02	0.32	6.10E-01	1	N
ENSG00000255452	RP11-107P7.1	-4.59	1.82	5.00E-05	1.60E-02	-0.49	4.50E-01	1.00E+00	0	1.00E+00	1	N
ENSG00000267654	RP11-973H7.4	-4.22	1.67	5.30E-05	1.70E-02	-0.13	8.30E-01	1.00E+00	1.28	5.10E-02	1	N
ENSG00000104267	CA2	-1	1.93	5.50E-05	1.80E-02	-0.32	4.30E-01	1.00E+00	-0.17	7.30E-01	1	Y
ENSG00000259383	RP11-403B2.6	-4.17	-1.73	6.50E-05	2.10E-02	0	1.00E+00	1.00E+00	0	1.00E+00	1	N
ENSG00000255184	RP11-313I2.7	-4.76	1.67	6.70E-05	2.10E-02	-1.41	7.70E-03	9.30E-01	0	1.00E+00	1	Y

Supplemental Table S 3.2. Morpholino sequences directed at the *DUX4* transcript.

PMO	**Sequence**
FM4	TCTCACCGGGCCTAGACCTAGAAGG
FM8	CCAGGAGATGTAACTCTAATCCAGG
FM9	TATATCTCTGAACTAATCATCCAGG
FM10	GGGCATTTTAATATATCTCTGAACT
Standard Control (Gene Tools, LLC)	CCTCTTACCTCAGTTACAATTTATA

Supplemental Table S 3.3. 46 genes differentially expressed (with p-value < 10^{-4}) in FM10 vs. control PMO-treated FSHD myotubes, sorted by p-value. Column names beginning LCPM, LFC, P and FDR indicate $\log_2$(counts per million), $\log_2$(fold-change), p-value, and false-discovery rate, respectively, and the suffix of the column name indicates the comparison: FvsU for FSHD vs. control myotubes; FM10.F for FM10 vs. control PMO in FSHD myotubes; and FM10.U for FM10 vs. control PMO is unaffected myotubes. The column Yao.S1 is Y if the gene appears in Supplemental Table S1, "Robust DUX4 regulated genes in human myoblasts transduced with human DUX4", of Yao et al (86), N otherwise.

gene_id	gene_name	LCPM.FvsU	LFC.FvsU	P.FvsU	FDR.FvsU	LFC.FM10.F	P.FM10.F	FDR.FM10.F	LFC.FM10.U	P.FM10.U	FDR.FM10.U	Yao.S1
ENSG00000157765	SLC34A2	3.38	5.7	1.10E-12	6.70E-10	-1.99	1.20E-20	4.60E-16	1.25	2.10E-03	1	Y
ENSG00000164879	CA3	0.12	1.53	5.50E-03	6.10E-01	-1.64	3.30E-13	6.20E-09	-0.26	3.90E-01	1	N
ENSG00000120952	PRAMEF2	0.67	5.37	1.50E-22	2.20E-19	-1.75	4.40E-11	5.40E-07	1.57	2.10E-02	1	Y
ENSG00000116721	PRAMEF1	0.75	5.7	2.00E-27	8.60E-24	-1.97	2.40E-10	2.20E-06	-0.05	9.40E-01	1	Y
ENSG00000144010	TRIM43B	0.22	5.27	1.50E-17	1.30E-14	-1.61	3.00E-10	2.20E-06	0.3	6.30E-01	1	Y
ENSG00000179172	HNRNPCL1	-0.25	5.44	1.00E-23	1.90E-20	-1.76	5.70E-10	3.50E-06	1.54	2.30E-02	1	Y
ENSG00000116726	PRAMEF12	1.21	5.5	5.90E-13	3.90E-10	-1.69	1.10E-09	5.90E-06	-0.54	4.50E-01	1	Y
ENSG00000204481	PRAMEF14	-3.31	3.72	9.90E-17	7.90E-14	-1.43	2.80E-09	1.30E-05	0	1.00E+00	1	Y
ENSG00000144015	TRIM43	0.31	5.47	1.20E-20	1.60E-17	-1.85	4.10E-09	1.60E-05	2.76	1.20E-04	0.78	Y
ENSG00000237706	TRIM51EP	-3.55	2.97	9.40E-11	5.10E-08	-1.79	4.30E-09	1.60E-05	0	1.00E+00	1	Y
ENSG00000229616	RP11-369J21.11	-4.69	1.42	8.80E-02	1.00E+00	-2.36	1.30E-08	4.20E-05	0	1.00E+00	1	N
ENSG00000251258	RFPL4B	0.83	5.72	7.70E-28	4.40E-24	-1.55	1.40E-08	4.20E-05	0.08	8.90E-01	1	Y
ENSG00000176979	TRIM60	-2.28	4.43	3.50E-28	2.30E-24	-1.92	2.80E-08	7.90E-05	0	1.00E+00	1	N
ENSG00000156510	HKDC1	0.13	1.41	1.40E-04	4.30E-02	-1.88	3.00E-08	8.00E-05	-0.25	5.00E-01	1	N
ENSG00000229571	PRAMEF26	-1.16	5.5	9.80E-35	3.90E-30	-1.67	3.60E-08	8.90E-05	0	1.00E+00	1	Y
ENSG00000205718	MBD3L4	-5.38	0.31	1.80E-01	1.00E+00	-4.74	6.40E-08	1.50E-04	0	1.00E+00	1	Y
ENSG00000204513	PRAMEF11	-1.08	5.01	1.80E-17	1.50E-14	-1.53	1.10E-07	2.30E-04	0.97	1.90E-01	1	Y
ENSG00000204532	ZSCAN5C	-3.99	2.5	5.30E-08	2.40E-05	-2.22	1.30E-07	2.70E-04	0	1.00E+00	1	Y
ENSG00000213921	LEUTX	1.41	5.83	2.00E-22	2.90E-19	-1.62	1.50E-07	3.00E-04	2.04	4.60E-03	1	Y
ENSG00000267908	ZSCAN5D	-0.96	3.76	3.80E-27	1.50E-23	-1.51	1.90E-07	3.60E-04	1.01	1.00E-01	1	N
ENSG00000239776	AC079949.1	6	-0.06	7.30E-01	1.00E+00	-1.93	3.00E-07	5.40E-04	0.68	6.10E-02	1	N
ENSG00000136943	CTSV	-0.66	-0.02	9.60E-01	1.00E+00	-1.59	3.20E-07	5.40E-04	-0.11	7.40E-01	1	N
ENSG00000133101	CCNA1	3.94	4.2	6.90E-18	7.00E-15	-1.73	5.00E-07	8.20E-04	0.96	1.20E-02	1	Y
ENSG00000179412	HNRNPCP5	-0.89	4.85	1.30E-25	3.10E-22	-1.36	5.90E-07	9.20E-04	1	9.80E-02	1	Y
ENSG00000180532	ZSCAN4	1.94	4.79	2.40E-30	4.80E-26	-1.65	6.70E-07	1.00E-03	0.43	4.10E-01	1	Y
ENSG00000236941	RP11-366M4.8	-0.98	2.25	9.10E-08	4.00E-05	-1.27	1.90E-06	2.70E-03	-0.54	3.10E-01	1	N
ENSG00000158246	FAM46B	0.22	0.59	6.40E-02	1.00E+00	-1.45	1.90E-06	2.70E-03	0.13	6.90E-01	1	N
ENSG00000181652	ATG9B	-2.68	0.06	8.40E-01	1.00E+00	-2.21	2.10E-06	2.80E-03	-1.67	5.70E-03	1	N
ENSG00000204495	PRAMEF13	-2.41	4.21	1.30E-24	3.10E-21	-1.49	2.10E-06	2.80E-03	0.97	1.10E-01	1	Y
ENSG00000243073	PRAMEF4	-2.12	3.93	7.10E-24	1.40E-20	-1.48	4.80E-06	6.00E-03	0	1.00E+00	1	Y
ENSG00000236217	C1DP2	-2.74	3.19	4.20E-12	2.60E-09	-1.78	5.00E-06	6.00E-03	0	1.00E+00	1	Y
ENSG00000214534	ZNF705E	-1.32	2.68	1.40E-09	7.10E-07	-1.19	7.30E-06	8.50E-03	0.28	5.50E-01	1	Y
ENSG00000239275	RP4-675G8.2	-3.72	3.22	8.20E-13	5.30E-10	-1.29	7.50E-06	8.50E-03	0	1.00E+00	1	Y
ENSG00000196946	ZNF705A	-1.12	4.1	9.70E-09	4.60E-06	-1.55	1.80E-05	2.00E-02	1.12	1.20E-01	1	Y
ENSG00000235605	RP5-827C21.1	-1.67	-0.15	5.60E-01	1.00E+00	-2.64	1.80E-05	2.00E-02	1.75	9.40E-04	1	N
ENSG00000125966	MMP24	-1.06	0.05	8.90E-01	1.00E+00	-1.53	2.20E-05	2.30E-02	-0.13	7.00E-01	1	N
ENSG00000235268	KDM4E	0	5.45	1.30E-18	1.40E-15	-1.52	2.20E-05	2.30E-02	-0.01	9.90E-01	1	Y
ENSG00000260808	CTD-2007L18.5	-4.72	-0.17	7.40E-01	1.00E+00	-2.58	3.40E-05	3.40E-02	0.57	2.50E-01	1	N
ENSG00000204455	TRIM51BP	-2.07	4.76	2.10E-29	2.10E-25	-1.55	3.60E-05	3.40E-02	-0.01	9.80E-01	1	Y
ENSG00000249620	RP11-321E2.10	-1.1	4.67	8.10E-26	2.50E-22	-1.28	4.70E-05	4.30E-02	-0.01	1.00E+00	1	Y
ENSG00000269466	RP11-432M8.17	-0.47	4.57	1.30E-17	1.20E-14	-1.67	5.00E-05	4.50E-02	1.27	5.30E-02	1	N
ENSG00000265150	RN7SL2	6.62	-0.31	1.80E-01	1.00E+00	0.91	5.30E-05	4.60E-02	0.18	4.00E-01	1	N
ENSG00000188536	HBA2	-4.3	2.42	1.90E-09	9.70E-07	-1.9	5.30E-05	4.60E-02	0.57	2.50E-01	1	Y
ENSG00000183150	GPR19	-3.25	0.22	5.50E-01	1.00E+00	-2.12	6.50E-05	5.50E-02	0.59	2.70E-01	1	N
ENSG00000197409	HIST1H3D	-4.04	-0.06	9.30E-01	1.00E+00	-2.41	6.80E-05	5.60E-02	-1.76	1.20E-02	1	N
ENSG00000250386	RP11-432M8.11	-1.25	3.7	2.10E-16	1.60E-13	-1.25	7.70E-05	6.20E-02	1.75	1.20E-02	1	Y
ENSG00000170684	ZNF296	-1.92	1.28	1.30E-04	3.90E-02	-1.26	8.30E-05	6.60E-02	-0.91	1.60E-01	1	Y

Supplemental Table S 3.4. RT Primer Sequences

Gene	Forward Primer Sequence	Reverse Primer Sequence
*RPL13A**	AACCTCCTCCTTTTCCAAGC	GCAGTACCTGTTTAGCCACGA
*CCNA1**	TGAAGCAGATCCATTCTTGAAA	ACCCTGTAAATGCAGCAAGG
*MBD3L2**	GCGTTCACCTCTTTTCCAAG	GCCATGTGGATTTCTCGTTT
*TRIM43**	ACCCATCACTGGACTGGTGT	CACATCCTCAAAGAGCCTGA
*ZSCAN4**	TGGAAATCAAGTGGCAAAAA	CTGCATGTGGACGTGGAC
MYH1	TACGCCAGGGTCCTTAACTG	CAGTAGCTCCAGCTTCGGTC
DUX4-fl	AGCTTTAGGACGCGGGGTTGGGAC	GCAGGTCTGCWGGTACCTGG

* from Geng et al., 2012

Supplemental Table S 3.5. Clinical characteristics of FSHD Subjects and Unaffected Donors*

Donor[a]	Familial Relations	Gender	Age At Enrollment	EcoRI/BlnI Sizes (kb)[b]	Biceps Strength[c]
33A	Proband	F	49	28 kb (4qB), **20 kb** (4qA)	5/5
33U	Sister of 33A	F	45	77 kb (4q[d]), 47 kb (4qB), 27 kb (4qB)[e]	5/5
41A	Proband	F	34	**14 kb** (4qA), 102 kb (4qA)	4+/4+
58A	Proband	M	50	**27kb**(4qA), 157kb(4qA)	4+/4+
61A	Proband	M	61	**17kb**(4qA), 77kb(4qA), 82 kb (4qB)[e]	5/5
61B	Sister of proband	F	60	**17kb**(4qA), 72kb(4qA), 82 kb (4qB)[e]	5/5

* Clinical characteristics of subjects not listed here were published previously (25).

[a]Donors are designated by cohort (family) number (01, 03, etc.) followed by A, B or C for the FSHD subjects or U, V or W for the unaffected first-degree relative(s).

[b]FSHD1 was confirmed by presence of a shortened 4qA type D4Z4 repeat array identified by an EcoRI/BlnI restriction fragment of <35 kb (Supplementary Material). Shortened repeat arrays are shown in bold.

[c]Muscle strength (right/left) is presented using a modified MRC scale where 5 is full strength and side of biopsy is underlined.

[d]4qA/4qB status was not determined.

[e]Subjects with three BlnI resistant chromosomes (designated as chromosome 4q-

type array) showed only one BlnI-sensitive chromosome (designated as chromosome 10-type array) resulting in an apparent chromosome 4q:10q array ratio of 3:1.

Supplemental Fig. S 3.1. RT-qPCR analysis of primary FSHD myotube cultures treated with 10 uM standard control (n=4), FM4 (n=2), FM8 (n=3), FM9 (n=4) or FM10 (n=4) morpholinos. Data are plotted as ΔCt values, normalized to *RPL13A* expression, and mean ±SEM is noted. Significant differences in FSHD biomarker expression levels between control and FM10 morpholino-treated samples were determined by Student's t-test (* $p<0.05$).

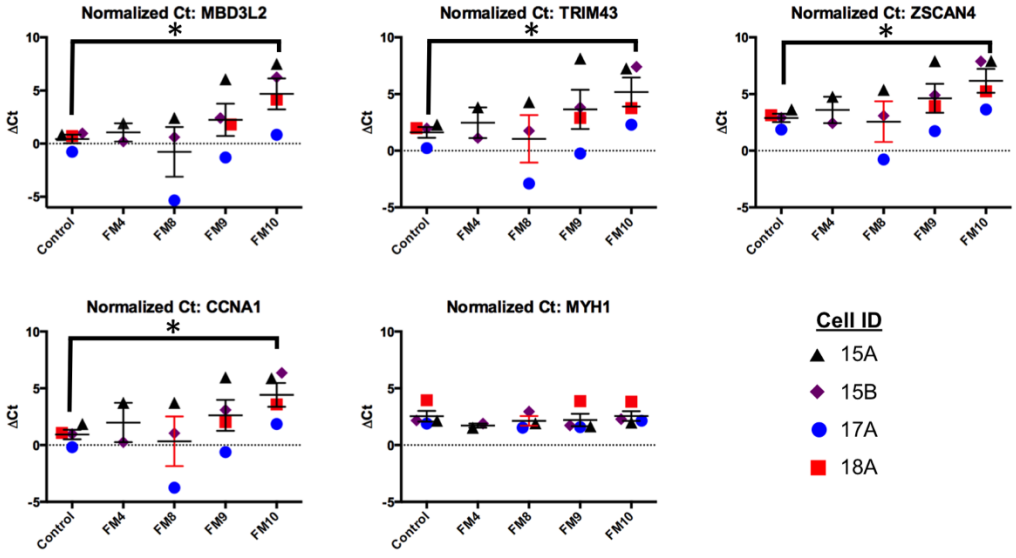

Supplemental Fig. S 3.2. FM10 and standard control MOs were conjugated to Peptide B and tested for cytotoxicity. FM10-PPMO treatment was not associated with significant in vitro cytotoxicity over 48 hour treatment with 0 to 500 uM PPMO. Data is plotted as mean corrected Relative Fluorescence Units (RFU)±SEM (n=3).

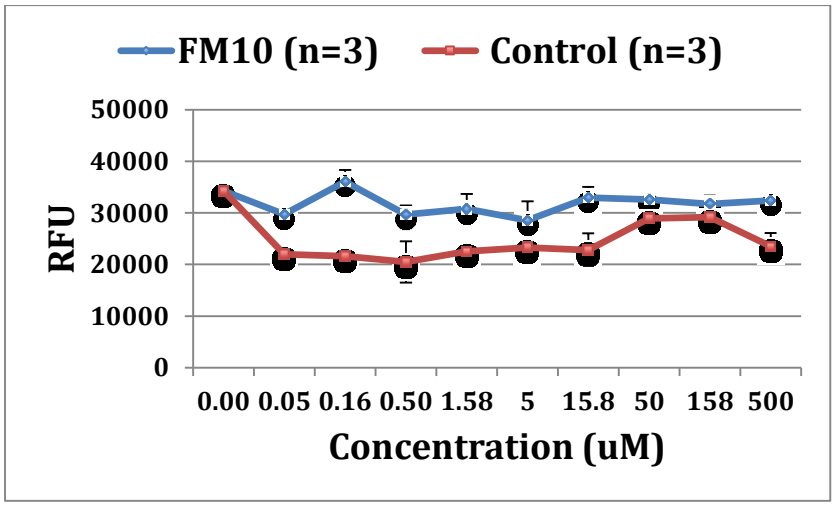

Supplemental Fig. S 3.3. ED50 assay of FM10. *MBD3L2 and ZSCAN4* biomarker expression was assayed by RT-qPCR in primary myotubes from FSHD subjects 17A, 18A, and 41A treated with 0 to 15 uM FM10 or standard control (Ctrl) MO. Data are plotted as ΔCt normalized to *RPL13A* with mean ± SEM noted (top) and average fold change relative to untreated (bottom) ± SEM. Maximal effects were observed at 12.5 uM, and ED50 ≤ 2.5 uM.

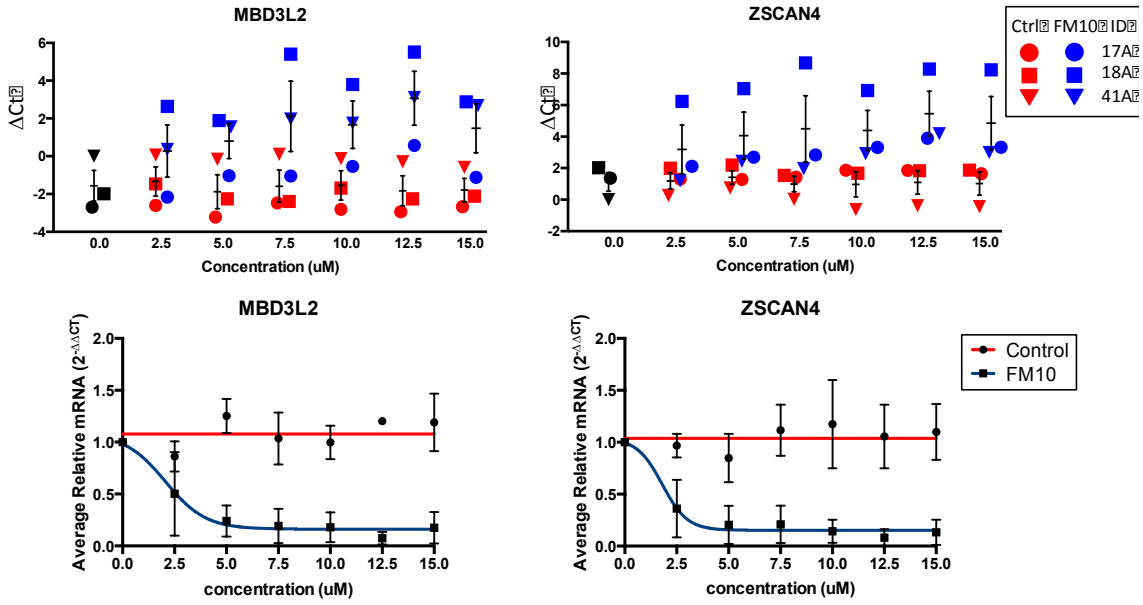

Supplemental Fig. S 3.4. RNA-seq counts for five DUX4 target genes and *MYH1*, a marker of myogenic cell differentiation. Vertical axes show $\log_2$(counts per million reads), with 1 prior count added before scaling; this gives genes with no counts scores around -6, and small changes in counts have larger effects on $\log_2$(CPM) when counts are low. Gene names are shown at the top of each plot, and each gene has two associated plots: (1) the FSHD vs. unaffected myotube study, with six FSHD (red circles) and six unaffected subjects (black circles), and dashed lines connecting first-degree relatives; (2) the PMO study, with four subjects (two FSHD in red, two unaffected in blue), each in three conditions, Opti-MEM medium alone (Opti, empty circles), standard control PMO (Ctrl, saturated solid circles), and FM10 PMO (FM10, pale solid circles). Dashed lines connect first-degree relatives in Opti-Mem, and solid lines connect treatments of the same sample (bold line connects Opti-MEM and control PMO, pale line connects control PMO and FM10). Treatments for 17A and 17U are done in duplicate, with triangles replacing circles for the second replicate. Note that because the two RNA-seq experiments were done at different times there may be batch effects that remain even after normalization, so

direct comparisons of levels between the two experiments may be biased.

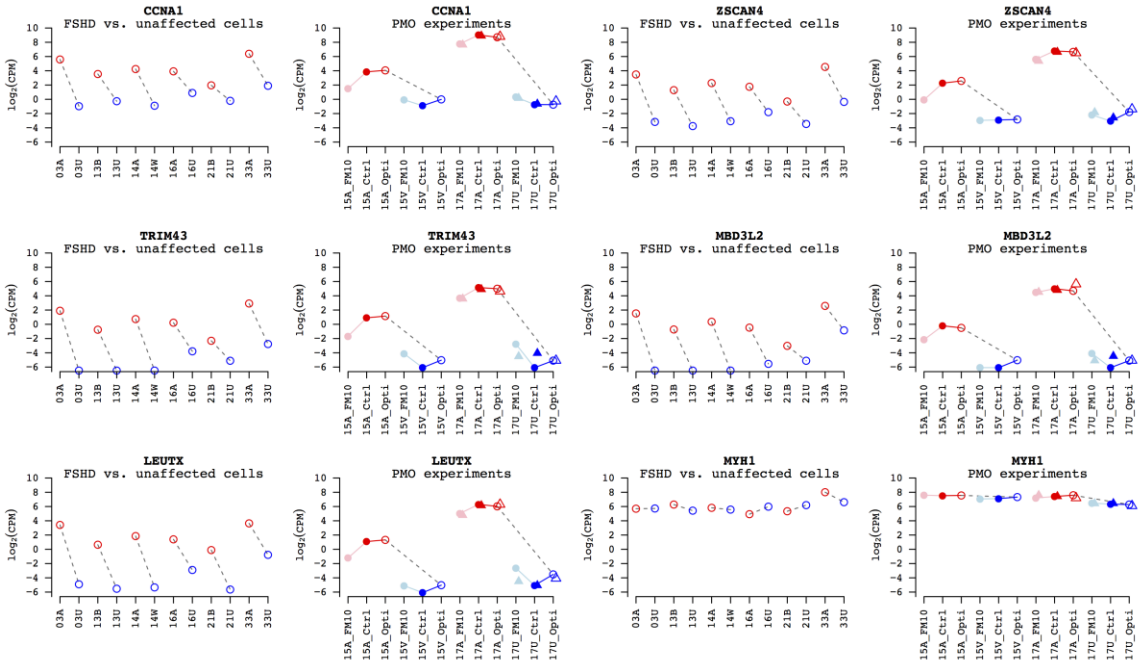

Chapter 4. Summary and future directions

Summary

In this work, we described the successful establishment a novel human skeletal muscle xenograft model for FSHD by transplanting FSHD affected donor muscle into the anterior tibial compartment of immunodeficient NRG mice hind limbs. The grafted muscles from fresh biopsy donors and autopsy donors were regenerated by graft myocytes, re-vascularized by graft and host blood vessels, and re-innervated by host motor neurons. Currently, the loss of transcriptional repression of DUX4 in the D4Z4 macrosatellite repeats at chromosome 4q35 is believed to be the causative genetic defect of FSHD. In our human muscle xenografts, DUX4 expression as well as the FSHD biomarker profile mirrored those of the donor muscle tissue, making this model a feasible and valid preclinical tool to predict the response to novel therapeutics for FSHD (Chapter 2). We report a proof-of-concept study to investigate the therapeutic potential of DUX4 targeting antisense oligonucleotide therapy for FSHD in our human muscle xenograft model and show promising knockdown of DUX4 expression and significant reduction in two FSHD biomarkers (Chapter 3).

Future Directions

This xenograft model provides an opportunity to study the effects of age and disease on the innate regenerative and growth capacity of human skeletal muscle *in vivo*. The fact that the regenerated muscle was integrated into the mouse host's vascular and nervous system but retained the clear separation from mouse muscle guaranteed the recreation of the human muscle microenvironment and cell-cell interactions in a physiological condition.

The recapitulation of disease biomarker profile in the FSHD xenografts compared to the original patient biopsy showed great promise to apply this xenograft model in disease pathogenesis investigation and pre-clinical therapeutic development of more skeletal muscle myopathies. Preliminary experiments have been done to create xenograft from patient biopsies from Duchenne muscular dystrophy (DMD) and inclusion body myositis (IBM) to investigate the disease pathogenesis, and it could be adapted to many more.

Our xenograft model also provides a platform to study human muscle regeneration *in vivo*. The transplanted muscle tissue is damaged from the biopsy process, but retained the intact 3-D structure of muscle tissue, and we have shown that the satellite cell activation and new muscle fiber formation happen within the extracellular matrix structure of the original muscle fibers. Further exploration of the specific progression of cellular events in human skeletal muscle regeneration can be done in this xenograft model.

References

1. Janssen I, Heymsfield SB, Wang Z, and Ross R. Skeletal muscle mass and distribution in 468 men and women aged 18–88 yr. *Journal of Applied Physiology.* 2000;89(1):81-8.
2. Landouzy L, and Dejerine J. De la myopathie atrophique progressive. *Rev Med Franc.* 1885;5(
3. . Orphanet: an online database of rare diseases and orphan drugs. http://www.orpha.net. 2016.
4. Tawil R, Kissel JT, Heatwole C, Pandya S, Gronseth G, and Benatar M. Evidence-based guideline summary: Evaluation, diagnosis, and management of facioscapulohumeral muscular dystrophy: Report of the Guideline Development, Dissemination, and Implementation Subcommittee of the American Academy of Neurology and the Practice Issues Review Panel of the American Association of Neuromuscular & Electrodiagnostic Medicine. *Neurology.* 2015;85(4):357-64.

5. Leung DG, Carrino JA, Wagner KR, and Jacobs MA. Whole-body magnetic resonance imaging evaluation of facioscapulohumeral muscular dystrophy. *Muscle & Nerve.* 2015;52(4):512-20.
6. Tawil R, van der Maarel SM, and Tapscott SJ. Facioscapulohumeral dystrophy: the path to consensus on pathophysiology. *Skeletal muscle.* 2014;4(12.
7. Zatz M, Marie SK, Cerqueira A, Vainzof M, Pavanello RC, and Passos-Bueno MR. The facioscapulohumeral muscular dystrophy (FSHD1) gene affects males more severely and more frequently than females. *American journal of medical genetics.* 1998;77(2):155-61.
8. Zatz M, Marie SK, Passos-Bueno MR, Vainzof M, Campiotto S, Cerqueira A, Wijmenga C, Padberg G, and Frants R. High proportion of new mutations and possible anticipation in Brazilian facioscapulohumeral muscular dystrophy families. *Am J Hum Genet.* 1995;56(1):99-105.
9. Lin F, Wang ZQ, Lin MT, Murong SX, and Wang N. New Insights into Genotype-phenotype Correlations in Chinese Facioscapulohumeral Muscular Dystrophy: A Retrospective Analysis of 178 Patients. *Chinese medical journal.* 2015;128(13):1707-13.
10. Goto K, Lee JEH, Matsuda C, Hirabayashi K, Kojo T, Nakamura A, Mitsunaga Y, Furukawa T, Sahashi KO, and Arahata K. DNA rearrangements in Japanese facioscapulohumeral muscular dystrophy patients: clinical correlations. *Neuromuscular Disorders.* 1995;5(3):201-8.
11. Lek A, Rahimov F, Jones PL, and Kunkel LM. Emerging preclinical animal models for FSHD. *Trends in molecular medicine.* 2015;21(5):295-306.
12. Mayes MB, Morgan T, Winston J, Buxton DS, Kamat MA, Smith D, Williams M, Martin RL, Kleinjan DA, Cooper DN, et al. Remotely acting SMCHD1 gene regulatory elements: in silico prediction and identification of potential regulatory variants in patients with FSHD. *Human genomics.* 2015;9(25.
13. Larsen M, Rost S, El Hajj N, Ferbert A, Deschauer M, Walter MC, Schoser B, Tacik P, Kress W, and Muller CR. Diagnostic approach for FSHD revisited: SMCHD1 mutations cause FSHD2 and act as modifiers of disease severity in FSHD1. *Eur J Hum Genet.* 2015;23(6):808-16.
14. Himeda CL, Jones TI, and Jones PL. Facioscapulohumeral Muscular Dystrophy As a Model for Epigenetic Regulation and Disease. *Antioxid Redox Sign.* 2015;22(16):1463-82.
15. Gabellini D, D'Antona G, Moggio M, Prelle A, Zecca C, Adami R, Angeletti B, Ciscato P, Pellegrino MA, Bottinelli R, et al. Facioscapulohumeral muscular dystrophy in mice overexpressing FRG1. *Nature.* 2006;439(7079):973-7.
16. van Deutekom JC, Lemmers RJ, Grewal PK, van Geel M, Romberg S, Dauwerse HG, Wright TJ, Padberg GW, Hofker MH, Hewitt JE, et al. Identification of the first gene (FRG1) from the FSHD region on human chromosome 4q35. *Hum Mol Genet.* 1996;5(
17. Rijkers T, Deidda G, van Koningsbruggen S, van Geel M, Lemmers RJ, van Deutekom JC, Figlewicz D, Hewitt JE, Padberg GW, Frants RR, et al. FRG2, an FSHD candidate gene, is transcriptionally upregulated in differentiating primary myoblast cultures of FSHD patients. *J Med Genet.* 2004;41(

18. Pirozhkova I, Petrov A, Dmitriev P, Laoudj D, Lipinski M, and Vassetzky Y. A functional role for 4qA/B in the structural rearrangement of the 4q35 region and in the regulation of FRG1 and ANT1 in facioscapulohumeral dystrophy. *PLoS One.* 2008;3(
19. Caruso N, Herberth B, Bartoli M, Puppo F, Dumonceaux J, Zimmermann A, Denadai S, Lebosse M, Roche S, Geng L, et al. Deregulation of the protocadherin gene FAT1 alters muscle shapes: implications for the pathogenesis of facioscapulohumeral dystrophy. *PLoS Genet.* 2013;9(
20. Bosnakovski D, Lamb S, Simsek T, Xu Z, Belayew A, Perlingeiro R, and Kyba M. DUX4c, an FSHD candidate gene, interferes with myogenic regulators and abolishes myoblast differentiation. *Exp Neurol.* 2008;214(
21. Bosnakovski D, Choi SH, Strasser JM, Toso EA, Walters MA, and Kyba M. High-throughput screening identifies inhibitors of DUX4-induced myoblast toxicity. *Skeletal muscle.* 2014;4(1):1-11.
22. Bosnakovski D, Xu Z, Gang EJ, Galindo CL, Liu M, Simsek T, Garner HR, Agha-Mohammadi S, Tassin A, Coppee F, et al. An isogenetic myoblast expression screen identifies DUX4-mediated FSHD-associated molecular pathologies. *EMBO J.* 2008;27(
23. Lemmers RJLF, van der Vliet PJ, Klooster R, Sacconi S, Camaño P, Dauwerse JG, Snider L, Straasheijm KR, Jan van Ommen G, Padberg GW, et al. A Unifying Genetic Model for Facioscapulohumeral Muscular Dystrophy. *Science.* 2010;329(5999):1650-3.
24. Kowaljow V, Marcowycz A, Ansseau E, Conde CB, Sauvage S, Matteotti C, Arias C, Corona ED, Nunez NG, Leo O, et al. The DUX4 gene at the FSHD1A locus encodes a pro-apoptotic protein. *Neuromuscular disorders : NMD.* 2007;17(8):611-23.
25. Jones TI, Chen JCJ, Rahimov F, Homma S, Arashiro P, Beermann ML, King OD, Miller JB, Kunkel LM, Emerson CP, et al. Facioscapulohumeral muscular dystrophy family studies of DUX4 expression: evidence for disease modifiers and a quantitative model of pathogenesis. *Human Molecular Genetics.* 2012;21(20):4419-30.
26. Rickard AM, Petek LM, and Miller DG. Endogenous DUX4 expression in FSHD myotubes is sufficient to cause cell death and disrupts RNA splicing and cell migration pathways. *Human Molecular Genetics.* 2015;24(20):5901-14.
27. Sharma V, Harafuji N, Belayew A, and Chen YW. DUX4 differentially regulates transcriptomes of human rhabdomyosarcoma and mouse C2C12 cells. *PLoS One.* 2013;8(5):e64691.
28. Leidenroth A, and Hewitt JE. A family history of DUX4: phylogenetic analysis of DUXA, B C and Duxbl reveals the ancestral DUX gene. *BMC Evol Biol.* 2010;10(
29. McGreevy JW, Hakim CH, McIntosh MA, and Duan D. Animal models of Duchenne muscular dystrophy: from basic mechanisms to gene therapy. *Disease models & mechanisms.* 2015;8(3):195-213.
30. Plantie E, Migocka-Patrzalek M, Daczewska M, and Jagla K. Model organisms in the fight against muscular dystrophy: lessons from drosophila and Zebrafish. *Molecules (Basel, Switzerland).* 2015;20(4):6237-53.

31. Mitsuhashi H, Mitsuhashi S, Lynn-Jones T, Kawahara G, and Kunkel LM. Expression of DUX4 in zebrafish development recapitulates facioscapulohumeral muscular dystrophy. *Hum Mol Genet.* 2013;22(3):568-77.
32. Wallace LM, Liu J, Domire JS, Garwick-Coppens SE, Guckes SM, Mendell JR, Flanigan KM, and Harper SQ. RNA interference inhibits DUX4-induced muscle toxicity in vivo: implications for a targeted FSHD therapy. *Mol Ther.* 2012;20(
33. Krom YD, Thijssen PE, Young JM, den Hamer B, Balog J, Yao Z, Maves L, Snider L, Knopp P, Zammit PS, et al. Intrinsic epigenetic regulation of the D4Z4 macrosatellite repeat in a transgenic mouse model for FSHD. *PLoS Genetics.* 2013;9(4):e1003415.
34. Hidalgo M, Amant F, Biankin AV, Budinská E, Byrne AT, Caldas C, Clarke RB, de Jong S, Jonkers J, Mælandsmo GM, et al. Patient-Derived Xenograft Models: An Emerging Platform for Translational Cancer Research. *Cancer Discovery.* 2014;4(9):998-1013.
35. Tentler JJ, Tan AC, Weekes CD, Jimeno A, Leong S, Pitts TM, Arcaroli JJ, Messersmith WA, and Eckhardt SG. Patient-derived tumour xenografts as models for oncology drug development. *Nat Rev Clin Oncol.* 2012;9(6):338-50.
36. Siolas D, and Hannon GJ. Patient-Derived Tumor Xenografts: Transforming Clinical Samples into Mouse Models. *Cancer Research.* 2013;73(17):5315-9.
37. Richardson PG, Hideshima T, and Anderson KC. Bortezomib (PS-341): a novel, first-in-class proteasome inhibitor for the treatment of multiple myeloma and other cancers. *Cancer control : journal of the Moffitt Cancer Center.* 2003;10(5):361-9.
38. McBride A, and Ryan PY. Proteasome inhibitors in the treatment of multiple myeloma. *Expert review of anticancer therapy.* 2013;13(3):339-58.
39. Cooper R, Irintchev A, Di Santo J, Zweyer M, Morgan J, Partridge T, and Wernig A. A new immunodeficient mouse model for human myoblast transplantation. *Human Gene Therapy.* 2001;12(823-31.
40. Vallese D, Negroni E, Duguez S, Ferry A, Trollet C, Aamiri A, Vosshenrich CA, Fuchtbauer EM, Di Santo JP, Vitiello L, et al. The Rag2(-)Il2rb(-)Dmd(-) mouse: a novel dystrophic and immunodeficient model to assess innovating therapeutic strategies for muscular dystrophies. *Mol Ther.* 2013;21(10):1950-7.
41. Rando TA. The adult muscle stem cell comes of age. *Nature medicine.* 2005;11(8):829-31.
42. Collins CA, Olsen I, Zammit PS, Heslop L, Petrie A, Partridge TA, and Morgan JE. Stem Cell Function, Self-Renewal, and Behavioral Heterogeneity of Cells from the Adult Muscle Satellite Cell Niche. *Cell.* 2005;122(2):289-301.
43. Duan D. Duchenne muscular dystrophy gene therapy: Lost in translation? *Research and Reports in Biology.* 2011;21(1051-69.
44. Partridge TA. The mdx mouse model as a surrogate for Duchenne muscular dystrophy. *FEBS J.* 2013;280(17):4177-86.
45. Griggs RC, Moxley RT, 3rd, Mendell JR, Fenichel GM, Brooke MH, Pestronk A, and Miller JP. Prednisone in Duchenne dystrophy: A randomized, controlled

trial defining the time course and dose response. Clinical Investigation of Duchenne Dystrophy Group. *Arch Neurol.* 1991;48(383-8.
46. Mendell JR, Moxley RT, Griggs RC, Brooke MH, Fenichel GM, Miller JP, King W, Signore L, Pandya S, Florence J, et al. Randomized, double-blind six-month trial of prednisone in Duchenne's muscular dystrophy. *New Engl J Med.* 1989;320(24):1592-7.
47. Sali A, Guerron AD, Gordish-Dressman H, Spurney C, Iantorno M, HOffman EP, and Nagaraju K. Glucocorticoid-treated mice are an inappropriate positive control for long-term preclinical studneis in the mdx mouse. *PLoS One.* 2012;7(4):e34204.
48. . Orphanet: an online database of rare diseases and orphan drugs. http://www.orpha.net. Accessed October 21, 2013, 2013.
49. van Deutekom J, C W, EA vT, and al. e. FSHD associated DNA arrangements are due to deletions of integral copies of a 3.2 kb tandemly repeated unit. . *Hum Mol Genet.* 1993;2(12):2037-42.
50. Wijmenga C, Hewitt J, Sandkuijl L, and al. e. Chromosome 4q DNA rearrangements associated with facioscpulohumeral muscular dystrophy. *Nat Genet.* 1992;2(1):26-30.
51. Statland JM, and Tawil R. Facioscapulohumeral muscular dystrophy: molecular pathological advances and future directions. *Curr Opin Neurol.* 2011;24(423-8.
52. Lemmers RJ, Wohlgemuth M, van der Gaag K, van der Vliet P, van Teijlingen CM, de Knijff P, Padberg GW, Frants RR, and van der Maarel SM. Specific sequence variations within the 4q35 region are associated with facioscapulohumeral muscular dystrophy. *Am J Hum Genet.* 2007;81(5):884-94.
53. Snider L, Geng Linda N, Lemmers RJ, Kyba M, Ware CB, Nelson AM, Tawil R, Filippova GN, van der Maarel SM, Tapscott Stephen J, et al. Facioscapulohumeral dystrophy: incomplete supression of a retrotransposed gene. *PloS Genetics.* 2010;6(10):e1001181.
54. Adams J. Development of the proteosome inhibitor PS-341. *The Oncologist.* 2002;7(9-16.
55. Pegram M, and Ngo D. Application and potential limitations of animal models utilized in the development of trastuzumab (Herceptin®): A case study. *Advanced Drug Delivery Reviews.* 2006;58(5–6):723-34.
56. Benchaouir R, Meregalli M, Farini A, G DA, M B, A G, M B, N B, R B, L G, et al. Restoration of human dystrophin following transplantation of exon-skipping-engineered DMD patient stem cells into dystrophic mice. *Cell Stem Cell.* 2007;1(6):646-57.
57. Meng J, Adkin CF, Xu S-w, Muntoni F, and Morgan JE. Contribution of Human Muscle-Derived Cells to Skeletal Muscle Regeneration in Dystrophic Host Mice. *PLoS ONE.* 2011;6(3):e17454.
58. Riederer I, Negroni E, Bencze M, Wolff A, Aamiri A, Di Santo J, Silva-Barbosa S, Bulter-Browne G, Savino W, and Mouly V. Slowing down differentiation of engrafted human myoblasts into immunodeficient mice correlates with increased proliferation and migration. *Mol Ther.* 2012;20(1):146-54.

59. Morgan J, Coultron G, and Partridge T. Mdx muscle grafts retain the mdx phenotype in normal hosts. *Muscle Nerve.* 1989;12(401-9.
60. McGeachie JK. Sustained cell proliferation in denervated skeletal muscle of mice. *Cell Tissue Res.* 1989;257(455-457.).
61. Dorsey S, Lovering R, Renn C, Leitch C, Liu X, Tallon L, Sadzewicz L, Pratap A, Ott S, Sengamalay N, et al. Genetic deletion of trkB.T1 increases neuromuscular function. *Cell Physiolog.* 2012;302(C141-C53.
62. Khairallah RJ, Shi G, Sbrana F, Prosser BL, Borroto C, Mazaitis MJ, Hoffman EP, Mahurkar A, Sachs F, Sun Y, et al. Microtubules Underlie Dysfunction in Duchenne Muscular Dystrophy. *Sci Signal.* 2012;5(236):ra56-.
63. Olojo R, Ziman A, Hernandez-Ochoa E, Allen P, Schneider M, and Ward C. Mice null for calsequestrin 1 exhibit deficits in functional performance and sarcoplasmic reticulum calcium handling. *PLoS One.* 2011;6(12):e27036.
64. Lovering R, L M, and CW W. Malformed mdx myofibers have normal cytoskeletal architecture yet altered EC coupling and stress-induced Ca2+ signaling. *Am J Physiol Cell Physiol.* 2009;297(C571-80.
65. Homma S, Chen JCJ, Rahimov F, Beermann ML, Hanger K, Bibat GM, Wagner KR, Kunkel LM, Emerson CP, Jr., and Miller JB. A unique library of myogenic cells from facioscapulohumeral muscular dystrophy subjects and unaffected relatives: family, disease and cell function. *Eur J Hum Genet.* 2012;20(4):404-10.
66. Rahimov F, King OD, Leung DG, Bibat GM, Emerson CP, Kunkel LM, and Wagner KR. Transcriptional profiling in facioscapulohumeral muscular dystrophy to identify candidate biomarkers. *Proceedings of the National Academy of Sciences.* 2012;109(40):16234-9.
67. Geng Linda N, Yao Z, Snider L, Fong Abraham P, Cech Jennifer N, Young Janet M, van der Maarel Silvere M, Ruzzo Walter L, Gentleman Robert C, Tawil R, et al. DUX4 Activates Germline Genes, Retroelements, and Immune Mediators: Implications for Facioscapulohumeral Dystrophy. *Developmental Cell.* 2012;22(1):38-51.
68. Latil M, Rocheteau P, Chatre L, Sanuli S, Memet S, Ricchetti M, Tajbkhsh S, and Chretien F. Skeletal muscle stem cells adopt a dormant cell state post mortem and retain regenerative capacity. *Nat Comm.* 2012;12(3):903.
69. Pearson T, Shultz LD, Miller D, King M, Laning J, Fodor W, Cuthbert A, Burzenski L, Gott B, Lyons B, et al. Non-obese diabetic-recombination activating gene-1 (NOD-Rag 1 null) interleukin (IL)-2 receptor common gamma chain (IL2 rγ null) null mice: a radioresistant model for human lymphohaematopoietic engraftment. *Clin Exp Immunol.* 2008;154(2):270-84.
70. Osborne RJ, Welle S, Venance SL, Thornton CA, and Tawil R. Expression profile of FSHD supports a link between retinal vasculopathy and muscular dystrophy. *Neurology.* 2007;68(8):569-77.
71. Mitsuhashi H, Mitsuhashi S, Lynn-Jones T, Kawahara G, and Kunkel LM. Expression of DUX4 in zebrafish development recapitulates facioscapulohumeral muscular dystrophy. *Hum Mol Genet.* 2013;22(568-77.

72. Bosnakovski D, Daughters RS, Xu S, Slack JM, and Kyba M. Biphasic myopathic phenotype of mouse DUX, an ORF within conserved FSHD-related repeats. *PLos ONE.* 2009;e7003(
73. Wallace LM, Garwick SE, Mei W, Belayew A, Coppee F, and al. e. DUX4, a candidate gene for facioscapulohmeral muscualr dystrophy, causes p53-dependent myopath in vivo. *Ann Neurol.* 2011;69(540-552).
74. Yokota T, Lu Q, TA P, Kobayashi M, Nakamura A, Takeda S, and Hoffman E. Efficacy of systemic morpholino exon-skipping in Duchenne dystrophy dogs. *Ann Neurol.* 2009;65(667-76.
75. Aoki Y, Yokota T, Nagata T, Nagata T, Nakamura A, Tanihata J, Saito T, Duguez SM, Nagaraju K, Hoffman EP, et al. Bodywide skipping of exons 45-55 in dystrophic mdx52 mice by systemic antisense delivery. *Proc Natl Acad Sci USA.* 2012;109(34):13763-8.
76. Morrison BM, Lachey JL, Warsing LC, Ting BL, Pullen AE, Underwood KW, Kumar R, Sako D, Grinberg A, Wong V, et al. A soluble activin type IIB receptor improves function in a mouse model of amyotrophic lateral sclerosis. *Experimental Neurology.* 2009;217(2):258-68.
77. Bo Li Z, Zhang J, and Wagner KR. Inhibition of myostatin reverses muscle fibrosis through apoptosis. *Journal of Cell Science.* 2012;125(17):3957-65.
78. Miciak JJ, Warsing LC, Tibbs ME, Jasper JR, Jampel SB, Malik FI, Tankersley C, and Wagner KR. Fast skeletal muscle troponin activator in the dy2J muscular dystrophy model. *Muscle & Nerve.* 2013;48(2):279-85.
79. Goodall M, Ward CW, Pratt S, Bloch R, and RM L. Structural and functinal evaluation of branched myofibers lacking intermediate filaments. *Am J Cell Phys.* 2012;303(C224-C32.
80. Gabriels J, Beckers MC, Ding H, De Vriese A, Plaisance S, van der Maarel SM, Padberg GW, Frants RR, Hewitt JE, Collen D, et al. Nucleotide sequence of the partially deleted D4Z4 locus in a patient with FSHD identifies a putative gene within each 3.3 kb element. *Gene.* 1999;236(1):25-32.
81. Lemmers RJLF, Tawil R, Petek LM, Balog J, Block GJ, Santen GWE, Amell AM, van der Vliet PJ, Almomani R, Straasheijm KR, et al. Digenic inheritance of an SMCHD1 mutation and an FSHD-permissive D4Z4 allele causes facioscapulohumeral muscular dystrophy type 2. *Nat Genet.* 2012;44(12):1370-4.
82. de Greef JC, Lemmers RJ, van Engelen BG, Sacconi S, Venance SL, Frants RR, Tawil R, and van der Maarel SM. Common epigenetic changes of D4Z4 in contraction-dependent and contraction-independent FSHD. *Human mutation.* 2009;30(10):1449-59.
83. Snider L, Geng LN, Lemmers RJ, Kyba M, Ware CB, Nelson AM, Tawil R, Filippova GN, van der Maarel SM, Tapscott SJ, et al. Facioscapulohumeral dystrophy: incomplete suppression of a retrotransposed gene. *PLoS Genet.* 2010;6(10):e1001181.
84. van Overveld PG, Lemmers RJ, Sandkuijl LA, Enthoven L, Winokur ST, Bakels F, Padberg GW, van Ommen GJ, Frants RR, and van der Maarel SM. Hypomethylation of D4Z4 in 4q-linked and non-4q-linked facioscapulohumeral muscular dystrophy. *Nat Genet.* 2003;35(4):315-7.

85. Clapp J, Mitchell LM, Bolland DJ, Fantes J, Corcoran AE, Scotting PJ, Armour JA, and Hewitt JE. Evolutionary conservation of a coding function for D4Z4, the tandem DNA repeat mutated in facioscapulohumeral muscular dystrophy. *Am J Hum Genet.* 2007;81(2):264-79.
86. Yao Z, Snider L, Balog J, Lemmers RJLF, Van Der Maarel SM, Tawil R, and Tapscott SJ. DUX4-induced gene expression is the major molecular signature in FSHD skeletal muscle. *Human Molecular Genetics.* 2014;23(20):5342-52.
87. Wallace LM, Garwick SE, Mei W, Belayew A, Coppee F, Ladner KJ, Guttridge D, Yang J, and Harper SQ. DUX4, a candidate gene for facioscapulohumeral muscular dystrophy, causes p53-dependent myopathy in vivo. *Ann Neurol.* 2011;69(3):540-52.
88. Voit T, Topaloglu H, Straub V, Muntoni F, Deconinck N, Campion G, De Kimpe SJ, Eagle M, Guglieri M, Hood S, et al. Safety and efficacy of drisapersen for the treatment of Duchenne muscular dystrophy (DEMAND II): an exploratory, randomised, placebo-controlled phase 2 study. *The Lancet Neurology.* 2014;13(10):987-96.
89. Anthony K, Arechavala-Gomeza V, Ricotti V, and et al. BIochemical characterization of patients with in-frame or out-of-frame dmd deletions pertinent to exon 44 or 45 skipping. *JAMA Neurology.* 2014;71(1):32-40.
90. Zanetta C, Nizzardo M, Simone C, Monguzzi E, Bresolin N, Comi GP, and Corti S. Molecular Therapeutic Strategies for Spinal Muscular Atrophies: Current and Future Clinical Trials. *Clinical Therapeutics.* 2014;36(1):128-40.
91. Ionis Pharmaceuticals I. ClinicalTrials.gov [Internet]. Bethesda (MD): National Library of Medicine (US). http://clinicaltrials.gov/show/NCT02312011; 2014-[cited Jan 24, 2016].
92. Blum M, De Robertis Edward M, Wallingford John B, and Niehrs C. Morpholinos: Antisense and Sensibility. *Developmental Cell.* 2015;35(2):145-9.
93. Eisen JS, and Smith JC. Controlling morpholino experiments: don't stop making antisense. *Development.* 2008;135(10):1735-43.
94. . www.gene-tools.com.
95. Zhang Y, King OD, Rahimov F, Jones TI, Ward CW, Kerr JP, Liu N, Emerson CP, Kunkel LM, Partridge TA, et al. Human skeletal muscle xenograft as a new preclinical model for muscle disorders. *Human Molecular Genetics.* 2014;23(12):3180-8.
96. Ferreboeuf M, Mariot V, Bessieres B, Vasiljevic A, Attie-Bitach T, Collardeau S, Morere J, Roche S, Magdinier F, Robin-Ducellier J, et al. DUX4 and DUX4 downstream target genes are expressed in fetal FSHD muscles. *Hum Mol Genet.* 2014;23(1):171-81.
97. Krom YD, Dumonceaux J, Mamchaoui K, den Hamer B, Mariot V, Negroni E, Geng LN, Martin N, Tawil R, Tapscott SJ, et al. Generation of isogenic D4Z4 contracted and noncontracted immortal muscle cell clones from a mosaic patient: a cellular model for FSHD. *Am J Pathol.* 2012;181(4):1387-401.
98. Marsollier AC, Ciszewski L, Mariot V, Popplewell L, Voit T, Dickson G, and Dumonceaux J. Antisense targeting of 3'end elements involved in DUX4 mRNA processing is an efficient therapeutic strategy for

Facioscapulohumeral Dystrophy: a new gene silencing approach. *Hum Mol Genet.* 2016.
99. Vanderplanck C, Ansseau E, Charron S, Stricwant N, Tassin A, Laoudj-Chenivesse D, Wilton SD, Coppee F, and Belayew A. The FSHD atrophic myotube phenotype is caused by DUX4 expression. *PLoS One.* 2011;6(10):e26820.
100. Deidda G, Cacurri S, Piazzo N, and Felicetti L. Direct detection of 4q35 rearrangements implicated in facioscapulohumeral muscular dystrophy (FSHD). *J Med Genet.* 1996;33(5):361-5.
101. Lemmers RJ, de Kievit P, Sandkuijl L, Padberg GW, van Ommen GJ, Frants RR, and van der Maarel SM. Facioscapulohumeral muscular dystrophy is uniquely associated with one of the two variants of the 4q subtelomere. *Nat Genet.* 2002;32(2):235-6.
102. van Deutekom JC, Wijmenga C, van Tienhoven EA, Gruter AM, Hewitt JE, Padberg GW, van Ommen GJ, Hofker MH, and Frants RR. FSHD associated DNA rearrangements are due to deletions of integral copies of a 3.2 kb tandemly repeated unit. *Hum Mol Genet.* 1993;2(12):2037-42.
103. Wijmenga C, Hewitt JE, Sandkuijl LA, Clark LN, Wright TJ, Dauwerse HG, Gruter AM, Hofker MH, Moerer P, Williamson R, et al. Chromosome 4q DNA rearrangements associated with facioscapulohumeral muscular dystrophy. *Nat Genet.* 1992;2(1):26-30.
104. Homma S, Chen JC, Rahimov F, Beermann ML, Hanger K, Bibat GM, Wagner KR, Kunkel LM, Emerson CP, Jr., and Miller JB. A unique library of myogenic cells from facioscapulohumeral muscular dystrophy subjects and unaffected relatives: family, disease and cell function. *Eur J Hum Genet.* 2012;20(4):404-10.
105. Clayton NP, Nelson CA, Weeden T, Taylor KM, Moreland RJ, Scheule RK, Phillips L, Leger AJ, Cheng SH, and Wentworth BM. Antisense Oligonucleotide-mediated Suppression of Muscle Glycogen Synthase 1 Synthesis as an Approach for Substrate Reduction Therapy of Pompe Disease. *Molecular therapy Nucleic acids.* 2014;3(e206.
106. Jones TI, King OD, Himeda CL, Homma S, Chen JCJ, Beermann ML, Yan C, Emerson CP, Miller JB, Wagner KR, et al. Individual epigenetic status of the pathogenic D4Z4 macrosatellite correlates with disease in facioscapulohumeral muscular dystrophy. *Clinical Epigenetics.* 2015;7(1):1-22.
107. Kim D, Pertea G, Trapnell C, Pimentel H, Kelley R, and Salzberg SL. TopHat2: accurate alignment of transcriptomes in the presence of insertions, deletions and gene fusions. *Genome biology.* 2013;14(4):R36.
108. Langmead B, and Salzberg SL. Fast gapped-read alignment with Bowtie 2. *Nature methods.* 2012;9(4):357-9.
109. Anders S, Pyl PT, and Huber W. HTSeq--a Python framework to work with high-throughput sequencing data. *Bioinformatics.* 2015;31(2):166-9.
110. McCarthy DJ, Chen Y, and Smyth GK. Differential expression analysis of multifactor RNA-Seq experiments with respect to biological variation. *Nucleic acids research.* 2012;40(10):4288-97.

Curriculum Vitae

Tracy Yuanfan Zhang

Center for Genetic Muscle Disorders
The Hugo W. Moser Research Institute, Kennedy Krieger, Baltimore, MD 21205
www.linkedin.com/in/tracyyzhang tracyzh@jhmi.edu Phone: 443-923-9528

EDUCATION:

The Johns Hopkins University, School of Medicine **Baltimore, MD**
Ph.D. in Cellular and Molecular Medicine Aug. 2010-Mar. 2016
Dissertation: Xenograft model of human skeletal muscle disorders
Advisor: Kathryn R. Wagner, M.D, Ph.D.

The Johns Hopkins University **Baltimore, MD**
Master of Science in Biomedical Engineering (Full fellowship) Sept. 2008-Aug. 2010
Thesis: Small metabolic molecules influence stem cell differentiation: effects of l-carnitine and acetyl-l-carnitine
Advisor: Jennifer H. Elisseeff, Ph.D.

Zhejiang University **Hangzhou, China**
Bachelor of Science in Biomedical Engineering (5 year program) Sept. 2003-June. 2008
Thesis: Experimental research and computer simulation of electrical cell-substrate biosensor based on interdigitated electrodes
Advisor: Ping Wang, Ph.D.

REASEARCH & PROFESSIONAL EXPERIENCE:

Ph.D. Candidate Advisor: Dr. Kathryn Wagner Sept.2010 - current *The Center for Genetic Muscle Disorders*, Kennedy Krieger Institute and the Johns Hopkins Graduate Program of Cellular and Molecular Medicine

- Pioneered and established a novel muscle xenograft model for human skeletal muscle diseases, including facioscapulohumeral muscular dystrophy (FSHD), Duchene Muscular Dystrophy (DMD), and Inclusion Body Myositis (IBM), to create a patient specific animal model for the study of disease mechanism, muscle regeneration and the evaluation of different therapeutics.
- Characterized the xenograft model specifically for FSHD by developing protocols and executing experiments from histopathological, physiologic and molecular level, including multiple biomarkers.
- Evaluated multiple therapeutics, including myostatin and TGF β inhibitors, Adeno Associated Virus (AAV) and antisense oligonucleotides in the muscle xenograft model.
- Examined muscle regeneration in vitro using primary myoblasts from FSHD patients and healthy donors.
- Studied disease pathogenesis and biomarker profile using induced Pluripotent Stem Cells (iPSCs) generated from primary cells from FSHD and DMD patients.
- Investigated the possibility of creating functional tissue engineered muscle using human adipose derived stem cells and biomaterial scaffold.

Visiting Researcher Advisor: Dr. Miguel Esteves March.2014 - June 2014

Gene Therapy Center, *Senator Paul D. Wellstone Muscular Dystrophy Cooperative Research Center for FSHD,* University of Massachusetts Medical School

- Cloned and tested new AAV-miRNA targeting FSHD causal gene DUX4-fl knockdown *in vitro*.

Graduate Student Fellow Advisor: Dr. Jennifer Elisseeff Sept.2008 - June.2010
Biomaterials and Tissue Engineering Lab, The Johns Hopkins University Department of Biomedical Engineering

- Examined the possibility of employing multiple kinds of stem cells as a reliable resource for cell therapy to promote cartilage regeneration for osteoarthritis patients.
- Analyzed the different effects of small molecules such as carnitine on therapy for osteoarthritis as well as on stem cell differentiation.

Research Assistant Advisor: Dr. Ping Wang Feb.2008 - June.2008
Biosensor National Special Laboratory (BNSL), Zhejiang University Department of Biomedical Engineering

- Designed and simulated the gold interdigitated array structure to optimize electrode parameters.
- Co-developed a system for real-time bacteria DNA detection and carried out the experiment.

PUBLICATIONS:

IN PREPARATION:

1. **Zhang Y**, Chen J, King OD, et al. Morpholino-Mediated Knockdown of DUX4 Towards Facioscapulohumeral Muscular Dystrophy Therapeutics. (Submitted)
2. **Zhang Y**, Partridge T, Wagner KR et al. Human muscle regeneration and aging: a new model in immuno-deficient mice. (Manuscript in preparation)
3. Choi IY, Lim H, Estrellas K, Mula J, Cohen TV, **Zhang Y** et al. Concordant but varied phenotypes among patient-specific myoblasts of Duchenne muscular dystrophy revealed by human iPSC-based model. (Submitted)
4. Choudhury SR, Fitzpatrick Z, Harris AF, Maitland SA, Ferreira JS, **Zhang Y** et al. In vivo selection yields novel AAV-B1 capsid for CNS and muscle gene therapy. (Submitted)

PEER-REVIEWED:

5. **Zhang Y**, King OD, Rahimov F, et al. Human Skeletal Muscle Xenograft as a New Preclinical Model for Muscle Disorders. **Human Molecular Genetics** 2014 Jun 15;23(12):3180-8.
6. Lu Q, **Zhang Y**, and Elisseeff JH. Carnitine and acetylcarnitine modulate mesenchymal differentiation of adult stem cells. **J Tissue Eng Regen Med.** 2013 Apr 29.
7. Wang L, Liu Q, Hu Z, **Zhang Y**, Wu C, Yang M, Wang P. A novel electrochemical biosensor based on dynamic polymerase-extending hybridization for E. coli O157:H7 DNA detection. **Talanta**, Volume 78, Issue 3, 15 May 2009.
8. Wang L, Wei Q, Wu C, Hu Z, **Zhang Y**, et al. The Escherichia coli O157:H7 DNA Detection on a Gold Nanoparticle-enhanced Piezoelectric Biosensor. Chinese Science Bulletin, 2007.

PRESENTATIONS:

TALKS:

1. **Zhang Y**, Chen J, King OD et al. An antisense oligonucleotide-mediated therapy for FSHD. **FSHD International Research Consortium 2015.**
2. **Zhang Y**, Esteves M, Wagner KR et al. New AAV-miRNA vector development for FSHD. **Senator Paul D. Wellstone Muscular Dystrophy Cooperative Research Center Retreat**

2014.

3. **Zhang Y**, Wagner KR et al. A Novel Muscle Tissue Xenograft Model for FSHD. **Senator Paul D. Wellstone Muscular Dystrophy Cooperative Research Center Retreat 2011, 2012, 2013.**

POSTERS:

4. **Zhang Y,** Partridge T et al. Human muscle regeneration and aging: a new model in immuno-deficient mice. **New Directions in Biology and Disease of Skeletal Muscle 2014.**
5. Partridge T, Liu H, Cohen T, **Zhang Y** et al. Nuclear membrane protein lamin A/C does not play by the rules. **New Directions in Biology and Disease of Skeletal Muscle 2014.**
6. **Zhang Y**, Wagner KR et al. A Xenograft Model of Skeletal Muscle for Preclinical Gene Therapy Studies. **The Sixteenth Annual Meeting of the American Society of Gene & Cell Therapy 2013.**
7. **Zhang Y**, Wagner KR et al. A Novel Xenograft Model for FSHD. **FSHD International Research Consortium Meeting. 2011, 2013.**
8. **Zhang Y**, Lu Q, Wu I, and Elisseeff JH. Small molecules modulate human adipose derived stem cell differentiation. **Experimental Biology Conference Proceeding FASEB J 2011**. Poster Award Finalist.
9. Hu Z, **Zhang Y**, Wang L, et al. Detecting Bacteria DNA via Ionic Conductance by a Novel Nanopore Biosensor, ***The 3rd Annual IEEE International Conference on Nano/Micro Engineered and Molecular Systems*, 2007.**
10. Wang L, Hu Z, **Zhang Y**, et al. A Novel Integrated Immunobiosensor Array for Detection of *Escherichia coli* O157:H7, ***Biosensor 2008: The Tenth World Congress on Biosensors***

HONORS & AWARDS:

Research fellowship by FSH Society	2016
Johns Hopkins University Graduate Student Travel Award	2015
Senator Paul D. Wellstone Muscular Dystrophy Predoctoral Fellowship	2011-2013
Experimental Biology Conference Travel Award	2011
Graduate Student Teaching Fellowship, School of Engineering	2008-2010
Graduate Student Research Fellowship	2008-2010
Graduate with Distinction	2008
Excellent Undergraduate Academic Scholarship	2004-2008